Modeling of High Voltage Pollution Discharge to Investigate Hot Stick Flashover

by

Dean Reske

A Thesis submitted to the Faculty of Graduate Studies of
The University of Manitoba
in partial fulfillment of the requirements for the degree of
MASTER OF SCIENCE

Department of Electrical and Computer Engineering
University of Manitoba
Winnipeg, Manitoba, Canada

Acknowledgment

I would like to thank my academic advisors Dr. Behzad Kordi and Dr. David Swatek for their guidance, support, and encouragement. I would also like to thank Manitoba Hydro for their support; in particular my supervisor Dr. Ioni Fernando, past and current section heads Brett Davies and Pei Wang, my department manager Ron Mazur, Stephanie Diakiw for help with computer drawings, and Bill McDermid and Tyler Black of the Manitoba Hydro High Voltage Test Facility. I also need to thank from the University of Manitoba Dr. Hassan Soliman and Dr. Ormiston in the Mechanical and Manufacturing Engineering Department, and Dr. Carl Bartels and Dr. Michael Freund in the Department of Chemistry; and Dr. Wiliam Likos at the University of Wisconsin-Madison Geological Engineering Department, and Dr. Ling Lu of the Colorado School of Mines Department of Civil and Environmental Engineering Department, all for helping me with my many questions. Finally, I would like to thank the members of the examining committee, Dr. Derek Oliver, Dr. Arkady Major, and Dr. Mohammad Jafari Jozani, for their constructive comments.

Abstract

Electric "flashover" or insulation breakdown has occurred on "hot stick" safety tools used on live AC transmission lines at Manitoba Hydro in 1997 and 2002. Investigations showed pollution flashover as the cause, whereby leakage currents cascade into flashover. Prior to reinstating live-line work with mitigation procedures, DC voltage experiments suggested an atypical flashover uncharacteristic of pollution flashover without leakage currents, which may require a different mitigation strategy. In this thesis, statistical analysis shows that relative humidity has a greater correlation than voltage with the type of flashover. Labeled a "fast flashover", it seems to be distinct from pollution flashover, although not statistically significant. A time-stepping computer model was developed to calculate a critical voltage for flashover as a function of relative humidity. However, lack of data prevents the model from making firm conclusions. A list of recommended research is proposed to remedy these deficiencies to allow future model refinement.

Table of Contents

List of Figures

Copyright Figures

List of Tables

Nomenclature

κ_c	Condensation coefficient.
κ_e	Evaporation coefficient.
ρ	Resistivity.
σ	Conductivity.
σ_s	Surface conductivity.
τ	Kendall Tau test coefficient.
A	Empirically derived constant used in the Obenaus arc voltage equation $V_a = Axi^{-n}$.
D	Diameter of insulator.
$D(l)$	Diameter of an insulator at position l along distance from cap to position.
E	Electric field magnitude.
E_a	Electric field stress of arc.
E_c	Critical electric field stress over which can lead to flashover.
h	heat transfer coefficient.
i	Current flowing through arc and pollution regions. Can be equal to the arc current i_a if no current flows in the substrate
i_a	Arc current.
i_c	Critical current over which can lead to flashover.
L	Total leakage length equal to length of arc x and pollution layer x_p, where $x_p = L - x$.
n	Empirically derived constant used in the Obenaus arc voltage equation $V_a = Axi^{-n}$.
R_p	Pollution layer resistance.

r_p	Pollution layer resistance per unit length.
T	Temperature.
t	Time.
V_a	Arc voltage.
V_c	Critical voltage over which can lead to flashover.
V_m	Minimum voltage needed to sustain an arc over bridged region of pollution layer leakage length.
V_s	Source voltage.
V_{fo}	Flashover voltage.
x	Length of arc.
x'_s	Length of arc for some specific applied source voltage V_s over x_c which can lead to flashover.
x_c	Critical length of arc over which can lead to flashover.
x_s	Length of arc for some specific applied source voltage V_s.
ESDD	Equivalent Salt Deposit Density
FFO	Fast flashover
FO	Flashover
FOw	Flashover withstand
PFO	Pollution flashover
RH	Relative humidity

Chapter 1

Introduction

In 1997, an incidence occurred on a Manitoba Hydro 500 kilovolt (kV) alternating-current (AC) high-voltage (HV) transmission line whereby an electric flashover or the breakdown of the electrical insulating effect of a dielectric insulating surface occurred over the length of a hot stick being used by a transmission line worker performing live (energized) transmission line maintenance work [13]. Live-line work was ceased and an internal investigation was conducted, attributing the incident to a pollution flashover, a mitagatable phenomenon. The hot stick, shown being employed in Figure 1.1, is essentially a long pole made from an electrical insulating material with a grappling hook on the end allowing the transmission-line worker to work on live (energized) lines, connecting and disconnecting, grabbing, pulling, and handling apparatus at a high voltage safely from the other end of the pole. A pollution flashover is a well-known mechanism of flashover whereby microscopic levels of pollution with conductive salts present on the insulating surface become wet which lead to leakage currents that dry out small surface regions, resulting in arcs bridging over those regions [14]. The current continues to dry out successive regions that arc over to keep the current continuous, propagating the arc activity until the entire length of the

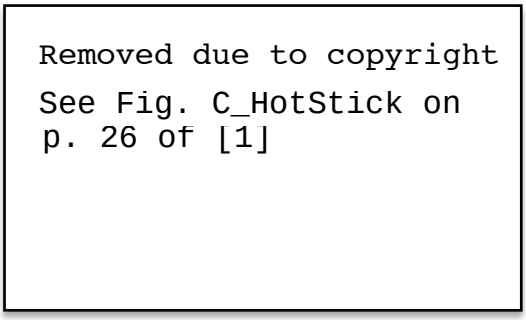

Figure 1.1: Illustration of Hot Stick in Use. Adopted from [1], ©2012 TE Connectivity.

insulating surface is breached and flashover occurs. Established mitigation procedures exist for prevention of this occurring on hot sticks, such as keeping the hot sticks clean, and restricting use of the tool to low humidity and low wind conditions [13]. Not exclusive to Manitoba Hydro, unexpected flashovers have been experienced at other utilities, although rarely reported in academic literature.

With the resolution of the cause of the 1997 incident, live-line work was reinstated until another incident occurred on the 500 kVAC transmission line system in 2002 [15]. With this incident, all high voltage live-line work was ceased and a full experimental investigation was commissioned into the cause(s) of these unexpected flashovers. Experimental investigation into the HVAC flashovers was conducted at L'Institut de Recherche d'Hydro Quebec (IREQ) in 2003 [16]. These experiments involved running a series of industry standard flashover experiments varying the applied voltage, relative humidity, and other derivatives of these two parameters while collecting data on the resulting currents and changes in ambient temperature in addition to the independent variables. This was done in an effort to discover unknown factors that may be cause for the flashovers. However, the

findings of the 2003 IREQ study concluded that pollution flashover again was the cause of the 2002 incident at Manitoba Hydro.

Prior to reinstating live-line work, additional prudent experimental investigations were conducted on the hot sticks at IREQ in 2004 under direct-current (DC) voltage, as live-line work also takes place on the Manitoba Hydro HVDC system. Although the pollution flashover mechanism was also found to be responsible for flashovers in these experiments, an additional anomalous unexplainable mechanism was discovered. This possible new mode of insulation breakdown, labeled as a"fast flashover", occurred without the precursor leakage current observed in pollution flashovers. Discharges occured at voltage gradients approximately 1/3 of that required for air-gap flashover. Very little is known about this new mode of flashover. An immediate reporting of these findings was made and disclosed to the academic and industrial HV insulation research community [17], [16]. With only the absence of precursor current being used to identify the fast flashover phenomenon, academia and industry has been reticent to accept the existence of this new phenomenon.

1.1 Motivation of the research

The possibility of a new mode of flashover is of serious concern. With different properties, a new mode of flashover most likely will require a different mitigation strategy. If the mitigation strategy is to monitor leakage current and a mode of flashover exists that does not exhibit this leakage current (at least to a measurable, detectable degree) then the mitigation strategy of monitoring leakage current will not work, and a new strategy would be necessary. Failure to appreciate the possibility of a new mode of flashover and merely attribute this phenomenon as a manifestation of the pollution mechanism is dangerous, as this may lead to incorrect mitigation resulting in future destruction to apparatus, and

injury or even possible fatality to transmission line workers. In lieu of experimental testing, statistical analysis was performed on the data from the 2004 IREQ experiments to see if anything could be found that may shed insight into the phenomenon using linear and non-parametric methods which have been used previously in similar applications [18]. In addition to this, a time-stepping mathematical model of the flashover process was created to investigate the mechanism within the context of the 2004 experimental data.

1.2 Work Performed and Results

A comprehensive literature review was first conducted to develop an understanding of the known electrical breakdown processes associated with pollution and air gap flashover. Results from the 2004 IREQ tests were acquired and the general question was posed if anything could be learned from the experimental data incorporating what had been acquired by the literature review. The IREQ test data was comprised of applied constant voltage and relative humidity as controlled independent variables, and leakage / discharge current and ambient temperature as dependent variables. It was deemed from an initial examination of the data that if a model could be developed to better understand the IREQ experiments, it would have to focus on the relative humidity data. This is because relative humidity was the only one of the two independent variables that varied (the applied voltage was held constant). Although the level of the applied voltage influences whether or not flashover occurs [4], it was thought that a property of the system would have to be varying in order to vary the type of flashover outcome. With only humidity varying out of the two independent variables, focusing on this variable seemed to be the best chance for gaining insight into the mechanism.

An exploratory analysis was first performed using descriptive statistics on the data by

identifying 19 variables describing the data, and examining the values of those variables for correlations and patterns. This was also carried out to identify redundant variables in order to reduce the variable set down to those that explained the most variation in experimental outcomes. Simple single variable regression tools and correlation matrices were employed for this purpose. Seven of the original variables were identified as being the most optimal for describing the outcomes. Two tests were employed to deduce if the fast flashover population data was distinct from the pollution flashover to support or refute the existence of fast flashover as a distinct mode of discharge. Statistically significant support was not obtained for this assertion due to small sample sizes.

To further investigate this anomalous observation, it was decided to build a computer based time-stepping pollution flashover model and apply it to the IREQ 2004 data to see if the fast flashover would meet the critical voltage criteria known for the pollution flashover. This criteria states that there is a critical voltage for which if the applied voltage exceeds it (or in the case of an applied voltage held constant, if the critical voltage drops below the applied voltage) pollution flashover can take place [8]. This is a necessary but not sufficient condition for pollution flashover [19]. It was thought that if the computer simulation tests on the fast flashover data failed to meet this pollution flashover criteria, this would support the proposition of a new mode of flashover. If the fast flashover data met the critical voltage criteria, the results would not support the fast-flashover proposition.

The model developed is a computational algorithm constructed from established mathematical formulas. Beginning with the critical voltage criteria that is a function of the pollution layer resistance per unit length, the model is essentially developed by adding equations to supply values to variables in previous equations until all values are calculated. Based on humidity, relationships were found from within thermodynamics and mass (mois-

ture) transfer to calculate a value for the varying resistance per unit length of the polluted hot stick due to changes in relative humidity. This effort unfortunately involved making assumptions to accommodate unavailable or non-existent data required for the model, but unavailable at this time. Although some insight was gained into the phenomenon from an examination of how intermediate variables change throughout the experiment compared with published results and HV experimental experience, the forced assumptions prevent the model from making firm conclusions. A list of recommended research is thus proposed to remedy these deficiencies in required data to allow for future model refinement that will give firm numerical results.

1.3 Conference publication

Resulting from the literature review, the following paper was presented at a conference, and has been invited for peer review in IEEE Transactions on Industrial Applications.

1. Dean Reske, David Swatek and Behzad Kordi, "A Study of Electric Breakdown Theory to Model Dielectric Surface Flashover," *Proc. 2012 Joint Electrostatics Conference*, Cambridge, Ontario, Canada, June 12-14, 2012.

    - A brief overview of concepts was presented from static models and experiments offering evidence of interaction between the discharge over an insulating surface and the surface itself, concepts from surface interaction models, and the Elenbass-Heller model for the leader component of the pre-discharge avalanche-streamer-leader model was examined. Discrepancies, contradictions, and proofs against some of the existing theories were discussed and recommendations for future research was proposed to rectify these deficiencies.

- To the author's knowledge, this was the first time links have been made between models from the avalanche-streamer-leader and surface interaction disciplines for the purpose of modeling dielectric surface flashover.

Chapter 2

Electric Breakdown of Air and Pollution Flashover

2.1 Electric Breakdown of Air

The breakdown of the electrical insulating effect of air has been investigated since the beginning of the last century. The air gap between two electrodes or materials at two different electric potentials is susceptible to its electrical insulating property breaking down and causing a conducting channel through the air in the event the electrical field strength due to the potential difference between the two electrodes becomes too strong for the air to prevent breakdown and conduction. Images of this phenomena occurring are shown in Figure 2.1.

The first scientific description of this phenomenon was proposed by Townsend around 1900 [4]. Labeled Townsend Electron Avalanche, the process is essentially described beginning with a newly free electron in the gap coming into existence from light or normally occurring cosmic rays from space ionizing air atoms in the gap. This unbound electron

Figure 2.1: Electric Breakdown a) Between HV Sphere and Electrode, b) Between Sphere and Sphere. Adopted with Modifications from [2], [3]. Photos ©2004 University of Michigan Demonstration Laboratory, and ©2006 Kurt Schraner Respectively. Both Images Used by Permission.

Removed due to copyright
See Fig. 5.8 on p. 296 of [4]

Figure 2.2: Schematic Representation of Townsend Electron Avalanche. a) Physical Gap b) Electron Multiplication. Adopted from [4], ©2000 Newnes.

in the gap is then accelerated by the electric field until it impacts another atom, exciting and ejecting a "secondary" electron by an ionization collision with that atom. The two resultant free electrons from the collision are then accelerated in the electric field until they both collide with more atoms producing two more ionization collisions and secondary electrons, and so on in a cascading manner. An illustration of this process is shown in Figure 2.2. Multiple instances of this process simultaneously occur at random positions throughout the air gap between the electrodes, but more so near the electrodes where the voltage gradient is more intense, and even more so near sharp edges of the electrode.

Ionizations are not only brought about by collisions, but also by photoionizations from

photons emitted from other collisions, thermal ionizations, and other ionization mechanisms. These ionization processes responsible for producing more electrons are also in competition with balancing "deionizing" processes that remove electrons by recombination with ions, or attachment to electronegative atoms producing negative ions [4].

This description of the avalanche process serves its purpose over short distances. However, weaknesses were found with the model in 1927 [20]. The discharge propagation speed in the Townsend model does not correlate with the speed in long discharges. This incited the development of new theories in 1928 dominated by the streamer and leader model of discharge that has continued to evolve until the present day. This theory begins with the avalanche process. Electron avalanches form in the strong electric field between the electrodes. The avalanche diffuses and drifts towards the anode. It stretches out due to its electron filled head being attracted to the anode, and positive ion filled tail dragging behind due to electrostatic pull and less mobility. The electrons flow into the anode and the positive ion charged tail remains behind extending the anode out into space. Subsequent avalanches drift towards the positive ion tail extending the anode, creating a further extension of a channel of ions outward from the anode. This positively charged ion channel growing outward built on electron avalanche building blocks is what is referred to as a "streamer," and the ionization state is kept in existence due to collisional ionization by the electrons flowing through to the anode from subsequent avalanches contacting the ionized space at the tip. The beginnings of this growth is illustrated in Figure 2.3 a-d on the following page.

For a short distance (up to 1 cm) this streamer channel can extend out, building on avalanche components until it reaches the cathode 2.3 e-f. However, with the discharge distances through air in power systems on the order of meters, another structure must come

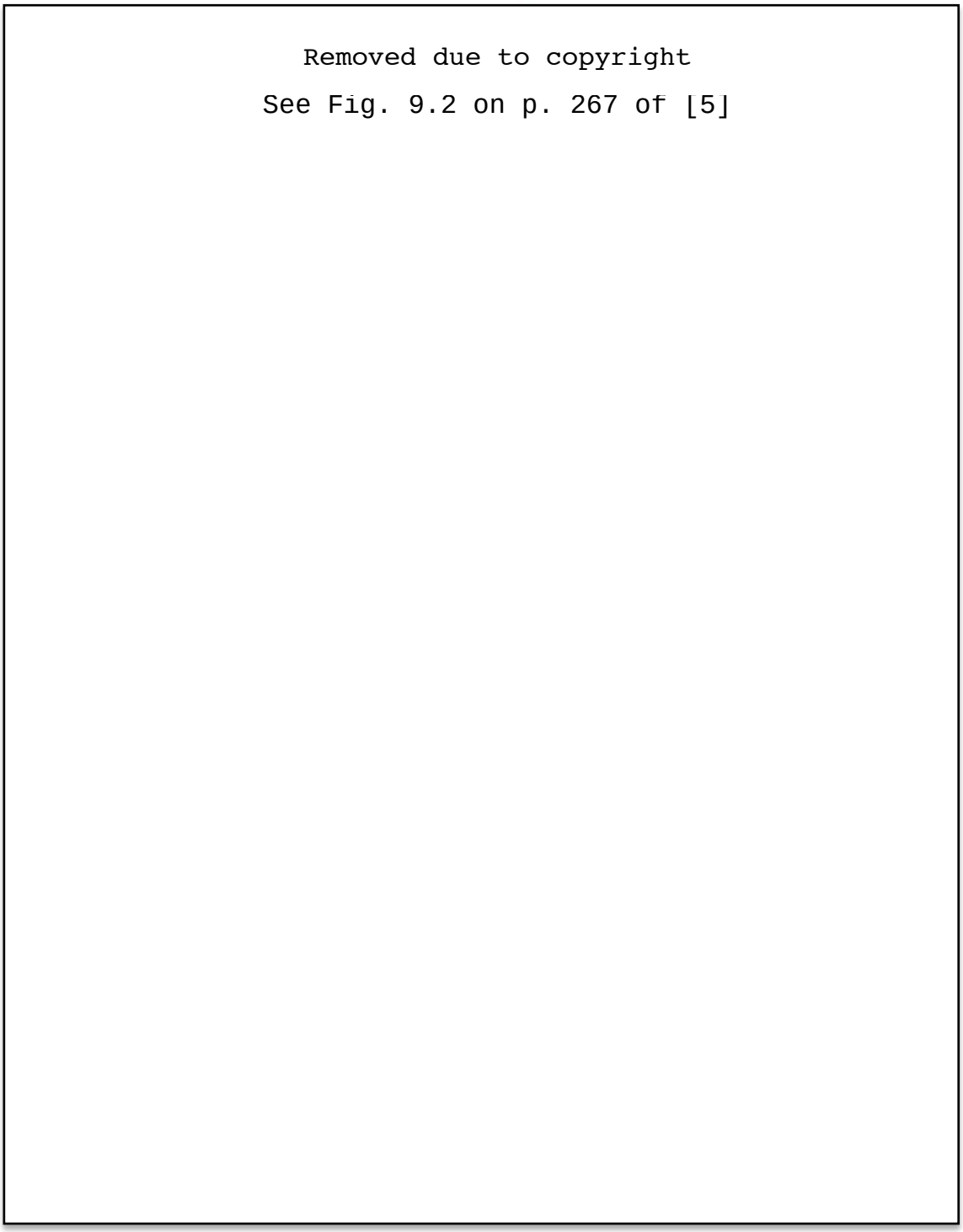

Figure 2.3: Avalanche and Streamer Formation. Adopted with modification from [5], ©1971 Wiley-Interscience.

into existence to represent the cross over in such large gaps. Just as multiple avalanches occur simultaneously and form the streamer, multiple streamers can also occur, extending outwards from a singular point at the anode. With the parallel currents from the electron avalanches flowing through the streamers converging to a singular point, and with all of this charge movement in a tight, condensed space, the ionization mechanism evolves from collisional and photonic ionization in the avalanche and streamers, to thermal ionization at the base of the streamers. Hence a new structure forms between the anode and the streamer tree where thermal ionization is occurring and growing out. This new structure is called a leader. With continual streamer currents flowing into the region heating and thermally ionizing the air, the leader will grow outward until it crosses the open gap from anode to cathode. Upon contact with the cathode, a conducting short circuit plasma channel exists between the cathode and anode. Thus, depending on the power and supply of charge at the electrodes, one of two outcomes will occur. In the event of a limited supply of charge, or a replenishable supply of charge with a weak power supply to deliver more charge as it is consumed, a brief transient explosion of charge transfer from anode to cathode will transpire (called a spark) transferring all available charge to the other electrode. However, in the event whereby a replenishable supply of charge exists with a strong enough power supply, the charge transfer will not die out, but will continue to burn with charge replenished. This phenomenon is called an arc. Both of these mechanisms are also dependent on the ionization supply and associated chemistry occurring in the air gap, as well as hundreds of other factors known to affect breakdown.

The above avalanche-streamer-leader mechanism has been described for the case of cathode directed breakdown [20]. However, another description of the mechanism was put forth by Raether in 1941 for the anode directed breakdown. Theoretically, it is also

possible for the discharge to initiate at any point in space between the electrodes and grow in both directions until a bridge linking the electrodes is formed [21], [22].

The streamers are characterized by their low current and high voltage drop, with collisional ionization bringing the local temperature up to approximately 700K-1000K. The leaders on the other hand have properties of high current and low voltage drop due to essentially being a thermally ionized plasma channel typically at a local temperature of 6000K-11000K that has reached complete equilibrium between free electron and ion reaction exchange [22]. Typical speeds in air of these discharge elements are $\sim 10^5 - 10^7$ m/s for streamers and $\sim 10^4$ m/s for leaders [21], and $\sim 1.3 - 2.1$ (cm/s)/(V/cm), or $\sim 14 - 25$ m/s for the Townsend avalanche breakdown at an average electric field gradient of 1100 V/cm.

2.2 Pollution Flashover

Electric insulation breakdown of air with the presence of a solid insulator placed between the electrodes introduces many other influencing factors into the process. In addition to the voltage potential difference and resulting electric field between the electrodes, chemistry of the air, and electric field intensities due to the geometry of the electrodes, other influencing factors can influence breakdown such as the geometry of the insulator and the junctions between it, the electrodes, and the air; and the insulator material itself. However, the most notable influence on breakdown from the power system perspective is the presence of pollution on the surface of the insulator. Pollution can contain various elements and compounds, and most notably ionic compounds that can disassociate in the presence of moisture and conduct electricity.

With the introduction of water moisture onto a "dry" pollution layer, any present ionic

salts in the pollution layer disassociate, and the electric field strength across the insulator surface will drive current due to free electrons in the solution. This current will generate heat and begin to evaporate the water moisture from the surface. This typically does not occur uniformly, and thus small regions will dry out before other areas on the surface of the insulator. Where these regions occur, forming a dry band around the insulator, an open circuit occurs in the conduction channel on the surface of the insulator and the whole voltage appears across the dry band. If the electric field intensity at the edges of the dry band is strong enough, a spark discharge or continuous arc breakdown occurs in the air above the surface in the dry band zone by the mechanisms described in the previous section. Heat from the continuing current flow in the pollution layer or from sparks or arcing contribute to further drying out and extension of the dry band, all the while other dry bands forming elsewhere along the length of the insulator. In the event dry banding covers enough of the surface so that the remaining surface length has a magnitude of electric field exceeding the breakdown voltage gradient, a final avalanche-streamer-leader structure can form resulting in the entire surface bridged by an ionized channel resulting in flashover of the entire insulator surface. This mechanism of insulation breakdown is called a pollution flashover. Pollution flashover is illustrated in Figure 2.4.

In the event the pollution is not conductive enough to produce enough heat to evaporate the moisture from the surface, dry bands will not form, or expand due to an equilibrium point being reached between evaporation and condensation.

2.3 Pollution Flashover - Mathematical Models

Pollution flashover can be mathematically represented generally in one of two ways; static models and dynamic models. Static models represent the relationship between parameters

Figure 2.4: Pollution Flashover. Adopted with modification from [6]. Photo ©2001 Stellenbosch University High Voltage Laboratory. Used by Permission.

of the pollution flashover at an instant in time, hence the term "static". Another type of model, the "dynamic" model, usually encompass a series of coupled equations to calculate rates of change in the parameters. For the most part, static models have been a mainstay of flashover modeling in power system and high voltage research. A majority of the papers on pollution flashover employ static models, with a very small minority using dynamic methods [23]

2.3.1 Pollution Flashover - Static Mathematical Model

Static flashover models have been reviewed in the past by Jolly [19, 24], and more recently by Rizk in his classic paper [25]. The static models were originally developed for describing polluted surface breakdown phenomenon, and hence by their nature require pollution and dry banding. These models describe electric flashover with physical parameters that can be measured from the terminal electrodes of a discharge such as arc voltage, arc current, arc length, and the pollution layer resistance in series with the arc.

The static approach often starts off with the discussion of the work of Fritz Obenaus

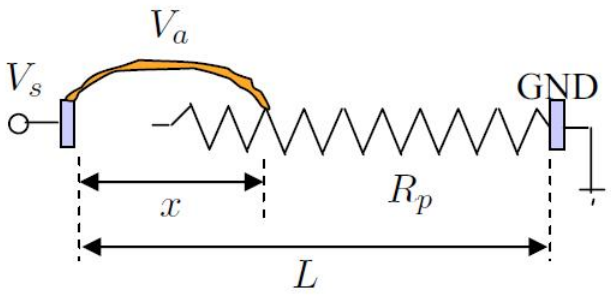

Figure 2.5: Static Arc/Pollution Flashover Circuit. Adopted with modification from [7], ©2010 IEEE. Used by Permission.

in 1958 [25] and the empirical static arc equation

$$V_a = Axi^{-n}, \tag{2.1}$$

where V_a is the potential across the arc, x is the length of the arc, i is the arc current, and $A, n \in \mathbb{R}$ are experimentally derived empirical constants. An illustration of the arc of length x jumping over a section of insulation surface (with total length L) in series with an unbreached pollution layer of length $L - x$ is given in Figure 2.5.

Equation 2.1 was one of the first to allow for quantitative discussion of electrical parameters of the arc. Writing out Kirchhoff's Voltage Law (KVL) around the closed circuit of Figure 2.5 with a voltage source V_s between the HV terminal and ground, we get the expression

$$V_s = V_a + iR_p = Axi^{-n} + iR_p, \tag{2.2}$$

with R_p the resistance of the pollution layer. The expression was mathematically manipulated by Obenaus by solving for x, then taking the derivative of x with respect to the current i and equating it to 0 to find the critical arc current i_c. This value was then substituted back into the expression for x to obtain the critical arc length x_c sustainable

at the current i_c. These equations are respectively given by

$$i_c = \frac{n}{n+1}\frac{V_s}{R_p}, \tag{2.3}$$

$$x_c = \frac{n^n}{(n+1)^{n+1}}\frac{V_s^{n+1}}{R_p^n\, A}. \tag{2.4}$$

Neumarker [26] focused his interest on conditions for arc extinction and concentrated on a more accurate and variable expression for the pollution resistance rather than the fixed one employed by Obenaus [25]. Assuming constant pollution resistance per unit length r_p, Neumarker functionalized the pollution layer resistance as a function of arc length $R_p = r_p(L - x)$. This resulted in a new expression for the circuit of Figure 2.5, given by

$$V_s = Axi^{-n} + ir_p(L - x), \tag{2.5}$$

where L is the sum length of the arc and pollution layer (Figure 2.5).

This formulation allowed for derivatives of both i and x to be taken by both Neumarker and later by Alston and Zoledziowski [8] to allow derivation of equations representing the minimum voltage V_m to sustain the arc (2.6), and from V_m the critical voltage V_c, critical arc length x_c, critical field E_c, and critical current i_c, all expressed as a function of a variable arc length x to incorporate arc growth over time into the model as given by

$$V_m = (n+1)\,(Ax)^{1/(n+1)}\,[(L - x)\,r_p/n]^{n/(n+1)}\,, \tag{2.6}$$

$$V_c = A^{1/(n+1)} r_p^{n/(n+1)} L, \tag{2.7}$$

$$x_c = L/\,(1+n)\,, \tag{2.8}$$

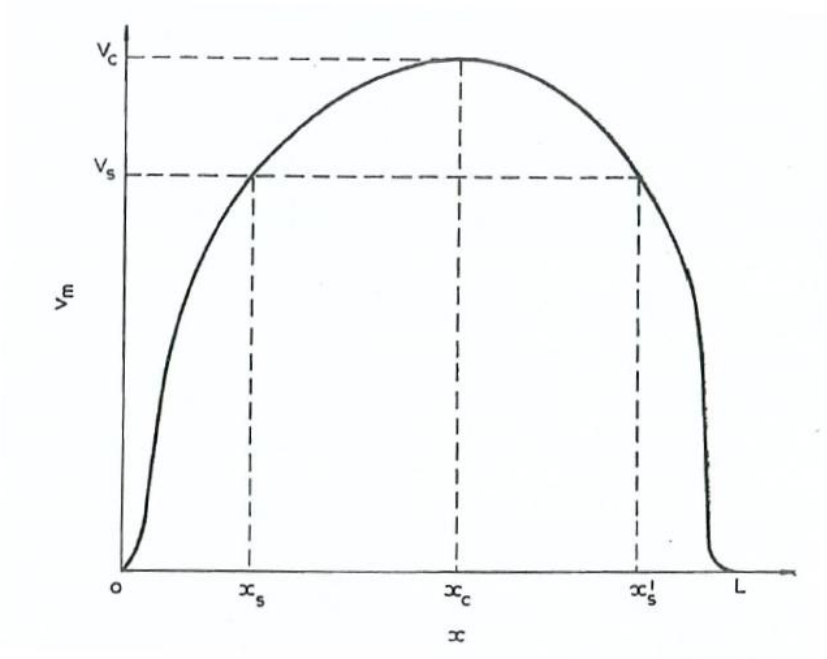

Figure 2.6: Dependence of the minimum voltage to sustain an arc V_m on the arc length x. Adopted from [8], ©1963 IET. Used by Permission.

$$E_c = A^{1/(n+1)} r_p^{n/(n+1)}, \tag{2.9}$$

$$i_c = (A/r_p)^{1/(n+1)} = E_c/r_p. \tag{2.10}$$

In plotting out the dependence of V_m on x as seen in Figure 2.6, Alston and Zoledziowski found the voltage required to maintain and propagate the discharge increases with discharge length. If the voltage required exceeds the supply voltage V_s (as it does for x_c in Figure 2.6) the discharge would extinguish without flashover. However, if the initial arc length is greater than the critical value ($x_s' > x_c$), the arc would propagate to flashover. The authors explained that as the pollution layer became more conducting, the electric field along the insulator would become more distorted and exceed the local field strength of the air resulting in flashover.

As these critical values would be fixed thresholds to their counterpart variables, it is

understood that the outcome of crossing that threshold is stochastic. Hence, to indicate this behavior, the critical threshold V_c is denoted by $V_{c,\,50\%}$ throughout this thesis to indicate it is the 50^{th} percentile.

Concentrating on the critical voltage formula, we have a criteria equation for pollution flashover

$$V_{c,\,50\%}\left(t\right) = A^{\frac{1}{n+1}} r_p\left(t\right)^{\frac{n}{n+1}} L, \tag{2.11}$$

with $V_{c,\,50\%}(t)$ as the critical voltage for which the applied voltage must exceed in order for pollution flashover to occur. L is the length of the hot stick surface under test, and A and n are empirical constants. The constant n is determined from the critical arc length (the maximum arc length attainable without full flashover) as expressed in equation 2.8

$$x_c = L/\left(1+n\right), \tag{2.8}$$

where x_c (as well as the other empirical constant A) is obtained from the experimental record discussed in the parameter settings section in chapter 6.

2.4 Pollution Resistance

Expressed as a function of time, the pollution resistance per unit length $r_p\left(t\right)$ is a function of the total pollution resistance

$$r_p\left(t\right) = \frac{R_p\left(t\right)}{L - x\left(t\right)}, \tag{2.12}$$

with $x\left(t\right)$ is the length of the dry banded area where the arc bridges the surface, $L - x\left(t\right)$ is the length of the remaining moist pollution layer that has not been bridged by arcing

and is in the process of drying out from the current. The pollution resistance is in turn a function of resistivity, the length of the resistive element, and the cross sectional area of the element [27] as shown by

$$R_p\left(t\right) = \frac{\rho_p\left(t\right)\left(L - x\left(t\right)\right)}{A_{H_2O}^{r\varphi}\left(t\right)}, \tag{2.13}$$

where $\rho_p(t)$ the resistivity of the pollution layer, and $A_{H_2O}^{r\varphi}\left(t\right)$ the cross-sectional area of the pollution layer the current is passing through.

There are many methods for calculating resistivity. One is to calculate the surface conductivity σ_s from the product of the specific conductivity σ_o and the depth of the moisture on the surface d

$$\sigma_s = \sigma_o d \tag{2.14}$$

as described by Wilkins [28]. Initially, there is always more salt that can dissolve into the water added to the surface. As moisture builds up on the surface at an initial constant maximum salt concentration, the conductivity will rise until a point is reached where no more dry salt is left to dissolve into the added water, and dilution begins. The amount of salt per volume of water begins to drop and continues to dilute until asymtotically reaching an equilibrium point given for a specific temperature. This method requires the specific conductivity to be found for each level of dilution and temperature, whether by tables or by calulation.

Another method for calculating the resistivity is given by an expression for the change in resistivitity or conductivity of a saline solution at a specific concentration for changes in temperature. This relationship is well known and is illustrated in Figure 2.7.

This relationship between salinity $[NaCl]$, temperature, and resistivity of the saline

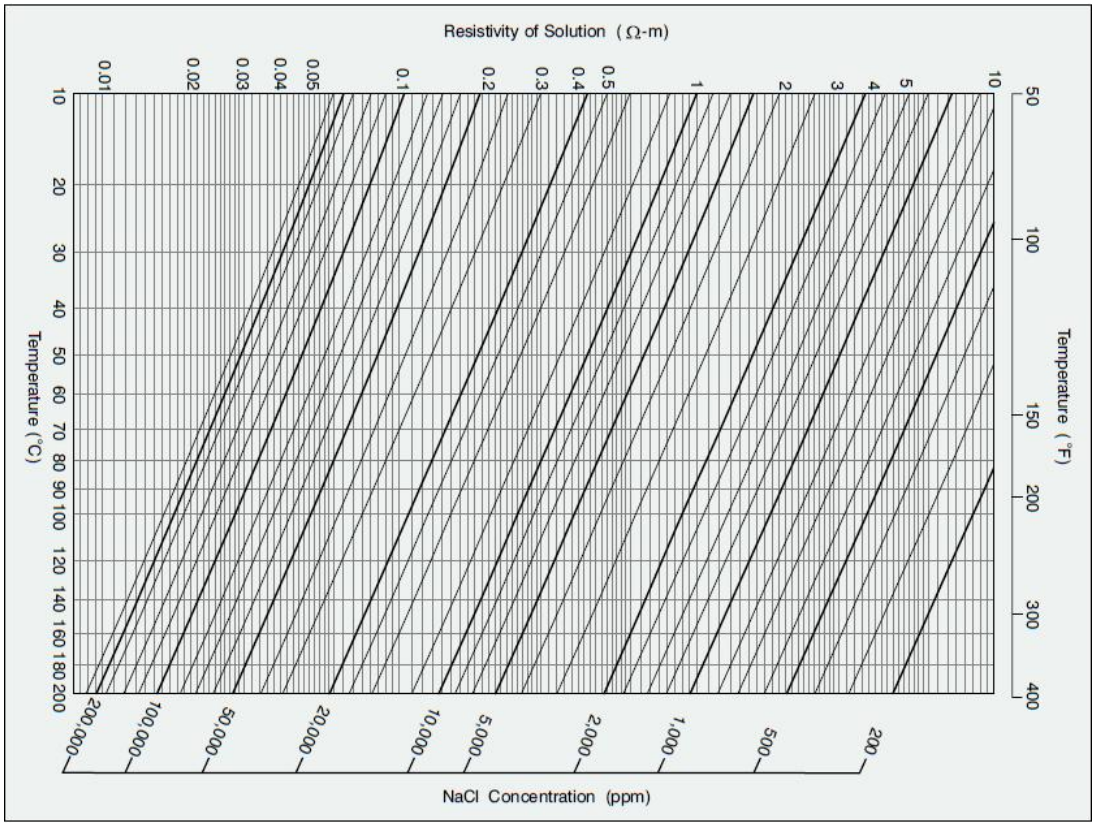

Figure 2.7: Resistivity of Saline Solution as a Function of Salt Concentration and Temperature. Adopted from [9], ©2007 Weatherford. Used by Permission.

solution pollutant ρ_p is described by the Hilchie equation [9], [29]

$$\rho_p(t) = R1\left\{\frac{T1_{\circ F} + x(t)}{T_{s^\circ F}(t) + x(t)}\right\}, \tag{2.15}$$

where $T1_{\circ F}$ and $x(t)$ are given by

$$T1_{\circ F} = \frac{9}{5}(50^\circ C) + 32 = 122^\circ F, \tag{2.16}$$

$$x(t) = 10^{-(0.340396\log_{10}[R1(t)] - 0.641427)}, \tag{2.17}$$

and R1 is the reference resistivity at the reference temperature $T1_{\circ F}$ lying on a specific [NaCl] concentration curve in Figure 2.7 given in ppm or NaCl (mg)/kg of water.

2.5 Moisture Transfer

In pollution flashover, the resistance is a function of wetting as discussed in the previous section. Hence, it is necessary to understand moisture transfer which in turn relies on thermodynamics and surface temperature.

Within the field of mass transfer in mechanical engineering, a relationship exists for the transfer of vapor to a fluid condensate on a surface, or from the water surface to vapor by evaporation in the air above the water surface. This relationship is based on the difference between the partial pressure of the vapor in the air above the surface, and the pressure exerted by the liquid on the vapor above. This mathematical relationship is described by the following expression

$$\left(\frac{dM}{dt}\right)'_t = \left[\kappa_c \frac{P_{H_2O(v)}(t)}{\sqrt{T_{H_2O(v)}(t)}} - \kappa_e \frac{P_{H_2O(l)}(t)}{\sqrt{T_{H_2O(l)}(t)}}\right] \sqrt{\frac{m_{H_2O}}{2\pi R}}. \tag{2.18}$$

In the equation, M represents the mass of water flux at the boundary, dM/dt the rate of that mass flux of water, $P_{H_2O(v)}(t)$ is the partial pressure of the water vapor in the ambient surroundings over the surface, $P_{H_2O(l)}(t)$ is the pressure of the "liquid water" on the ambient surroundings, m_{H_2O} is the molecular mass of H_2O, R is the ideal gas constant, $T_{H_2O(v)}(t)$ and $T_{H_2O(l)}(t)$ are the temperatures of the vapor and liquid respectively, and κ_c and κ_e are the condensation and evaporation coefficients. The equation simply states that the mass flux from vapor to a liquid surface is a function of the difference between the partial pressure of the vapor above the surface and the liquid's pressure at the surface. This form is the expression given by Marek and Straub [30] and is referred to as the Hertz-Knudsen-Schrage (HKS) equation. The relationship is often required in this form as different surface properties exhibit different degrees of absorbency and evaporation, thus requiring use of the condensation and evaporation constants.

With knowledge of the relative humidity, the partial pressure can be calculated from the definition of relative humidity

$$RH(t)(\%) = \frac{P_{H_2O(v)}(t)}{P_{H_2O(v)sat}(t)} \cdot 100\%, \tag{2.19}$$

where $\mathrm{P}_{H2O(v)sat}(t)$ is the saturation pressure of water vapor at the respective temperature [31]. Rearranging this relationship to find the partial pressure of the vapor in the air, we obtain

$$P_{H_2O(v)}(t) = \frac{RH(t)(\%)}{100\%} P_{H_2O(v)sat}(t). \tag{2.20}$$

The saturation pressure can be obtained from the saturated water-temperature table at

the back of any introductory textbook on engineering thermodynamics [31]. The data can be entered into a spreadsheet and a curve fit can be obtained. However, there are many empirical equations already available, one of which is the Antoine equation that calculates the saturation pressure at different air temperatures

$$P_{H_2O(v)sat}\left(t\right) = 10^{\left\{A - \frac{B}{C + T_{H_2O(v)}(t)}\right\}}, \tag{2.21}$$

with A, B, and C empirical constants given for water over varying intervals of ambient temperature [32].

The vapor pressure for the liquid is given by the Clausius Clapeyron equation, given here in a form to solve for the vapor pressure of the liquid

$$P_{H_2O(l)}\left(t\right) = \exp\left\{\frac{\Delta H}{R}\left(\frac{1}{T_1} - \frac{1}{T_{H_2O(l)}\left(t\right)}\right) + \ln\left(P_1\right)\right\}, \tag{2.22}$$

with ΔH the enthalpy of vaporization of water, P_1 the standard pressure of 101300 Pa, and T_1 the temperature of 373.15 K [33].

Another moisture transfer function $(dM/dt_{boil})_t$ must be defined for if the temperature of the surface water reaches 100°C or 373.15K and boils off surface water to the ambient surroundings. Typically, this would be equal to

$$\left(\frac{dM}{dt}_{boil}\right)_t = \frac{P\left(t\right)}{A^{z\varphi}_{H_2O}\left(t\right)\Delta H\left(t\right)}, \tag{2.23}$$

with $P\left(t\right)$ the power injected into the water by Joule Heating (in the case of a current flowing through a saline moist pollution layer on the surface of an insulator). This is formulated just by definition of the enthalpy or heat of vaporization (amount of energy

to vaporize 1kg of water at 373.15K), and is found in [27] for reference. Applying Joule heating to a saline water pollution layer to cause dry banding was originally applied by Salthouse [34].

2.6 Thermodynamics

In the previous section, it is observed that many of the moisture transfer and pressure functions are a function of the temperature of the water surface. An increase in the temperature of a polluted conductive water surface can be caused by Joule heating as stated in the previous section. A decrease in the temperature can be caused by the heat losses due to convection, conduction, and radiation [31]. These effects are given in terms of their energy change. For Joule heating, the change in energy is expressed as

$$\left(\frac{dQ}{dt}\right)_{Joule\ heat} = i^2\left(t\right) R_p\left(t\right). \tag{2.24}$$

At any time the heat Q generated is also being given off by the water due to natural convection to the ambient air at a rate $dQ/dt = \dot{Q}$ given by Newton's law of cooling [31]

$$\left(\frac{dQ}{dt}\right)_{conv,t} = h\left(t\right) A^{z\varphi}_{H_2O}\left(t\right)\left(T_{H_2O(l)}\left(t\right) - T_a\left(t\right)\right). \tag{2.25}$$

An expression for the total energy change in a system with energy sources and sinks such as the ones above is stated by the following equation [31]

$$\left(\frac{dQ}{dt}\right)_{total,t} = m\left(t\right) c_p\left(t\right)\left(\frac{dT_{H_2O(l)}}{dt}\right)_t \tag{2.26}$$

Assuming that only Joule heating as the source of heat energy input into the salt water

layer, and convection is the only method of cooling, an energy balance equation can be assembled whereby the total energy change is equal to the increase in energy due to Joule heating minus the losses in energy due to convection [35]

$$m\left(t\right)c_{p}\left(t\right)\left(\frac{dT_{H_{2}O(l)}}{dt}\right)_{t}=i^{2}\left(t\right)R_{p}\left(t\right)-h\left(t\right)A_{H_{2}O}^{z\varphi}\left(t\right)\left(T_{H_{2}O(l)}\left(t\right)-T_{a}\left(t\right)\right). \tag{2.27}$$

Dividing through by the mass and specific heat capacity, we arrive at an expression for the rate of change of temperature with respect to time for a wet saline surface being simultaniously heated by Joule heating and cooled by convection

$$\left(\frac{dT_{H_{2}O(l)}}{dt}\right)_{t}=\frac{i^{2}\left(t\right)R_{p}\left(t\right)}{m\left(t\right)c_{p}\left(t\right)}-\frac{h\left(t\right)A_{H_{2}O}^{z\varphi}\left(t\right)\left(T_{H_{2}O(l)}\left(t\right)-T_{a}\left(t\right)\right)}{m\left(t\right)c_{p}\left(t\right)}. \tag{2.28}$$

The above expressions require a value for the heat transfer coefficient $h(t)$. Unfortunately, the calculation of $h\left(t\right)$ is very complex and has a large dependence on geometry. Therefore, this review will discuss the calculation within the context of our specific cylindrical hot stick moisture surface boundary mounted vertically in the laboratory. Various formulas have already been derived for $h\left(t\right)$ and are given in Welty et al. for a variety of geometries: horizontal flat surfaces, vertical flat planes, horizontal cylindrical surfaces [36]. In Welty et al., an expression for $h\left(t\right)$ is given by Churchill and Chu for a horizontal vertical plane that can be used to approximate the vertical cylinder. The expression is

$$h\left(t\right)=\frac{k\left(t\right)}{L'}Nu_{L}\left(t\right), \tag{2.29}$$

where $k\left(t\right)$ is the thermal conductivity of air, L' is the length of the surface in the direction of gravity which for our situation is equal to the length of the hot stick test length L, and

$Nu_L(t)$ is the average Nusselt number (a dimensionless number). This approximation is only valid if the following condition is met

$$\frac{2r}{L'} \geq \frac{35}{Ra_L(t)^{0.25}}, \tag{2.30}$$

where r is the radius of the hot stick (more specifically, the distance from the axis of the hot stick to the surface of the water on the hot stick), and $Ra_L(t)$ is the average Raleigh number of the system, which can only be evaluated after all of the long series of calculations for $h(t)$ are completed.

The average Nusselt number $Nu_L(t)$ (dimensionless) is calculated by the expression

$$Nu_L(t) = \left(0.825 + \frac{0.387 Ra_L(t)^{\frac{1}{6}}}{\left[1 + \left(\frac{0.492}{Pr(t)}\right)^{\frac{9}{16}}\right]^{\frac{8}{27}}} \right)^2, \tag{2.31}$$

where $Ra_L(t)$ is the average Raleigh number (dimensionless), and $Pr(t)$ is the Prendtl number (dimensionless). The Prendtl number is calculated from the formula

$$Pr(t) = \frac{c_p(t)\,\mu(t)}{k(t)}, \tag{2.32}$$

where $\mu(t)$ is the dynamic viscosity of the air. The average Raleigh number is a product of the Prendtl number and another dimensionless number called the Grashof number, the average value denoted by $Gr_L(t)$, where

$$Ra_L(t) = Gr_L(t)\,Pr(t). \tag{2.33}$$

The average Grashof number is calculated from the following formula

$$Gr_L(t) = \frac{g\beta(t) L^3}{\nu(t)^2} \left(T_s(t) - T_a(t)\right), \tag{2.34}$$

where g is the gravitational constant, $\nu(t)$ is the kinematic viscosity, $T_s(t)$ and $T_a(t)$ are the surface and ambient temperatures, and $\beta(t)$ is the thermal expansion coefficient $= 1/T_f(t)$ where $T_f(t)$ is the 'film' temperature at the boundary of heat transfer equal to

$$T_f(t) = \frac{1}{2}\left(T_{s(t)} - T_a(t)\right), \tag{2.35}$$

which is the temperature that all the above parameters $c_p(t)$, $\mu(t)$, $\nu(t)$, and $k(t)$ are to be evaluated at.

In the event that the condition of equation 2.30 is not met, Cebeci offers a solution [37] whereby Nusselt number correction factors are tabulated for very narrow vertical cylinders. These correction factors are looked up in the table according to the corresponding Prendtl number and a calculated factor $\xi(t)$ found by the expression

$$\xi(t) = \frac{\sqrt{32}}{Gr_L(t)^{0.25}} \frac{L}{2r}, \tag{2.36}$$

reformulated and explained by Poliel et al. [38].

Chapter 3

Background Experimental Research and Data Reconstruction

For the 2004 IREQ DC hot stick investigation, a series of nine pollution flashover experiments designated "B01-B09" were conducted on lineman hot sticks. These experiments were standardized, controlled artificial pollution solid-layer tests performed according to IEC 61245 [39]. The hot sticks were spray-coated with a kaolin-salt-water slurry mixture resulting in an average equivalent salt deposit density (ESDD) of 2 μg/cm^2, and allowed to dry. The hot sticks were individually set up in a high voltage fog-chamber and tested by applying a clean fog steam into the chamber causing the relative humidity to rise while holding a constant voltage potential across the stick, until flashover occurred or until the 90 minute limit to the experimental run was reached. During the experiment, voltage, current, ambient temperature, and relative humidity data were collected.

Due to the time lapse since these experiments, the original data files were not available and only plots of the above four data traces were available for analysis (see Figures 3.2 - 3.5, and Appendix A). Hence, digitization of the data plots was performed to reacquire

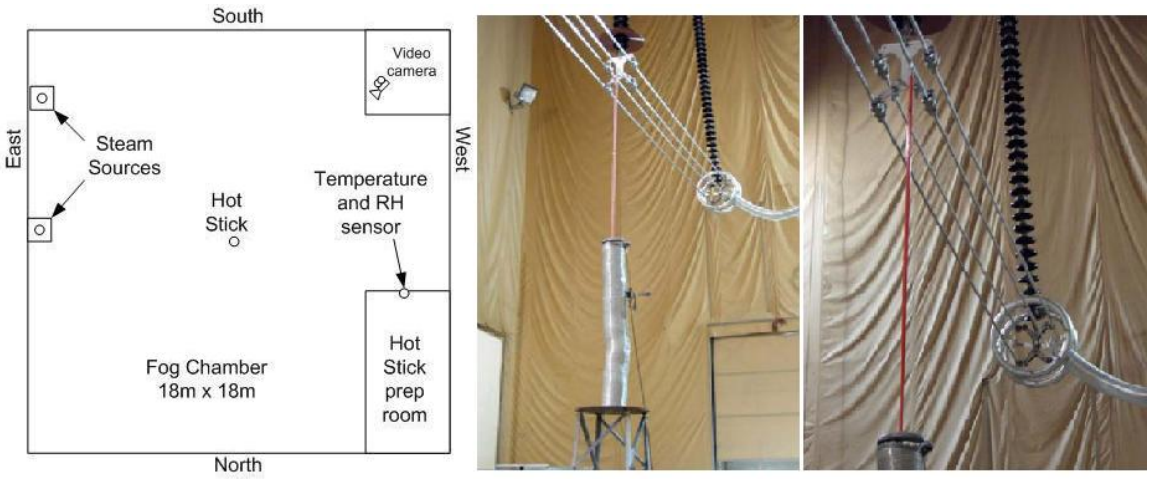

Figure 3.1: Floor Layout of IREQ Fog Chamber, and Images of Hot stick Setup in Lab. Photos Adopted with Modification from [10]. Used by Permission.

the measurements over the time of the experimental run of each of the 9 experiments.

3.1 Details

The tests were performed in the 18m x 18m square fog chamber at the IREQ HV test facility in Varannes, Quebec. Steam nozzles releasing steam into the chamber were located at the side wall, temperature and relative humidity transducers were located on top of a 3-3.5m high room sticking out into the chamber on the opposite side, and the hot stick was experimented on in the center of the chamber. A video camera was placed near the intermediate wall about 8.5m away from the hot stick vertical axis. The chamber layout and images of it are displayed in Figure 3.1.

The nine experiments were conducted with the intent of varying the voltage levels. The experiments, labeled B01 to B09, also had varying relative humidity level traces due to random experimental variation. The data was only available for examination in the format of plots. Figures 3.2 - 3.4 display the results for three of the experiments B04, B02,

Table 3.1: Artificial Pollution Slurry Composition

Component	Amount (g)	Constituent	Percentage (%)
Kaolin (Roger's)	480	SiO_2	46.50
		Al_2O_3	37.50
		TiO_2	1.30
		Fe_2O_3	1.00
		H_2O (OH)	12.78
		Trace Elements	0.92
NaCl	4.16		
H_2O	2,400		
Alcohol (95%)	9,600	C_2H_5OH	95.00
		H_2O	5.00

and B01 which also represent the three types of outcomes - pollution flashover (PFO), fast flashover (FFO), and flashover withstand or no flashover (FOw). Figure 3.5 displays experiment B03 which is divided into B03-01, a fast flashover outcome which occurs in the first 23 minutes, and B03-02, a flashover withstand resulting from the final 67 minutes of the experimental run (from 23 to 90 minutes). The plots for all of the 9 experiments can be found in Appendix A. Table 3.2 summarizes the results of the ten experiments with the applied voltage V and relative humidity at flashover RH_{fo}, or the RH at the end of the experiment.

Table 3.2: B01 - B09 Flashover Experiments Results

Case	Outcome	V_a (kV)	RH_{fo} (%)
B01	PFOW	-300	97.0
B02	FFO	-325	88.8
B03-1	FFO	-325	88.5
B03-2	PFOW	-300	97.2
B04	PFO	-315	97.9
B05	FFO	-300	67.1
B06	PFO	-285	98.3
B07	PFOW	-270	98.6
B08	PFOW	-300	98.1
B09	PFO	-315	97.3

Analysis of the data required transformation from the form of the plots as displayed in Figures 3.2 - 3.5 into digital representation. Hence, the plots were enlarged to a maximum size and digitized to obtain the smallest time division. However, this first attempt produced data that was unusable as the time division was on the order of 10's of seconds. It was then determined that the plot images should be divided up into the grid cells for more detailed digitization.

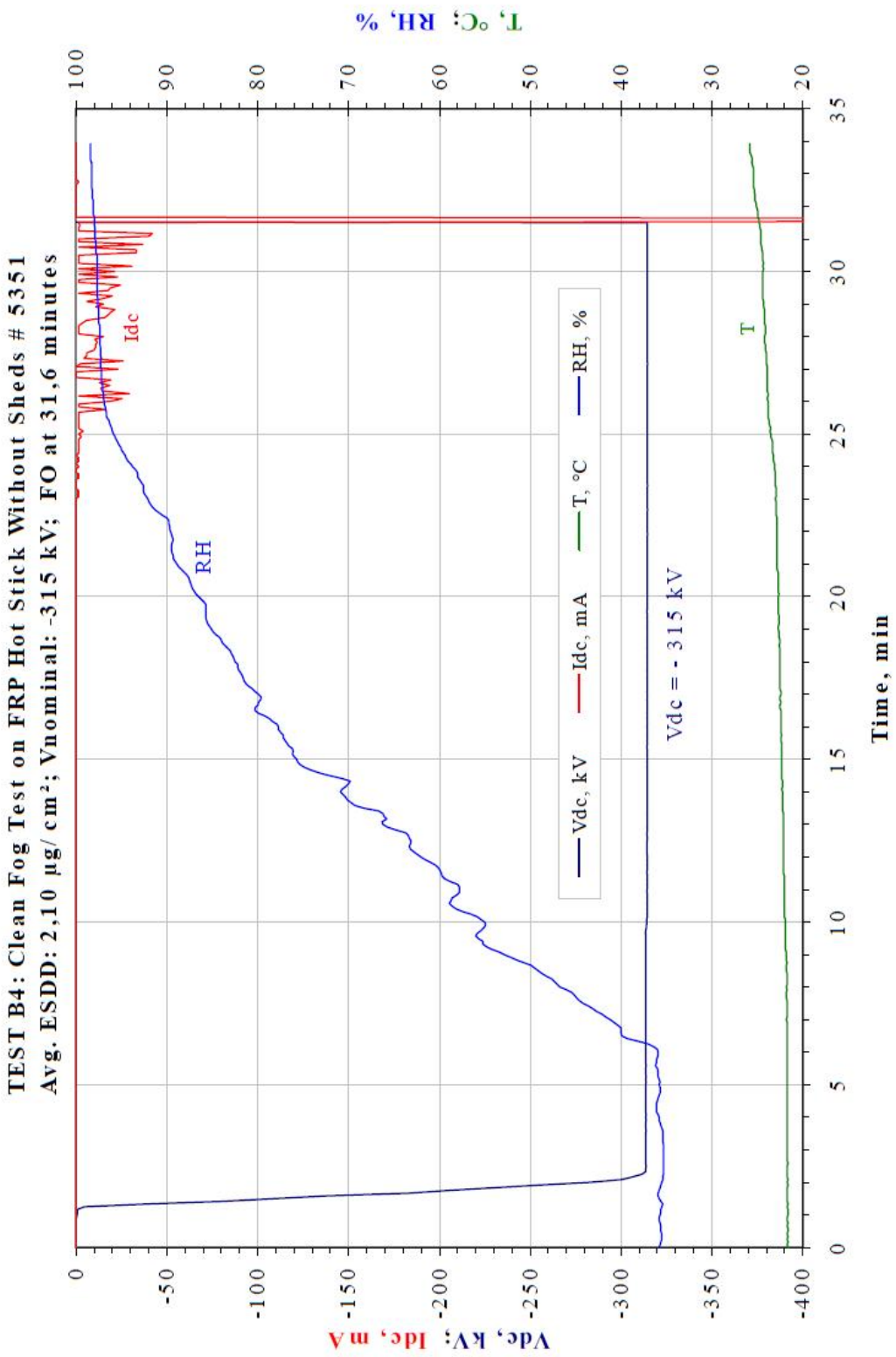

Figure 3.2: B04 Pollution Flashover - Original Data. Adopted from [10]. Used by Permission.

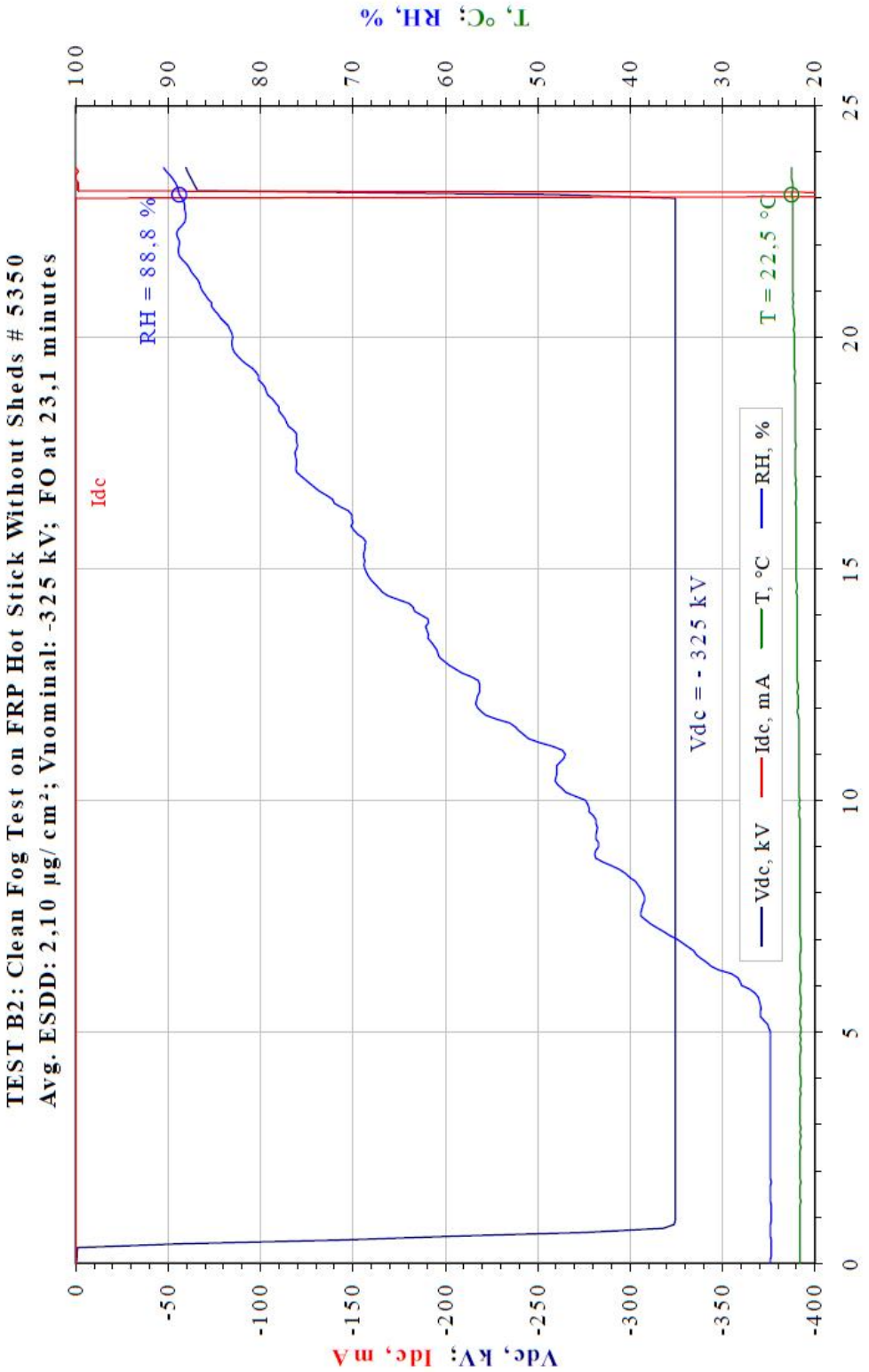

Figure 3.3: B02 Fast Flashover - Original Data. Adopted from [10]. Used by Permission.

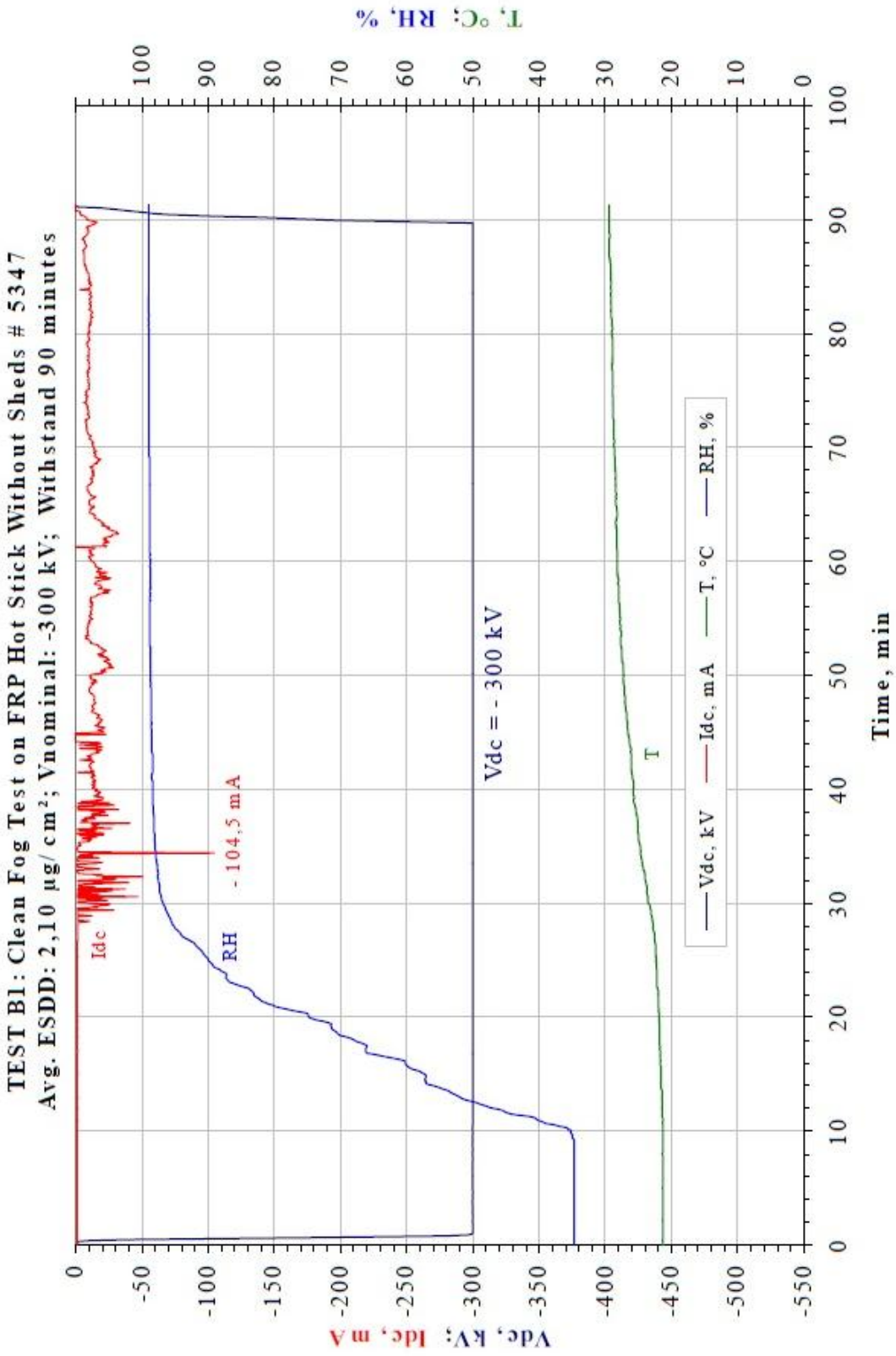

Figure 3.4: B01 Pollution Flashover Withstand - Original Data. Adopted from [10]. Used by Permission.

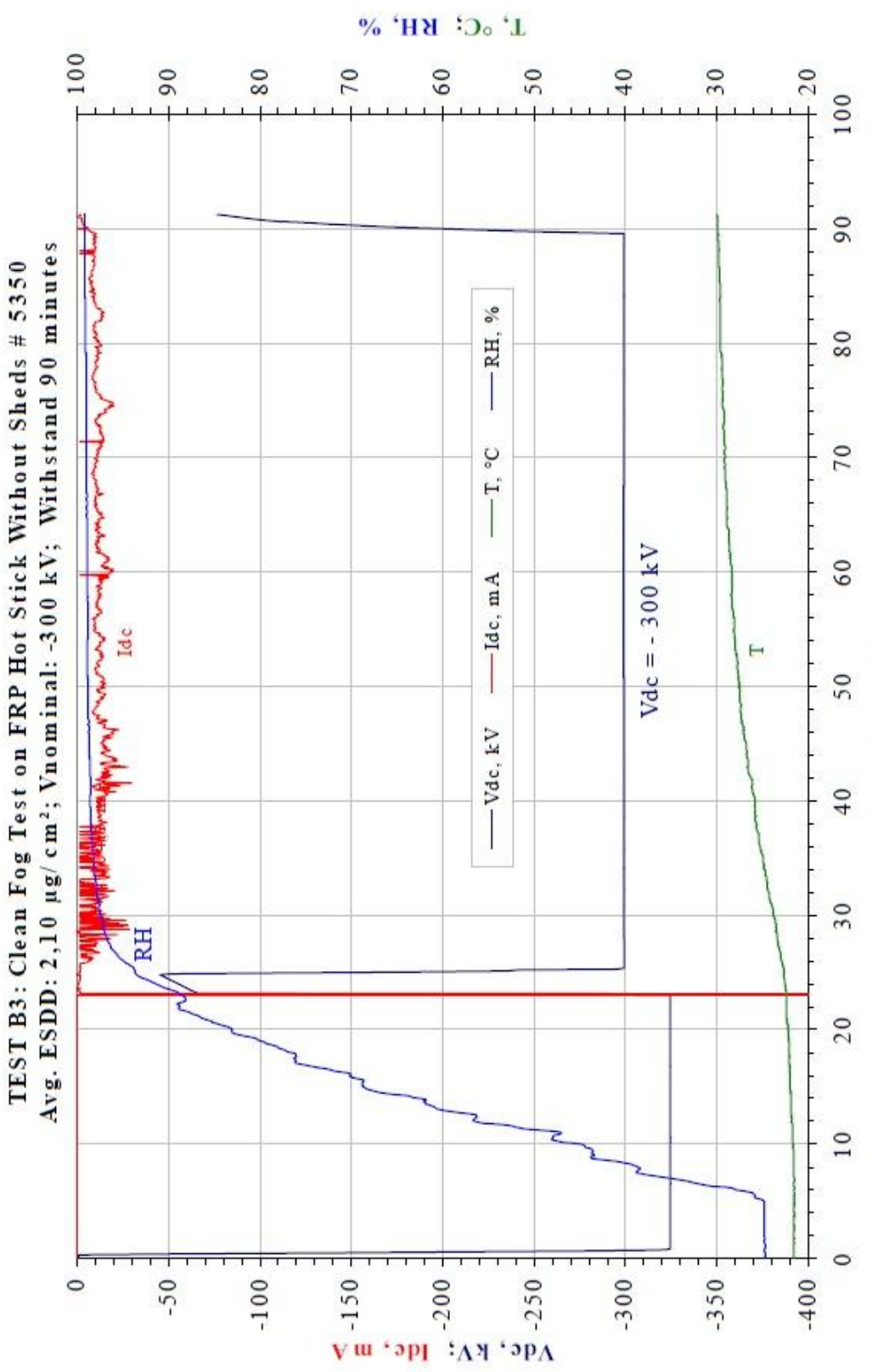

Figure 3.5: B03 Combination Fast Flashover Followed by Pollution Flashover Withstand - Original Data. Adopted from [10]. Used by Permission.

Dividing up the grid cells of the plots allowed for maximum enlargement while still maintaining reference points (the grid intersections) for proper scaling. This was done in order to get a small enough time division (0.5 seconds) that allowed reproduction of the activity in the leakage current. Images of the digitization process are shown in Figure 3.6 on the following page for the cell between 20 to 30 minutes and 0 to -50 mA of current in the experimental flashover withstand case B01 illustrated in Figure 3.4. After each cell in the figure was prepared, the traces were digitized and the points exported to csv files, as displayed in Figure 3.7.

After the data was exported to csv files for the separate cells, the data from each cell was assembled together for each case according to trace type (current, voltage, relative humidity, and ambient temperature). These traces were brought together in an Excel spreadsheet. However, there were still multiple second intervals between data points, and points for one trace would have different time coordinates from the other traces due to the digitization program optimizing these locations on each separate data trace for maximum data point generation. Therefore, linear interpolation was performed on the data traces to increase the data resolution as much as possible. This allowed for as near replication of the transient movements in the traces, and set all the data points of each separate trace to a common time step. Linear interpolation was performed by importing the columns of data into arrays in MATLAB and employing the interp() linear interpolation function to interpolate between the digitized sample points to achieve a final trace.

As there is no original digital data, we can not do a quantitative comparison between the original data and the digitized results. However, a qualitative comparison performed in Figure 3.8 shows that overall the digitization did replicate the plotted current data trace. However, where sharp transitions occur, the digitization did not cover the current trace as

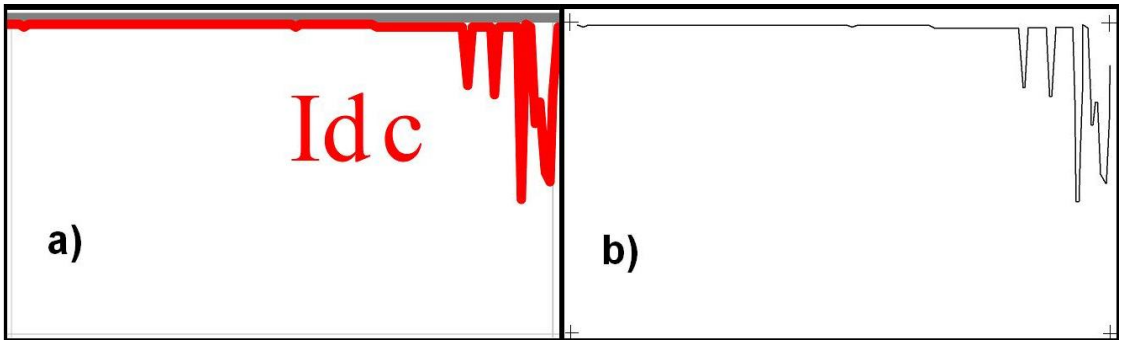

Figure 3.6: Digitization Process: a) zoom in, b) trace over and deletion of lines, resulting in final image with coordinate markers.

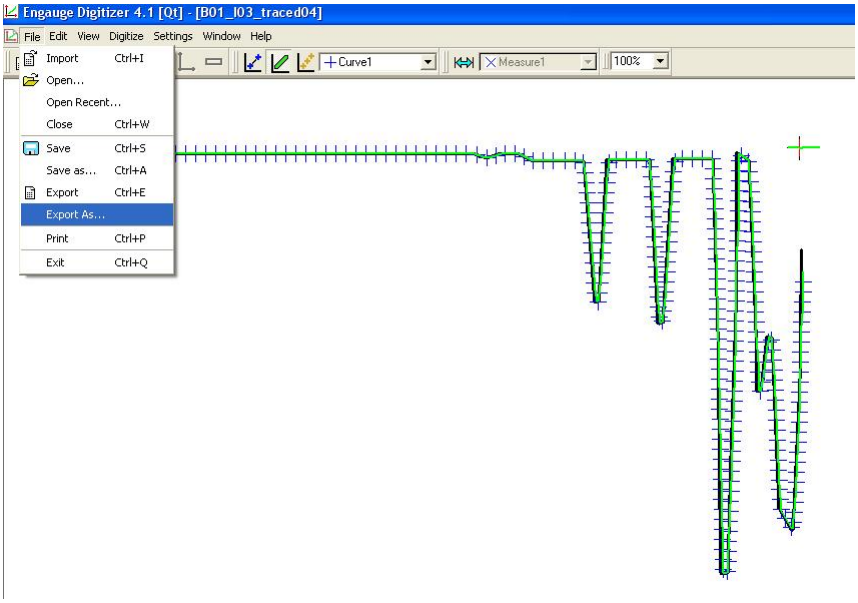

Figure 3.7: Digitization and export of data.

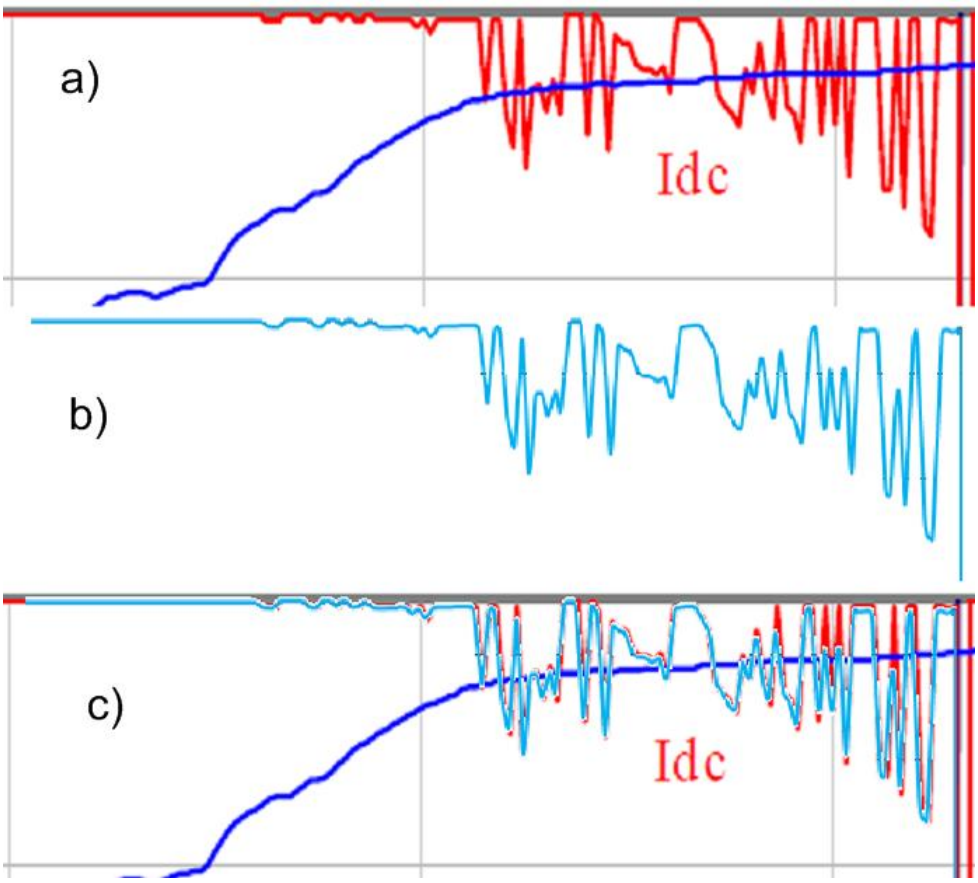

Figure 3.8: Comparison between a) original B04 current trace data and b) digitized current data, c) digitized current data overlaying original current data. Current magnitude scale 50mA between horizontal grey lines; time scale 5 minute interval between grey vertical lines.

displayed in the lower magnitude, upper portions of the overlay trace in Figure 3.8c. This would have the effect of overestimating the current during those brief time intervals.

Chapter 4

Statistical Analysis, Results, and Discussion

In order to support or refute the proposition that fast flashover is a new mode or class of flashover distinct from the pollution flashover, evidence had to be gained from the data. Within the discipline of statistical science, this question could be reframed to ask if it is possible for the fast flashover data values to have been drawn from a population distinct from the pollution flashover. Statistical analysis was used to evaluate the relative degree to which the independent controllable variables correlated with the experimental outcomes of flashover (FO) vs. flashover withstand (FOw), and with the type of flashover outcome, i.e. pollution flashover (PFO), flashover withstand (FOw), or fast flashover (FFO). The analysis showed that voltage level had the greater correlation with the outcome of FO vs. FOw. However, it was found that relative humidity had a greater correlation with the type of flashover outcome (PFO/FOw/FFO).

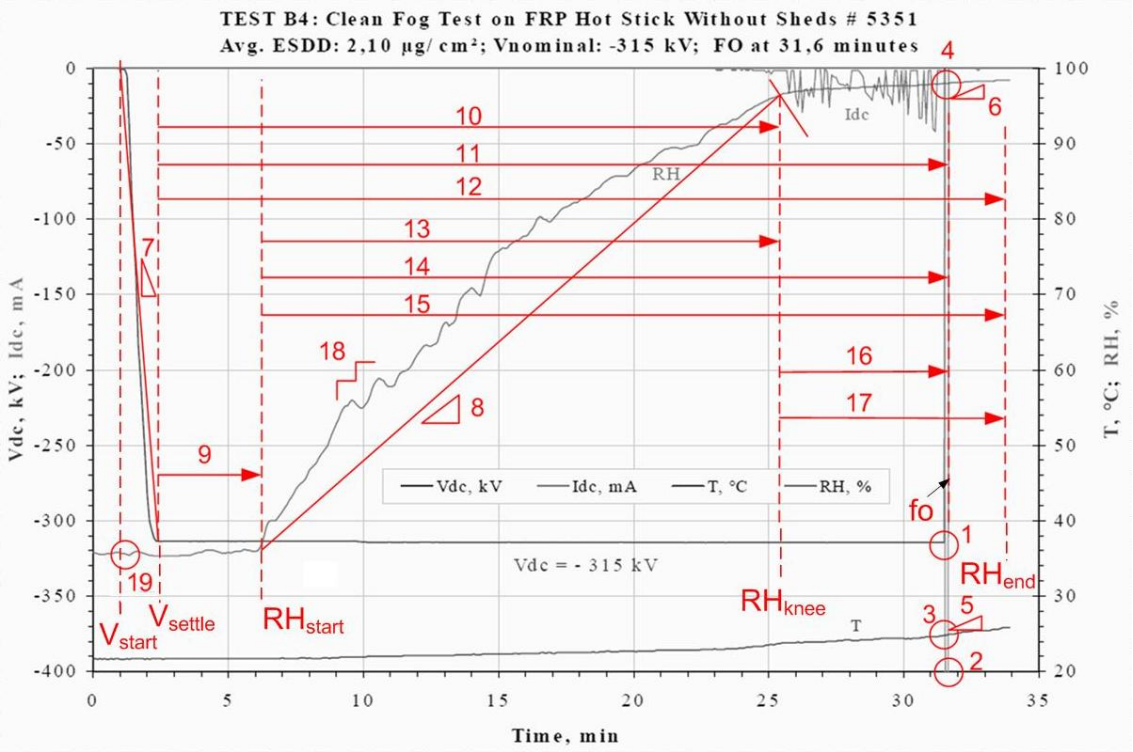

Figure 4.1: Case Variables for Statistical Analysis (See Table 4.1 for Variable Identification According to Numbers. Background Original Data, Adopted from [10]. Used by Permission.

4.1 Preliminary Analysis - Simple Linear Regression

The data was first analyzed to investigate relationships between variables describing the properties of the flashover or flashover withstand cases, and for patterns between these relationships and the type of flashover. The traces were examined and descriptive properties of the traces were defined to describe the data. An illustration of these variables describing the properties of the cases is shown in Figure 4.1.

As illustrated in Figure 4.1, the variables describe current (I), voltage (V), ambient temperature (T_a), and relative humidity (RH) levels, time derivatives, and slopes at specific points or over time intervals. The specific points are when the voltage is started (V_{start}),

settled to its final value ($V_{settled}$), when the steam fog is started (RH_{start}), the time it reaches the knee point where the RH levels out (RH_{knee}) the point of time at flashover (fo) or the end of the experiment in the event of withstand. A relative "smoothness" measurement for the RH curve was also extracted from the data. All of these variables are listed in Table 4.1 and a summary statistics for these variables is displayed in Table 4.2. The calculation for the smoothness of the RH curve was performed by summing up all the squares of the second derivative along the RH trace, according to [40]

$$RH_{smoothness} = \sum \left(\frac{d^2 RH}{dt^2} \right)^2, \tag{4.1}$$

where a sum of zero would indicate a perfectly smooth curve (only obtainable with a straight line).

Table 4.1: B01 - B09 Cases Variable List

Var.	Description	Var.	Description
1	V level (kV)	11	t: V_{settle} to fo (s)
2	I at fo (mA)	12	t: V_{settle} to RH_{end} (s)
3	T_a at fo (°C)	13	t: RH_{start} to RH_{knee} (s)
4	RH at fo (%)	14	t: RH_{start} to fo (s)
5	dT_a/dt at fo (°C/s)	15	t: RH_{start} to RH_{end} (s)
6	dRH/dt at fo (%/s)	16	t: RH_{knee} to fo (s)
7	dV/dt, V_{start} to V_{settle} (V/s)	17	t: RH_{knee} to RH_{end} (s)
8	dRH/dt, RH_{start} to RH_{knee}(%/s)	18	RH smoothness
9	t: V_{settle} to RH_{start} (s)	19	RH at start (%)
10	t: V_{settle} to RH_{knee} (s)		

After measuring these values off of the data sheet and tabulating them into Excel spreadsheets, all pair permutations of the parameters were regressed against each other via linear regression in "R" statistics software, and a correlation coefficient was calculated for each pairing. Regression the 19 variables against each other leads to 190 permutations. One regression that raises interest is displayed in Figure 4.2, which shows the regression of

Table 4.2: Summary Statistics for B01 - B09 Cases Variable List

Variable No.	Mean	Std. Dev.	Max.	Min.
1	-303.8	17.01	-270.6	-324.8
2	-224.9	164.1	-25.00	-400.0
3	23.85	1.303	25.48	22.30
4	92.94	9.863	98.60	67.11
5	0.003	0.001	0.005	0.0
6	0.017	0.024	0.077	0.001
7	-8.042	3.246	-1.451	-11.72
8	0.053	0.010	0.068	0.028
9	251.0	120.7	494.9	15.00
10	1199	432.1	1600	121.8
11	1495	398.8	1997	839.2
12	2835	1906	5353	812.0
13	948.1	365.4	1330	106.8
14	1243	372.1	1709	548.4
15	2584	1910	5136	513.2
16	295.8	271.5	851.6	0.0
17	1636	1932	4061	0.0
18	0.001	0.001	0.005	0.0
19	32.56	7.866	48.62	24.77

the RH_{fo} onto the value of the derivative of ambient temperature at flashover dT_a/dt_{fo}. This regression clearly shows grouping or clustering of the types of experimental outcomes, with all of the PFO, FOw, and FFO distinctly together in groups along the dT_a/dt_{fo} axis, showing itself to be an indicator of flashover type. Further investigation of the regressions found an interesting discovery. It is well known that voltage level is well correlated with whether or not flashover will occur [4]. However, it was found that regressions of dT_a/dt_{fo} as a categorical indicator of type of flashover against relative humidity variables (Figures 4.3 - 4.6 produced regressions with significant p-values for the regression coefficient (Table 4.4) and seem to have a linear relationship with the type of flashover. Regression of dT_a/dt against voltage level did not have significant p-values for the regression coefficients, as indicated by Table 4.4, and thus seems to have no linear relationship with the type of flashover.

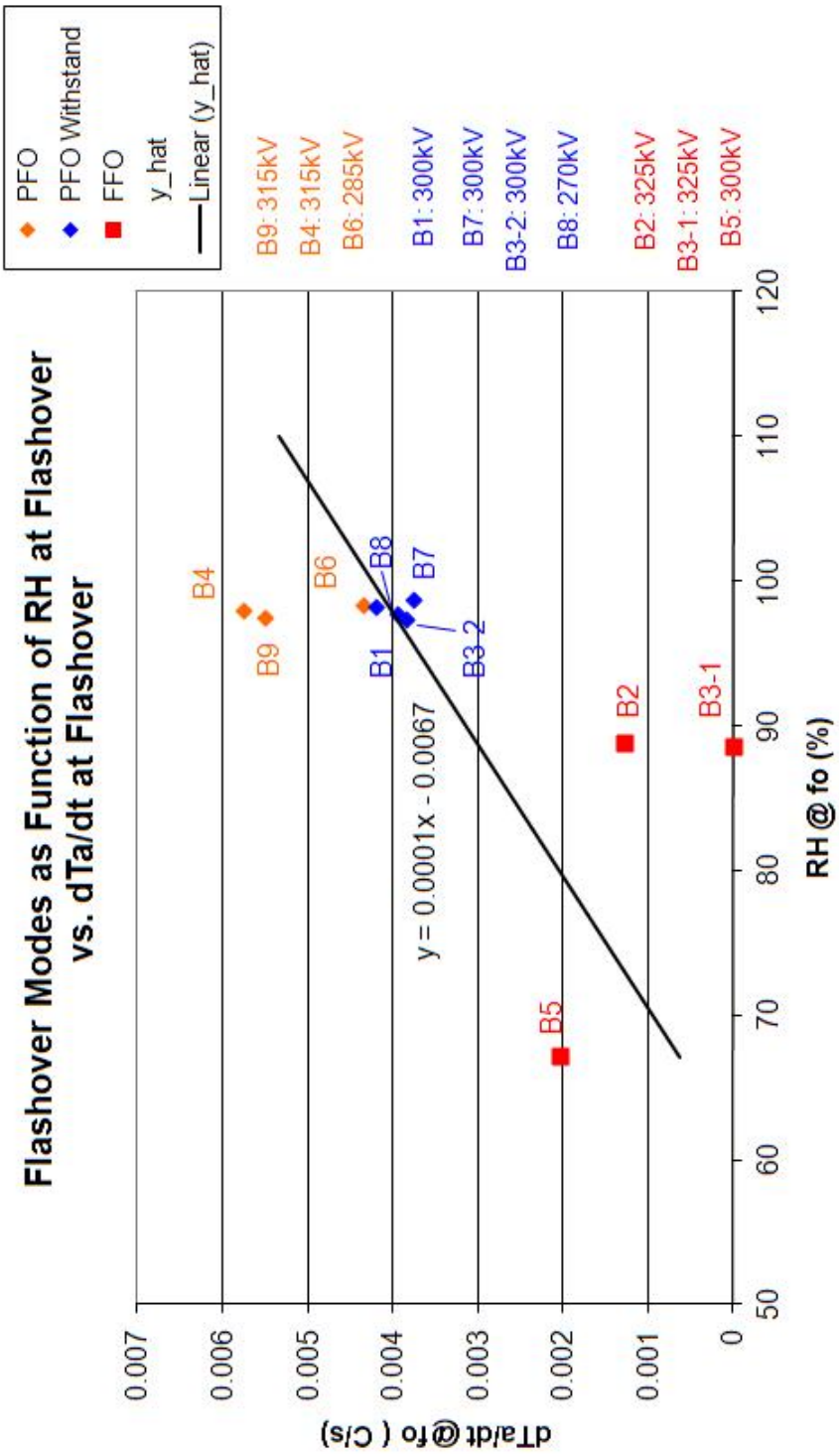

Figure 4.2: Regression of RH at fo onto dT/dt at fo.

Table 4.3: Coefficients Information for Regression of dT_a/dt onto the RH and V Variables in Figures 4.3 - 4.4

Variable	Coefficient	Estimate	Std. Error	t value	$P(>\|t\|)$	
RH_{fo}	β_0	-6.7e-03	4.9e-03	-1.36	0.21	
	β_1	1.1e-04	5.2e-05	2.07	0.07	*
dRH/dt_{fo}	β_0	4.3-03	5.6e-05	7.6	6.9e-05	*
	β_1	-4.9e-03	1.9e-02	-2.54	0.03	*
RH_{start}	β_0	-1.6e-03	2.0e-03	-0.77	0.45	
	β_1	1.5e-04	6.1e-05	2.54	0.03	*
V	β_0	1.4e-02	1.1e-02	1.31	0.22	
	β_1	3.5e-05	3.6e-05	0.98	0.35	

Table 4.4: Coefficients Information for Regression of I_{fo} onto the RH and V Variables in Figures 4.3 - 4.4

Variable	Coefficient	Estimate	Std. Error	t value	$P(>\|t\|)$	
RH_{fo}	β_0	-633	530	-1.19	0.26	
	β_1	4.39	5.67	0.77	0.46	
dRH/dt_{fo}	β_0	-182	63.46	-2.88	0.02	*
	β_1	-2438	2177	-1.12	0.29	
RH_{start}	β_0	-208	246	-0.84	0.42	
	β_1	-.49	7.37	-0.06	0.94	
V	β_0	2130	617	3.45	0.008	*
	β_1	7.753	2.03	3.18	0.005	*

Of additional fundamental interest is the correlation coefficients from these simple linear regressions. As many of the regressions in the 190 pairs were non-linearly related, a non-parametric correlation coefficient called Kendall-Tau which has no requirement of linearity or distribution type was used to measure the level of independence or degree of association between the pairs. The Kendall-Tau correlation coefficients were generated in "R" and are tabulated in Figure 4.5.

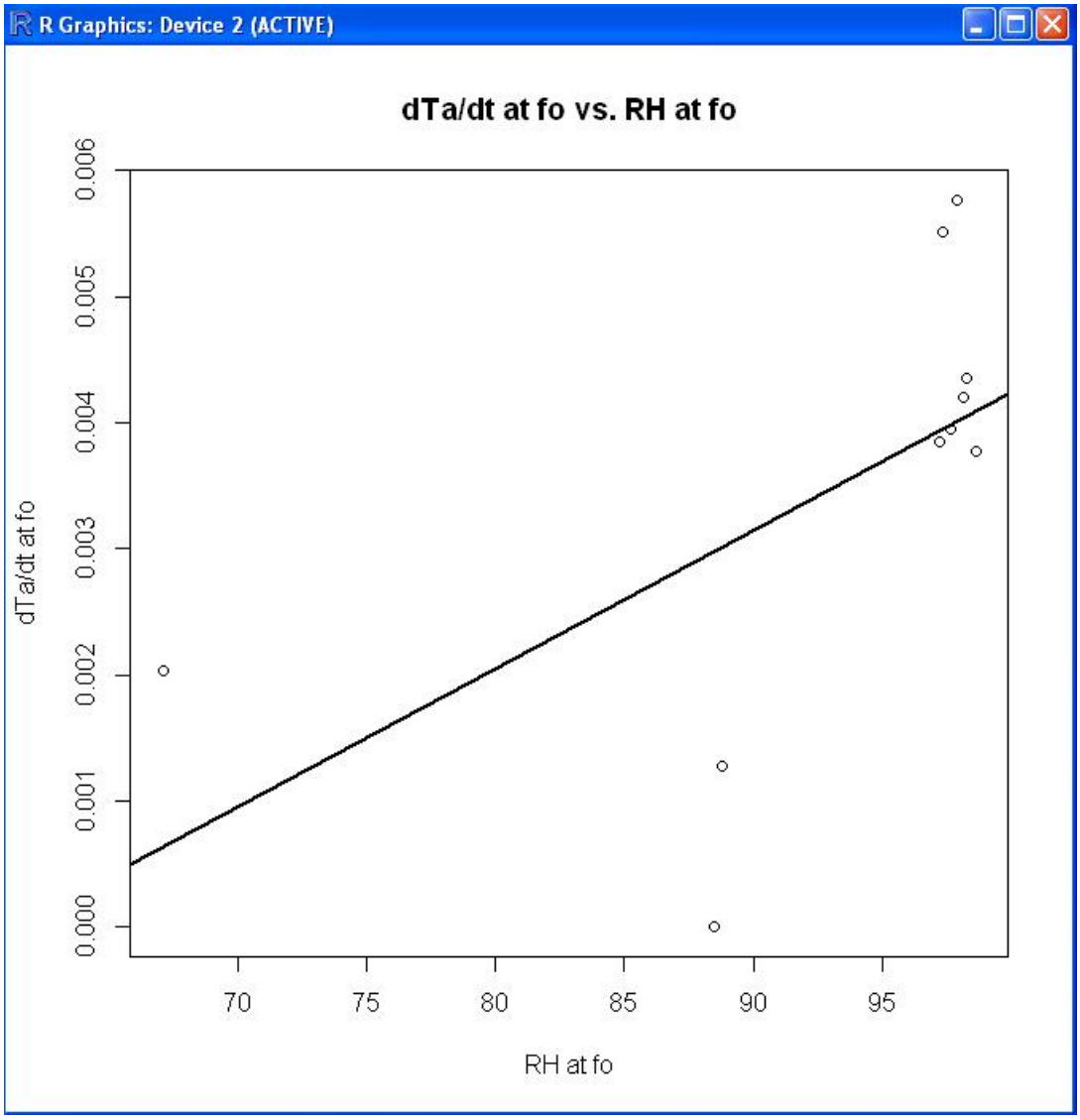

Figure 4.3: Regression in "R" of RH at fo onto dT/dt at fo.

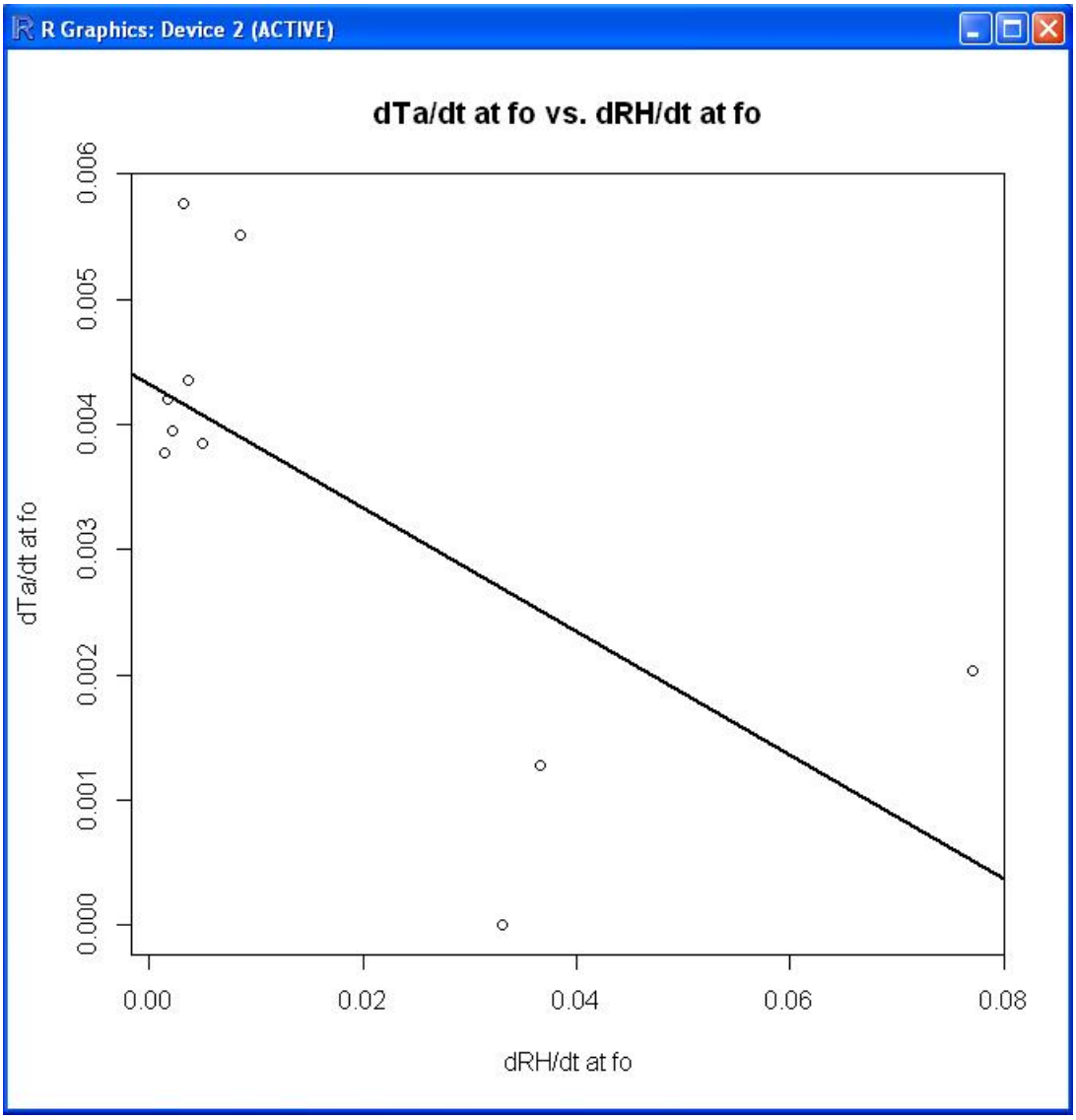

Figure 4.4: Regression in "R" of of dRH/dt at fo onto dT/dt at fo.

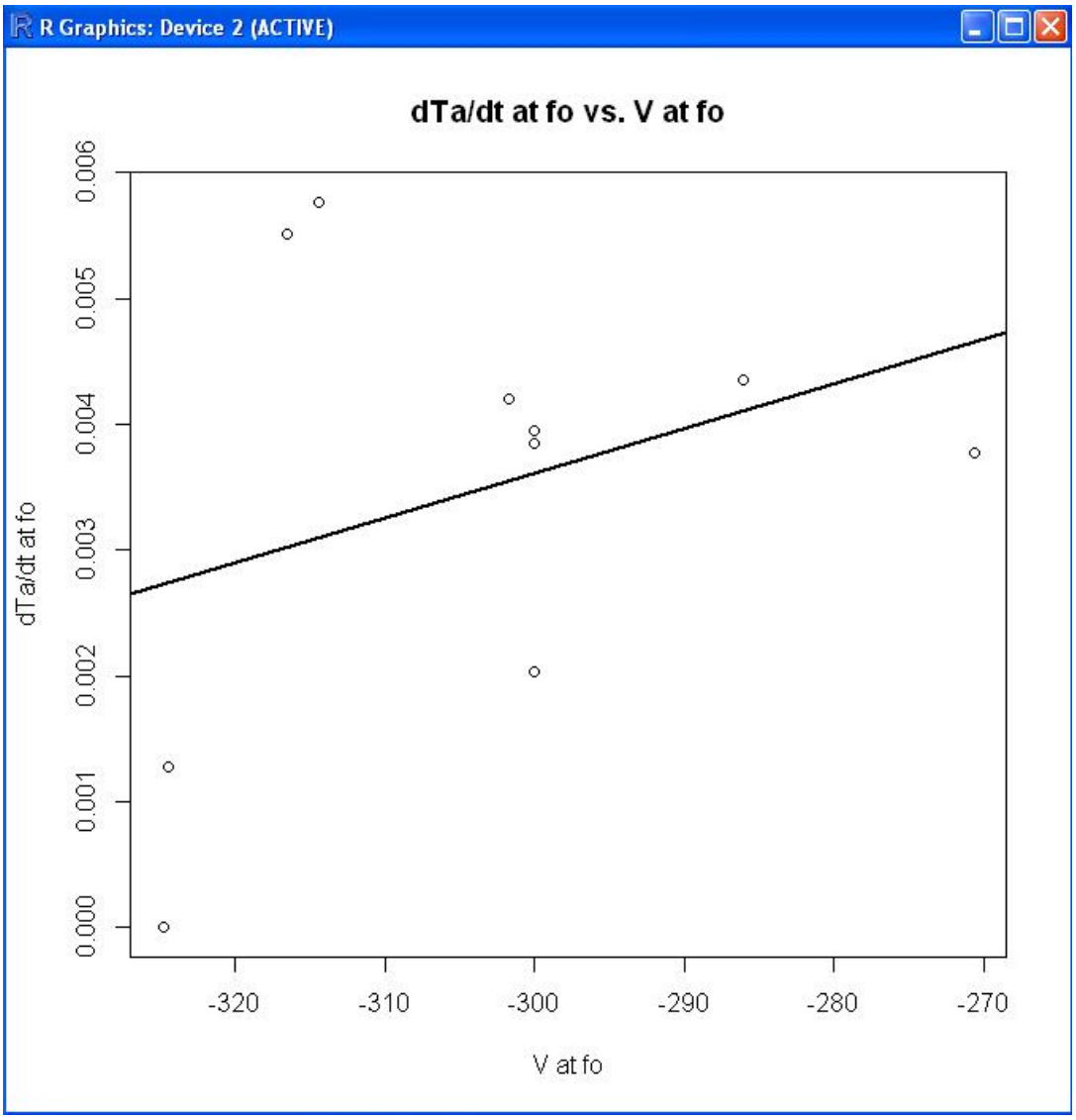

Figure 4.5: Regression in "R" of of dRH/dt at fo onto V.

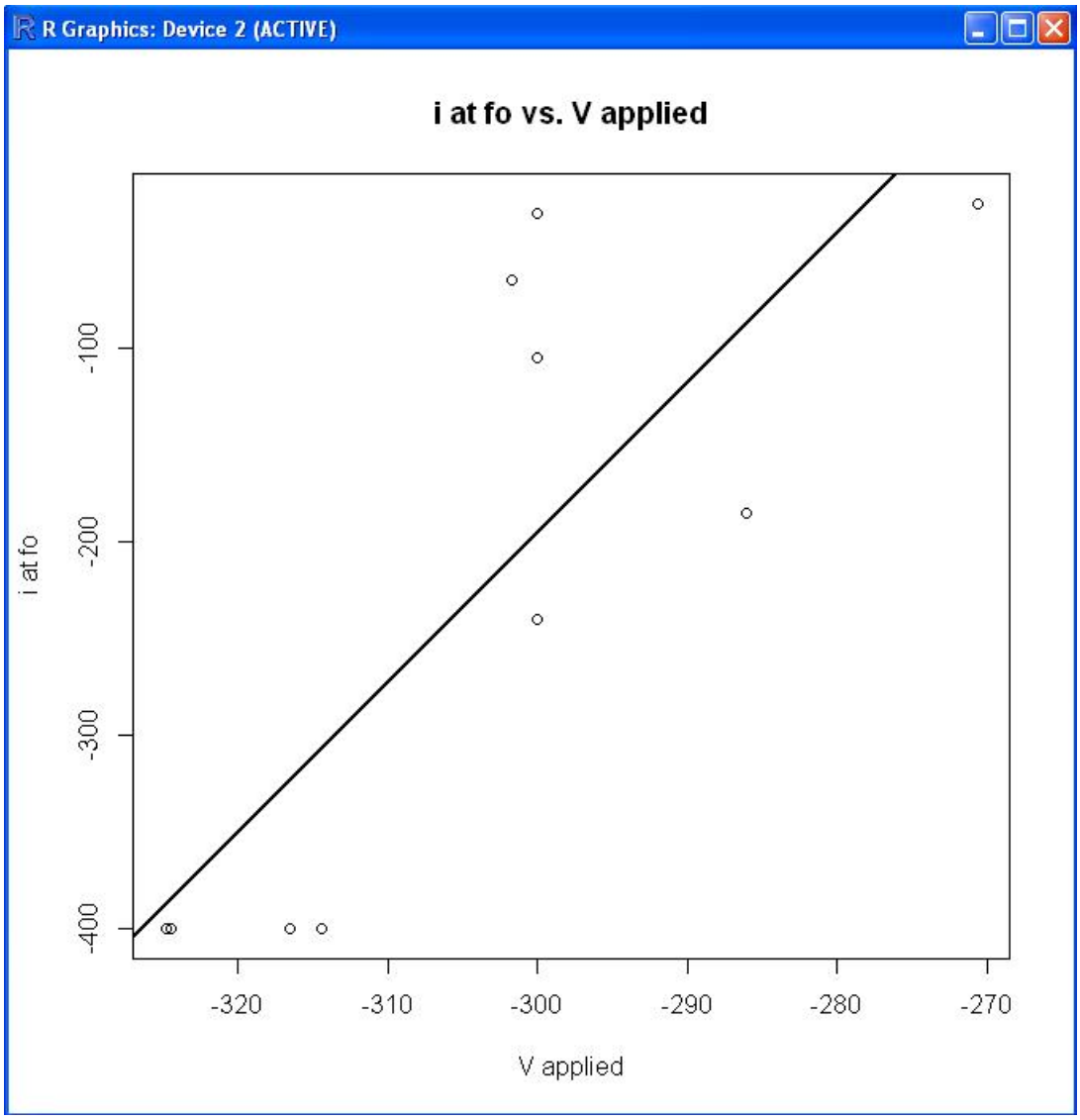

Figure 4.6: Regression in "R" of of I at fo onto V.

	V00	V01	V02	V03	V04	V05	V06	V07	V08	V09	V10	V11	V12	V13	V14	V15	V16	V17	V18	V19
V00	10	-4	-8	-5	-4	0	6	1	4	3	0	-2	-7	1	-2	-7	-6	-8	-1	-1
V01	-4	10	6	5	5	1	-4	1	-5	-2	0	2	5	0	3	4	6	5	-2	2
V02	-8	6	10	4	4	-1	-5	-1	-4	-4	-1	2	6	-1	2	6	6	8	0	1
V03	-5	5	4	10	7	4	-7	1	-5	0	5	7	6	4	6	6	7	6	0	4
V04	-4	5	4	7	10	4	-7	1	-6	-2	3	6	6	5	6	6	5	6	3	4
V05	0	1	-1	4	4	10	-2	6	-2	0	2	2	0	4	2	1	2	1	-2	5
V06	6	-4	-5	-7	-7	-2	10	-1	5	2	-2	-5	-7	-2	-5	-7	-6	-8	-4	-4
V07	1	1	-1	1	1	6	-1	10	1	1	0	0	-2	1	-1	-1	-1	0	-3	3
V08	4	-5	-4	-5	-6	-2	5	1	10	5	-2	-4	-5	-2	-6	-5	-8	-6	1	-1
V09	3	-2	-4	0	-2	0	2	1	5	10	1	-1	-4	-1	-2	-4	-3	-4	-1	2
V10	0	0	-1	5	3	2	-2	0	-2	1	10	8	4	8	6	3	2	1	2	2
V11	-2	2	2	7	6	2	-5	0	-4	-1	8	10	6	7	8	6	4	4	3	3
V12	-7	5	6	6	6	0	-7	-2	-5	-4	4	6	10	3	6	10	6	8	2	2
V13	1	0	-1	4	5	4	-2	1	-2	-1	8	7	3	10	7	3	1	1	2	2
V14	-2	3	2	6	6	2	-5	-1	-6	-2	6	8	6	7	10	6	4	4	3	3
V15	-7	4	6	6	6	1	-7	-1	-5	-4	3	6	10	3	6	10	6	8	3	2
V16	-6	6	6	7	5	2	-6	-1	-8	-3	2	4	6	1	4	6	10	8	-1	2
V17	-8	5	8	6	6	1	-8	0	-6	-4	1	4	8	1	4	8	8	10	1	3
V18	-1	-2	0	0	3	-2	-4	-3	1	-1	2	3	2	2	3	3	-1	1	10	1
V19	-1	2	1	4	4	5	-4	3	-1	2	2	3	2	2	3	2	2	3	1	10

Table 4.5: Kendall-Tau Correlation Coefficients for all Pairs of Variables.

For a sample size of n=10, we look up the Kendall-Tau coefficient from the tables in Daniel [42] and obtain a $\tau^* = 0.511$. For a Kendall Tau coefficient greater than 0.511, we reject the null hypothesis that the two variables are independent, and state that they are dependent. Hence, to reduce down our variable set desiring independent variables with a minimum of overlapping capacity to explain the variation in the dependent type of flashover variable, we drop variables resulting in Kendall Tau coefficients in combination with other variables greater than 0.511.

The Kendall-Tau correlation coefficients in Figure 4.5 were generated, multiplied by 10, and rounded in order to easily work with integers. Values greater than 5.11 (0.511 x 10) have been color coded in red to highlight variables with large correlations. It is evident from the chart that the voltage at flashover (V01) overall exhibits small correlations with the other variables, as the top row of the chart displays lower correlations between voltage at flashover and most of the other variables. An examination of the chart allows the same to be said for dV/dt from V_{start} to $V_{settled}$ (V07), dRH/dt from RH_{start} to RH_{knee} (V08), the time intervals from $V_{settled}$ to RH_{start} (V09) and from RH_{start} to RH_{knee} (V13), and for the RH value at start (V19) and the variable measuring the smoothness of the RH curve (V18).

Worthwhile to note from this chart is the correlation coefficients of the parameters involving voltage (V01) to the flashover outcome (V05), and comparing these with parameters involving relative humidity to the flashover outcome. A low correlation coefficient of 1 is observed for voltage at flashover V (V01) vs. the rate of change of ambient temperature at flashover dT_a/dt_{fo} (V05) which is correlated to the type of flashover, shown in Figure 4.2. Comparing the correlation between dT_a/dt_{fo} (V05) and the controllable RH variables such as the RH_{start} or V19 (having a value of 5), or the dRH/dt from RH_{start} to RH_{knee}

or V08 (-2), it would suggest that relative humidity has a stronger association with the type of flashover outcome than the voltage has.

After this preliminary examination, a variable reduction was done to reduce the data set down to variables independent of one another. The first variables that were removed are those that are not controllable by the experimenter and are derived from the outcome of the experiment, such as the current, RH at flashover, ambient temperature (due to heating from arcing on the insulating surface during the experiment), and its derivative dT_a/dt at flashover (variables 2, 3, 4, and 5 respectively, listed in Table 4.1).

Other non-controllable variables taken out are the time intervals up to the flashover (variables 11, 14, and 16) as it is not known when flashover will occur, and thus are also not controllable, and the time intervals to the end of the experiment encoded in variables 12, 15, and 17 (time intervals of V_{settle} to RH_{end}, RH_{start} to RH_{end}, and RH_{knee} to RH_{end})., which do not describe any intrinsic properties of the experiment. Significant correlations are observed between variables 4 and 6 (RH and dRH/dt at flashover) allowing removal of 6 as well as being another variable at flashover, and the correlation between 10 and 13 (time intervals of V_{settle} to RH_{knee} and RH_{start} to RH_{knee}), allowing for removal of 10, as the time interval of 10 can be described by both 9 and 13 as seen in Figure 4.1. Most of these variable combinations are removed as they together appear to be all a function of the shape of the relative humidity response curve, which is determined by the time the steam nozzles are turned on, by how much, and the amount of relative humidity already present at the beginning of the experiment. These controllable properties are described by the variables 9, 8 and 13, and 19 respectively (the time interval from V_{settle} to RH_{start}, dRH/dt from RH_{start} to RH_{knee} and the time interval from V_{settle} to RH_{start}, and the level of RH_{start}). After removing the "excess" variables that individually contribute little

	V01	V06	V07	V08	V09	V13	V18	V19
V01	10	-4	1	-5	-2	0	-2	2
V06	-4	10	-1	5	2	-2	-4	-4
V07	1	-1	10	1	1	1	-3	3
V08	-5	5	1	10	5	-2	1	-1
V09	-2	2	1	5	10	-1	-1	2
V13	0	-2	1	-2	-1	10	2	2
V18	-2	-4	-3	1	-1	2	10	1
V19	2	-4	3	-1	2	2	1	10

Table 4.6: Kendall-Tau Correlation Matrix for Final Reduced Variable Set.

additional explanation to the variation in the dependent variable, a correlation matrix is generated for the remaining variables and is shown in Figure 4.6.

4.2 Fast Flashover as a Distinct Type of Discharge

The next statistical analysis carried out was to investigate whether or not the data statistically supported the proposition that the fast flashover is indeed another type or mode of flashover and not just a pollution flashover, (i.e. that it is of a different statistical distribution). Due to low sample sizes, we use two parametric tests. Although exhibiting low statistical confidence, they are simple to carry out, and make no assumption on the underlying population distribution for the fast flashover, which we have no information on. The non-parametric tests we use to allow for testing for different population means with low sample sizes are the Mann-Whitney test, and the Mood test for dispersion.

The Mann-Whitney test is employed to examine whether the fast flashover tests derive from a different statistical distribution than the pollution flashovers is the Mann-Whitney test [42]. In this test, the two sets of sample values from the fast flashover (n_f) and pollution flashover (n_p) data are combined into a single sample of size $n = n_f + n_p$. All of the observations are ranked together keeping track of their origin populations, and a T

statistic is calculated from the sum of the ranks of observations from the fast flashovers.

The expression for calculating the T statistic is

$$T = S - \frac{n_f\,(n_f + 1)}{2}, \tag{4.2}$$

where S is the sum of the ranks in the fast flashover sample. The T statistic is then compared to a value in a table listing critical values for the Mann-Whitney test [43]. We then test if the populations are different vs. the populations are the same by the test H_0: $m_f = m_p$ vs. H_a: $m_f \neq m_p$, where m_f and m_p are the medians of the fast flashover and pollution flashover populations respectively. For a sample size of n=6, the critical value is T $>$ 8 if $\alpha/2 = 0.05$. This is associated with a low confidence level (90%) due to a low sample size, but it is the only level of confidence that allows us to ever reject the null hypothesis if it occurs with $n_f = n_p = 3$. The results for applying the Mann-Whitney test to the 2004 IREQ data is listed in Table 4.7 with a rejection of the null hypothesis indicated as $^*\mathrm{H}_a$. Only two variables reject the null hypothesis in the Mann-Whitney test, giving minor support (but support nonetheless) to the proposition that the fast flashover is distinct from the breakdown mode of pollution flashover. It is worth noting that both of the variables that support this proposition are relative humidity variables, possibly indicative that relative humidity is more correlated with the type of flashover then voltage.

A final non-parametric test employed to examine the statistical distinctiveness of the fast flashover observations from pollution flashover phenomenon is the Mood test. This test examines if any difference exists between the dispersion in the fast flashover data and the dispersion in the pollution flashover data, and whether or not that difference is statistically significant [42]. As we are testing for a difference and have no knowledge of whether the dispersion of the fast flashover population σ_f should be greater or less than

Table 4.7: Mann-Whitney Test for H_o:$m_f = m_p$ vs. H_a:$m_f \neq m_p$

Variable	M-W T-stat.	Test Result ($\alpha/2 = 0.05$)
V level	7	H_o
dV/dt from V_{start} -V_{settle}	6	H_o
dRH/dt, RH_{start} - RH_{knee}	9	$^*H_a$
t: V_{settle} - RH_{start}	6	H_o
t: RH_{start} - RH_{knee}	7	H_o
RH smoothness	5	H_o
RH at start	9	$^*H_a$

the dispersion of the pollution flashover population σ_p, we have to test the null hypothesis H_o: $\sigma_f = \sigma_p$ against the alternate hypothesis H_a: $\sigma_f \neq \sigma_p$.

The Mood test is performed by combining the values of both the fast flashover and pollution flashover data into one set, ordering them, and ranking the combined sample keeping track of which population the observations came from. Each rank value from the fast flashover data r_f is then used to calculate a test statistic M value from the expression

$$M = \sum_{i=1}^{n_f} \left(r_{fi} - \frac{n+1}{2} \right)^2, \tag{4.3}$$

where $n = n_f + n_p$.

The results of the Mood dispersion test for the IREQ data is given in Table 4.8. A value less than M=2.75 or greater than M=14.75 rejects the null hypothesis in a two sided test at $\alpha/2 = 0.05$ for $n_f = n_p = 3$ [44].

From the non-parametric tests, some statistically significant evidence is obtained for the proposition that the fast flashover is distinct and is derived from a population other than the pollution flashover. However, the confidence in these tests is low due to the constraint of a small sample size.

Table 4.8: Mood Test for H_o:$\sigma_f = \sigma_p$ vs. H_a:$\sigma_f \neq \sigma_p$

Variable	M value	Test Result ($\alpha/2 = 0.05$)
V level	10.75	H_o
dV/dt from V_{start} - V_{settle}	14.75	$^*H_a$
dRH/dt, RH_{start} - RH_{knee}	8.75	H_o
t: V_{settle} - RH_{start}	2.75	$^*H_a$
t: RH_{start} - RH_{knee}	6.75	H_o
RH smoothness	12.75	H_o
RH at start	8.75	H_o

4.3 Summary and Conclusion of Statistical Analysis

Small sample sizes introduce many difficulties into the statistical analysis of data. An ideal tool for this phenomenon would be a multiple linear analysis due to many independent variables influencing the outcome of the dependent type of flashover variable. However, the linearity of the relationship can not be guaranteed with such a small sample size. Another difficulty encountered is that with a new phenomena such as fast flashover and very few observations, no knowledge is possible on the distribution of the variables characterizing this type of flashover. This further restricts our analysis. However, a few relative humidity linear regressions were shown to have a significant p-value for the regression coefficient whereas voltage did not, appearing to indicate that relative humidity had more linear influence than voltage on the dependent variable indicating type of flashover. With the low sample size, we can not be completely confident in this, and only use it as an indicator. Statistical methods such as non-parametric methods which have no dependency on linearity nor distribution type show that the relative humidity rather than voltage is more correlated with the type of flashover outcome. In addition, non-parametric methods appear to indicate that fast flashover is a mode of flashover distinct from pollution flashover,

but with low statistical confidence due to low sample sizes.

Chapter 5

Computational Algorithm for Pollution Flashover, Simulation Results, and Discussion

It has been shown there is support for fast flashover being distinct from the pollution flashover mechanism, and that levels, derivatives, and time intervals involving relative humidity are more correlated with the type of flashover outcome than the level of applied voltage. With the fact that the only criteria for the fast flashover is the absence of leakage current, it is desired to find another criteria in an effort to further distinguish fast flashover from pollution flashover.

An examination of the pollution flashover critical voltage equation as a criteria for flashover shows that only the resistance per unit length r_p can vary during the experiment

$$V_{c,\,50\%}\,(t) = A^{\frac{1}{n+1}} r_p\,(t)^{\frac{n}{n+1}}\,L. \tag{5.1}$$

If we could make a link between r_p and relative humidity that correlates with the type of flashover, we would be able to add another criteria to our tool kit to analyse fast flashover. Many of the relationships found in the literature review of thermodynamic mass transfer concepts and equations can be used to assemble a computational model to represent pollution flashover as a function of relative humidity in a time-stepping manner. Assembly of this model is done with the goal of using the model to observe the critical voltage for pollution flashover being satisfied in the pollution flashover cases as expected, but not satisfied in the fast-flashover cases. It is also desired to gain insight into the fast-flashover process by exploring for differences between the two cases in the values of the underlying variables residing within the equations presented in Chapter 2.

5.1 Construction of a Pollution Flashover Computational Algorithm

The assembly of an algorithm is started with the criteria equation for pollution flashover

$$V_{c,\,50\%}\,(t) = A^{\frac{1}{n+1}} r_p\,(t)^{\frac{n}{n+1}}\,L, \tag{5.2}$$

with $V_{c,\,50\%}(t)$, L, A, and n previously discussed.

The resistance per unit length $r_p(t)$ by definition equals the total resistance divided by length of the moist pollution layer

$$r_p\,(t) = \frac{R_p\,(t)}{L - x\,(t)}, \tag{5.3}$$

where $x\,(t)$ is the length of the dry banded area where the arc bridges the surface, and

$L - x(t)$ is the length of the remaining moist pollution layer that has not been bridged by arcing and is in the process of drying out from the current. The total resistance $R_p(t)$ is obtained from the standard function of the resistivity of the pollution layer $\rho_p(t)$

$$R_p(t) = \frac{\rho_p(t)(L - x(t))}{A^{r\varphi}_{H_2O}(t)}, \tag{5.4}$$

with $A^{r\varphi}_{H_2O}(t)$ the cross-sectional area of the pollution layer the current is passing through [27].

The required cross-sectional area as well as the pollution layer surface area and depth are illustrated in the geometrical description in Figure 5.1. The cross-sectional area is found from the equation

$$A^{r\varphi}_{H_2O}(t) = \frac{Vol_{H_2O}(t)}{L - x(t)}, \tag{5.5}$$

or constructed from the radii of the hot stick and the water level

$$A^{r\varphi}_{H_2O}(t) = \pi r_w(t)^2 - \pi r_{hs}^2, \tag{5.6}$$

with $r_w(t)^2$ and r_{hs}^2 the squares of the radial distances to the hot stick surface and the water surface respectfully. $r_w(t)^2$ is obtained from the volume of water on the surface calculatted each iteration

$$r_w(t) = \sqrt{\frac{Vol_{H_2O}(t)}{\pi(L - x(t))} + r_{hs}(t)^2}, \tag{5.7}$$

With $r_w(t)$ calculated, we can now obtain the depth of the surface solution

$$d_{H_2O}(t) = r_w(t) - r_{hs}, \tag{5.8}$$

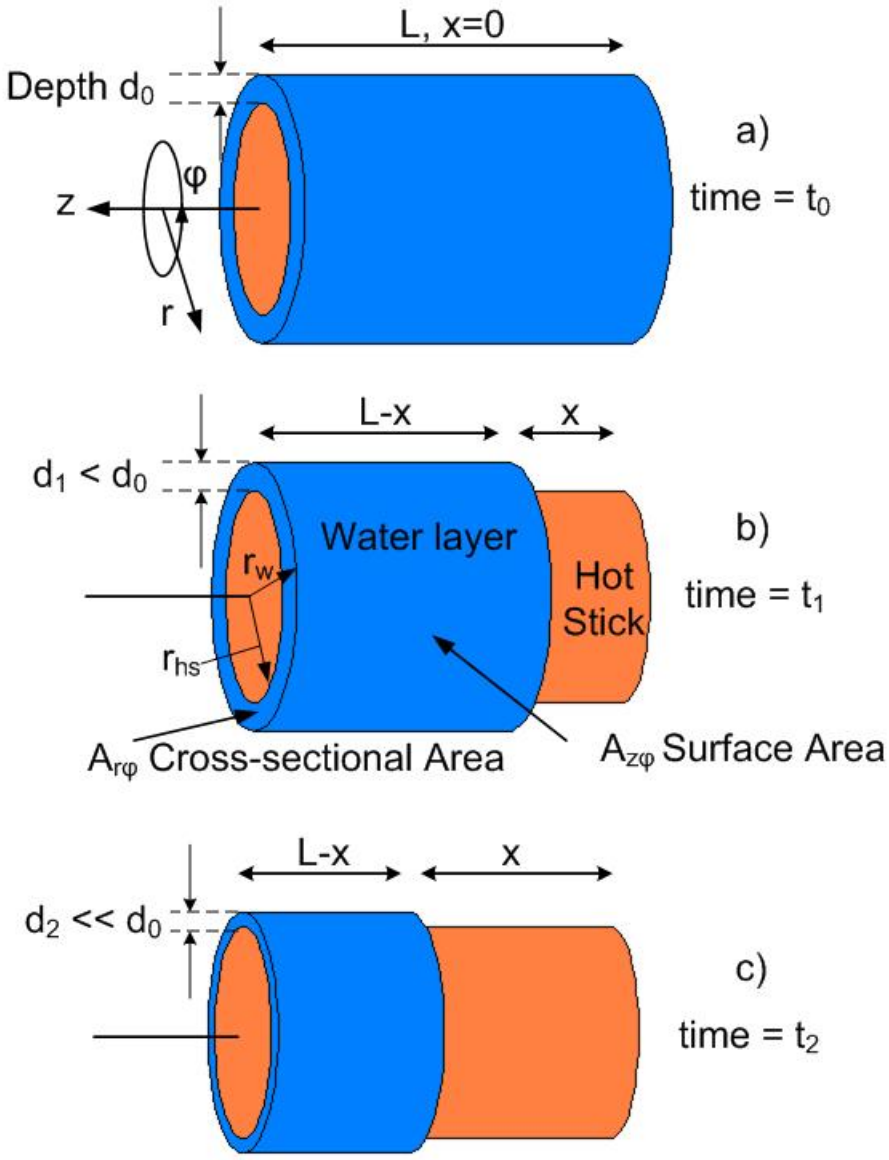

Figure 5.1: Equivalent Water Layer on Hot Stick.

and the solution surface area

$$A_{H_2O}^{z\varphi} = 2\pi r_w(t)\left(L - x(t)\right). \tag{5.9}$$

The final discussion point is in regard to the removal of water. The surface can be treated as uniformly polluted, with water being removed or added equally over the entire surface. Drybanding is implied as being implicitly occurring according to uniform drop in volume over the whole surface. Another more involved approach involves proportional factors that would fraction the drop in water volume between the reduction in depth and length proportionate to the non-uniformity of the pollution layer, as illustrated in moving from t_0 to t_1 to t_2 in Figure 5.1.

The above mathematical relationships are basic and obtainable from any introductory physics textbook. The development of a model to link relative humidity to changes in the pollution resistance per unit length requires three relationships to be build between the chain of variables that must be calculated, as illustrated in Figure 5.2. These are: 1, a mathematical expression relating relative humidity to the volume of water on the pollution surface; 2, an expression to derive the surface water temperature as a function of the Joule heating minus the convection losses due to the surface current and ambient temperature respectively; and 3, the relationship for the resistivity as a function of the concentration of salt or salt equivalent on the surface and the surface temperature.

The first relationship that must be addressed is between the relative humidity and the surface water volume (1). This is represented in part by the HKS Equation 2.18

$$\left(\frac{dM}{dt}\right)_t' = \left[\kappa_c \frac{P_{H_2O(v)}(t)}{\sqrt{T_{H_2O(v)}(t)}} - \kappa_e \frac{P_{H_2O(l)}(t)}{\sqrt{T_{H_2O(l)}(t)}}\right]\sqrt{\frac{m_{H_2O}}{2\pi R}}, \tag{2.18}$$

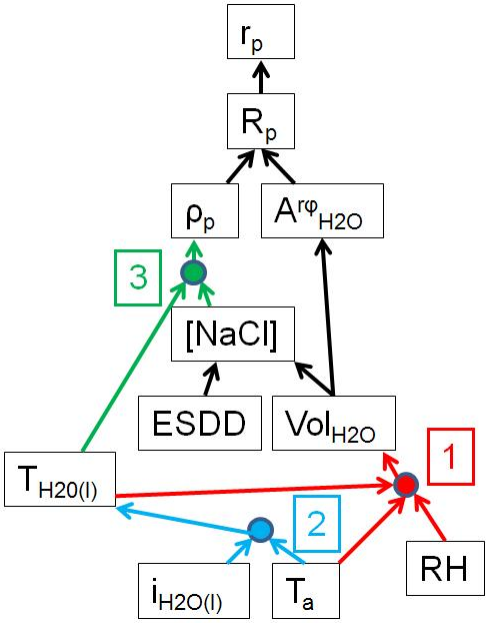

Figure 5.2: Relationships Between Variables and Required Connecting Equations 1-3 in Critical Voltage Time-Stepping Polution Flashover Model.

which would have to incorporate scaling constants for any change in mass flux due to the presence of the Kaolin, as its absorption activity will influence the ratio between the condensation/evaporation constants

$$\left(\frac{dM}{dt}\right)'_t = \left(\frac{dM}{dt}\right)^{(1)}_{Kaolin\ scale} \left[\kappa_c \frac{P_{H_2O(v)}(t)}{\sqrt{T_{H_2O(v)}(t)}} - \kappa_e \frac{P_{H_2O(l)}(t)}{\sqrt{T_{H_2O(l)}(t)}}\right] \sqrt{\frac{m_{H_2O}}{2\pi R}}, \tag{5.10}$$

with all of the same parameters and expressions for their evaluation as defined and expressed in Chapter 2. Taking into account mass water transfer when the surface water reaches 100°C and boils off of the surface

$$\left(\frac{dM}{dt}_{boil}\right)_t = \left(\frac{dM}{dt}\right)^{(2)}_{Kaolin\ scale} \frac{P(t)}{A^{z\varphi}_{H_2O}(t)\,\Delta H(t)}, \tag{5.11}$$

and summing the effect of the two water mass transfers

$$\left(\frac{dM}{dt}\right)_t = \left(\frac{dM}{dt}\right)'_t + \left(\frac{dM}{dt}_{boil}\right)_t, \tag{5.12}$$

we can now obtain an expression for the increase in the volume of water with each time step of the computer model, given as

$$Vol_{H_2O}(t) = Vol_{H_2O}(t-1) + \frac{A^{z\varphi}_{H_2O}(t)\,\Delta t}{1000}\left(\frac{dM}{dt}\right)_{t-1}, \tag{5.13}$$

where the rate of water mass flux $(dM/dt)_t$ is in kg/s. As the water volume is in m^3, we have to divide the kg of water (dm^3) by 1000 to get the amount in m^3 per square meter of surface, and then multiply by the surface area $A^{z\varphi}_{H2O}$ to get the total water mass transfer to or from the surface.

The second of the three relationships illustrated in Figure 5.2 to be incorporated into the model is an expression for the change in pollution layer water surface temperature. As illustrated in Chapter 2, a formula was derived for the surface saline water temperature change from the energy balance equation using the individual changes in energy from Joule heating, convection cooling, and total energy change, reproduced here as

$$m(t)\,c_p(t)\left(\frac{dT_{H_2O(l)}}{dt}\right)_t = i^2(t)\,R_p(t) - h(t)\,A^{z\varphi}_{H_2O}(t)\left(T_{H_2O(l)}(t) - T_a(t)\right). \tag{5.14}$$

which is further developed into what we require by dividing through by the mass and specific heat capacity to obtain an expression for the rate of change of temperature with respect to time for a wet saline surface simultaneously heated by Joule heating and cooled

by convection

$$\left(\frac{dT_{H_2O(l)}}{dt}\right)_t = \frac{i^2(t)\,R_p(t)}{m(t)\,c_p(t)} - \frac{h(t)\,A^{z\varphi}_{H_2O}(t)\left(T_{H_2O(l)}(t) - T_a(t)\right)}{m(t)\,c_p(t)}. \tag{5.15}$$

As with the final mass water transfer equation, we substitute this expression into a time stepping equation to calculate the current surface water temperature as a function of its value at the previous time step plus the rate of change of surface water temperature from the above equation to obtain

$$T_{H_2O(l)}(t) = T_{H_2O(l)}(t-1) + \left(\frac{dT_{H_2O(l)}}{dt}\right)_{t-1}\Delta t. \tag{5.16}$$

The final relationship to be put into the model is an equation to calculate the resistivity of the saline pollution layer $\rho_p(t)$ given the ESDD and surface water volume (both encompasing the salt concentration [NaCl]), and the surface water temperature $T_{H_2O(l)}$. The resistivity of the saline pollution layer $\rho_p(t)$ is calculated from the Hilchie equation as discussed in Chapter 2

$$\rho_p(t) = R1(t)\left\{\frac{T1_{\circ F} + x(t)}{T_{s^\circ F}(t) + x(t)}\right\}. \tag{2.15}$$

where $T1_{\circ F}$ and $x(t)$ are given by

$$T1_{\circ F} = \frac{9}{5}(50^\circ C) + 32 = 122^\circ F, \tag{5.17}$$

$$x(t) = 10^{-(0.340396\log_{10}[R1(t)] - 0.641427)}, \tag{5.18}$$

and R1 is the reference resistivity at the reference temperature $T1_{\circ F}$ lying on the specific [NaCl] concentration curve. This relationship is redisplayed in Figure 5.3 showing a solid

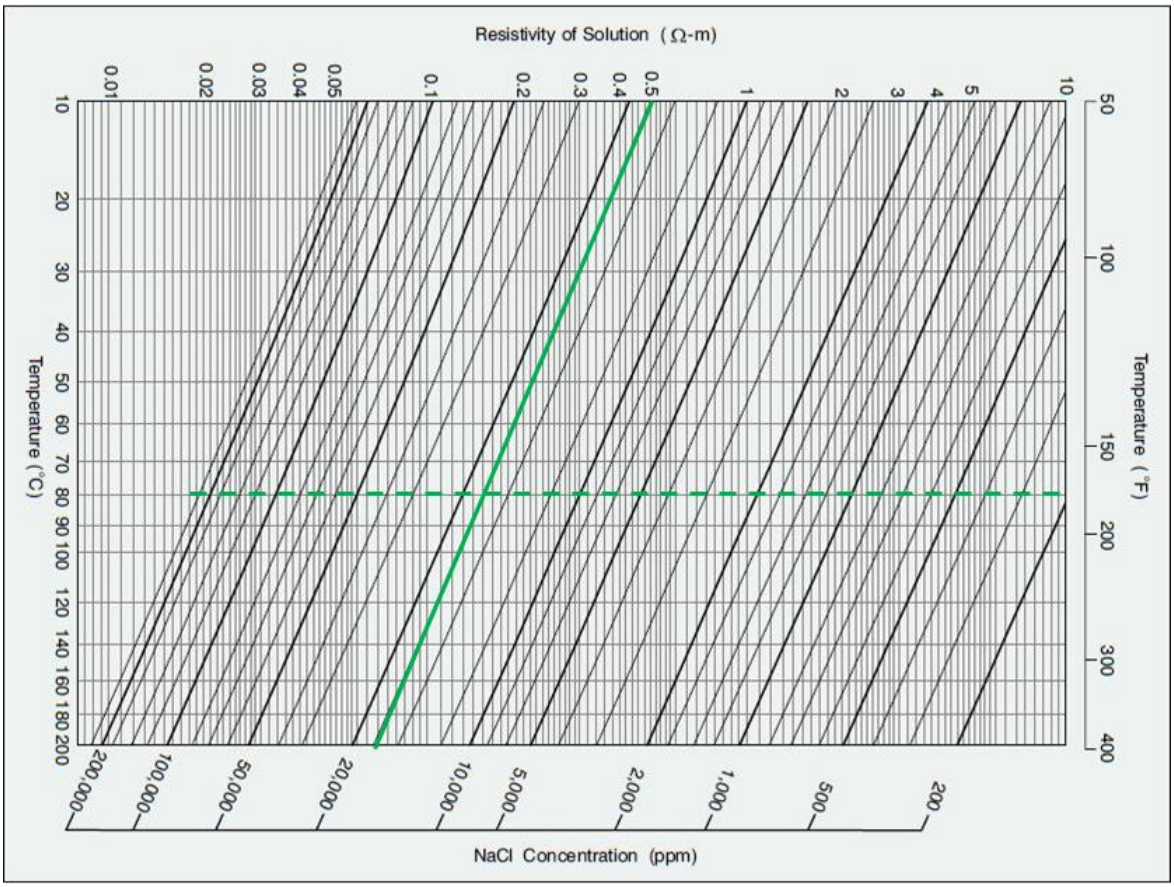

Figure 5.3: Relationship Between Resistivity, Water Temperature, and Salt Concentration [NaCl].

green line for constant salt concentration and a dashed green line for constant temperature.

In a computational model, we would want the program to be able to recalculate the resistivity at each time step with changes in surface volume water that take place by the equations previously discussed. Hence, to change the reference resistivity $R1(t)$, a curve was fit along the dashed green line in Figure 5.3 in order to calculate the reference resistivity $R1(t)$ for changes in $[NaCl(t)]$ This curve fit is given by the expression

$$R1\,(t) = \frac{R1'}{[NaCl\,(t)]}, \tag{5.19}$$

The resistivity is scaled through the numerator constant $R1'$ to obtain the expected total resistance with a Kaolin salt water pollution layer. This total resistance is another assumption required for the model, as surface resistivity measurements were not taken in the 2004 IREQ experiments. However, estimates can be gained from CIGRE monograph 158 - Polluted Insulators: A Review of Current Knowledge [12], and is discussed in the next section.

A flowchart summarizing all the calculations and their order is shown in Figure 5.4.

5.2 Parameter Settings

Out of the expressions that compose the model, values must be set for the empirical constants A and n in the critical voltage equation, the condensation and evaporation constants κ_c and κ_e from the Marek-Straub equation, the numerator constant $R1'$ from the equation for the reference resistivity, and the scale factors of equations (5.10) and (5.11)

Setting n is accomplished from the realization that approximately 2/3 of the surface is dry banded in the pollution flashover cases prior to flashover, and the largest arc (critical arc x_c) that can be seen without a flashover is

$$x_c = L/\left(1+n\right). \tag{2.8}$$

Rearranging equation 2.8 to obtain n results in

$$n = \frac{L}{x_c} - 1. \tag{5.20}$$

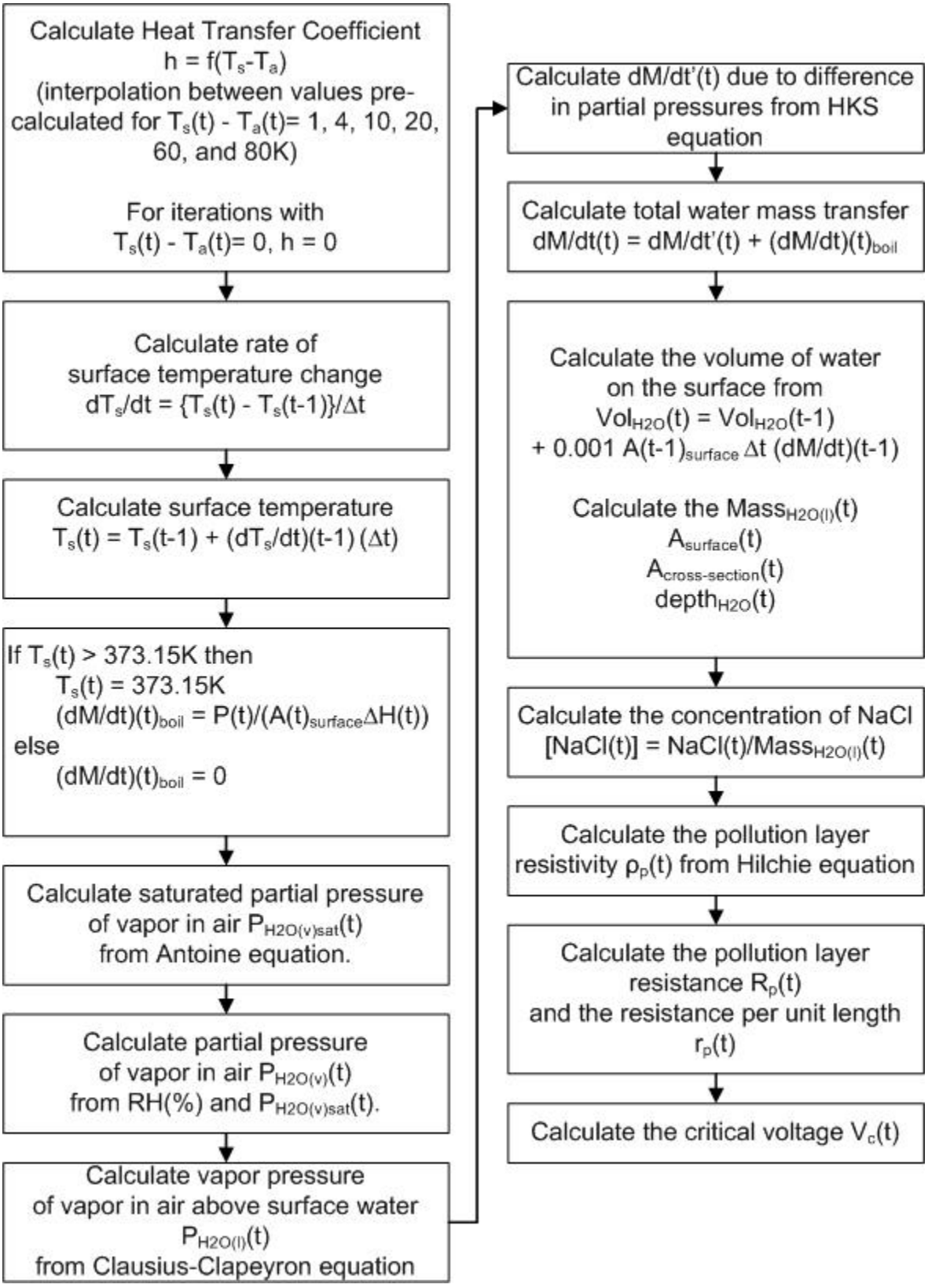

Figure 5.4: Summary Flowchart of Iterative Calculations for Pollution Flashover Algorithm.

Examining the video records of the two pollution flashovers B04 and B09, it was observed in B09 that just before flashover there was an arc discharge from the top electrode (assumed) down to a point on the hot stick that exceeded most other discharge lengths observed prior to flashover. The assumption had to be made with regard to the interpretation of the video record, as only half of the hot stick was recorded at any time in the IREQ experiments. In viewing all of the discharges throughout the entire series, discharges between glow points on the hot stick, and arc discharges from an end electrode to a point on the surface of the stick had specific audible signatures. Discharges between glow points on the hot stick had a characteristic "crackling" sound whereas long arc discharges gave off a "snap" sound. Using this audible signature and the excessive light flash coming from above the video frame top border, an assumption is made that the longest discharge viewed right before the flashover was originating from the top electrode. Four successive frames of the video record (with the flashover the last frame) are displayed in Figure 5.5.

To estimate the length of this longest arc before flashover, an assessment of the length of the remaining gap $L-x\,(t)$ on the hot stick in the video image is done by basic trigonometry. Knowing from the lab setup the height of the hot stick placement (5.7m from the floor to the bottom of the hot stick), the height of the camera (1.5m), and the distance from the camera to the axis of the hot stick (8.5m), a calculation can be made as to how much of the hot stick length is in view in the video frame. In examining the video archives, a video tilt was found to have been performed over the length of the hot stick prior to conducting experiment B08. Images from that tilt are shown in Figure 5.6 a,b with background ceiling rafter beams colored in blue to mark a reference position along the length of the stick.

Performing a trigonometric analysis using the law of sines (Figure 5.6c), the length of the hot stick in each view is found. The values for the analysis is in Table 5.1. It is found

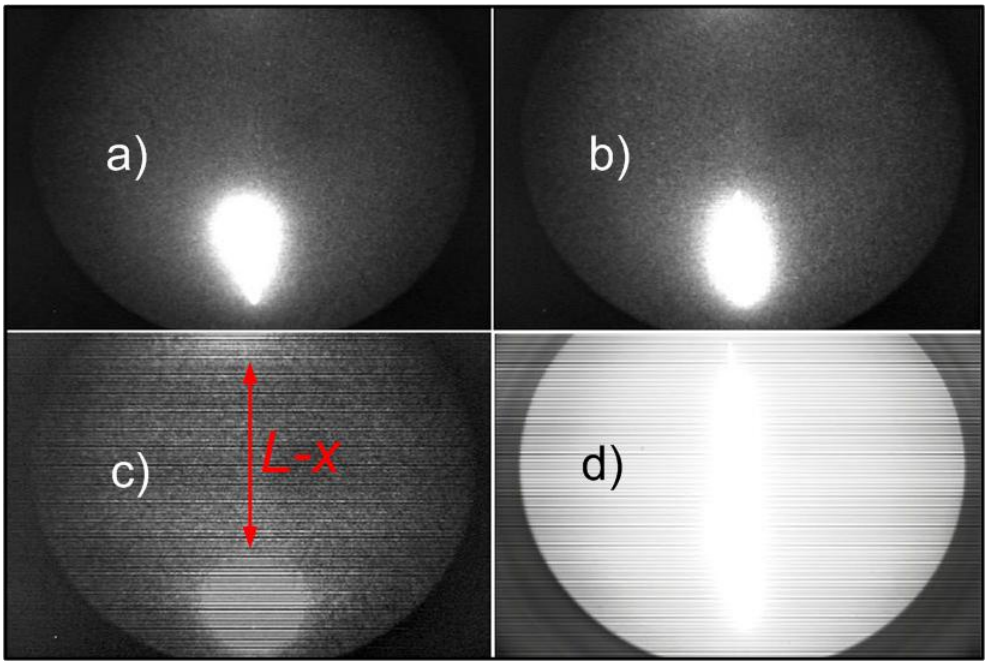

Figure 5.5: Longest Arc Discharge in B09 Prior to Pollution Flashover. Frames a-d in Sequence in Video Recording, with frame d final pollution flashover arc discharge. Video Images ©2004 Manitoba Hydro. Used by Permission.

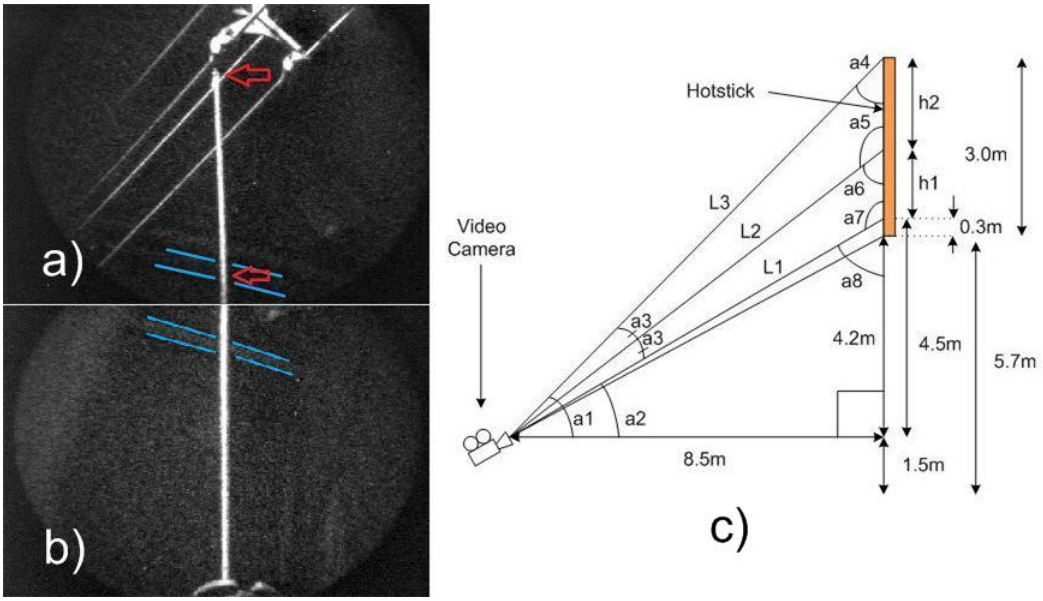

Figure 5.6: a, b: Top and bottom views of hot stick in video tilt. Background beam as reference for same position at midpoint along hot stick outlined in blue. c: Trigonometric analysis to determine hot stick lengths in top and bottom views. Video Images ©2004 Manitoba Hydro. Used by Permission.

Table 5.1: Angles and Lengths of Trigonometric Analysis of Camera View of Hot Stick

Angle	Angle Value (°)	Length	Length Value (m)
a1	40.27	L1	9.617
a2	27.90	L3	11.14
a3	6.18		
a4	49.73	h1	1.25
a5	124.08	h2	1.45
a6	55.92		
a7	117.90		
a8	62.10		

that the length of the hot stick in the bottom view is 1.25m and the length of the hot stick in the top view is 1.45m. Measuring the gap $L - x\,(t)$ at the point just before the flashover and averaging with various other long arcs not resulting in flashovers observed in B04 and B09, an average gap length of 0.95m was found, resulting in an average value for x_c of $L - (L - x_c)$ of 2.7-0.95 = 1.75m. This results in an x_c of about 1.75m/2.7m = 0.64 or about 65%, which is very close to the upper range of values observed x_c of 67% [45]. This results in a value for n of

$$n = \frac{L}{x_c} - 1 = \frac{2.7m}{1.75m} - 1 = 0.54. \tag{5.21}$$

Thus, using a value of n=0.5 corresponding to a 67% critical length ratio is justified.

Setting of κ_c, κ_e, and $\left(\frac{dM}{dt}\right)^{(1)}_{Kaolin\ scale}$ is governed by the amount of moisture we expect the surface to naturally accumulate due to Kaolin absorption with the surface at room temperature, and with no current heating up the moisture on the surface. The time response of water absorption is also required in order to assess at a specific relative humidity and temperature how fast the water absorption occurs. One of the most recent set of measurements on Kaolin absorption at different relative humidities and at a high relative

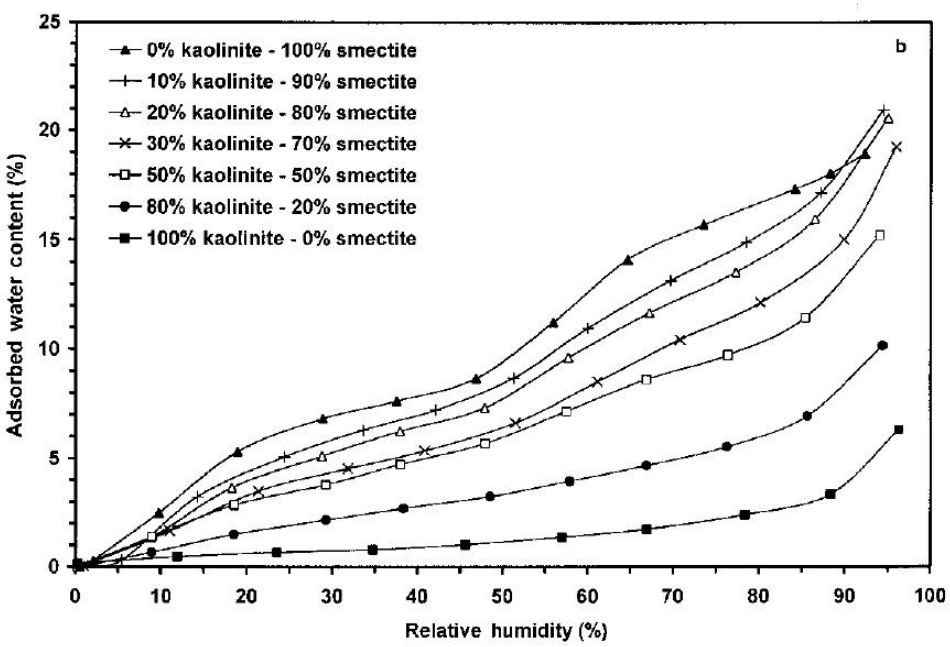

Figure 5.7: Absorbed Water Content of kaolinite as a Function of Relative Humidity. Bottom Curve for 100% kaolinite. Adopted from [11]. Used by Permission.

humidity over time was performed in 2002 by Likos and Lu [11]. The mass of water absorbed by Kaolin (mineral name kaolinite) at different relative humidities is observed in the bottom curve of Figure 5.7. These values for 100% kaolinite are summarized in Table 5.2.

Table 5.2: Kaolin Water Absorption for Different Values of Relative Humidity. Tabulated from Bottom Curve of Figure 5.7

RH (%)	Water (g/kg Kaolin)	RH (%)	Water (g/kg Kaolin)
10	4	60	15.5
20	6.5	70	19.5
30	8.0	80	26
40	10.0	90	40
50	15.5	95	60

Another item required is the time response of that absorption. Likos and Lu supply a time response water absorption curve for a 30% kaolinite - 70% smectite mixture, as seen in Figure 5.8. Exploding the first 25 hours of the plot into an enlarged view, it was

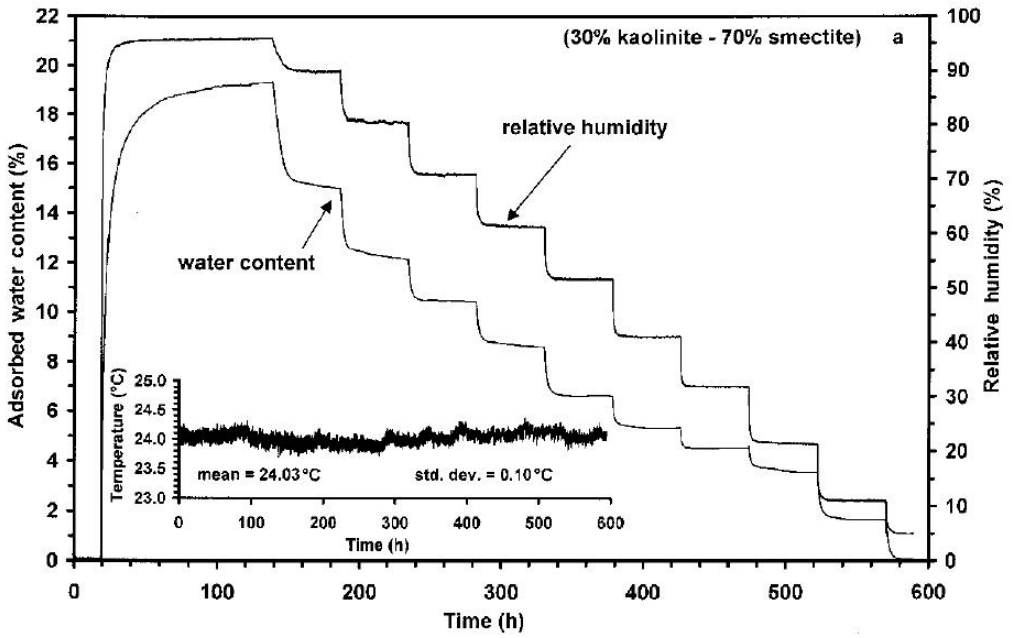

Figure 5.8: Time Response of Kaolinite - Smectite Water Absorption. Adopted from [11]. Used by Permission.

observed that the first 10 hours are essentially linear. A scaling factor (unpublished) was obtained from the authors, showing that the time for 100% kaolinite to reach the same level of water absorption as a 20% kaolinite - 80% smectite mixture was approximately double. The plot is be skewed out on the time line, keeping constant the magnitudes relative to the maximum level. Hence, we can use the values published by Likos and Lu to perform an approximation in order to estimate the mass of water accumulated on the surface of the Kaolin coated hot stick. As a level of 16% out of a maximum 19.3% is attained in 10 hours on the 30% kaolinite - 70% smectite curve (Figure 5.8), this same level is assumed to be attained in 20 hours in the 100% kaolinite sample from the scaling factor supplied by the authors. From the 95% relative humidity absorption of 60g/kg of Kaolinite (Table 5.2), we can expect a level of 48.7g water absorbed at 20 hours per kg of kaolinite. As the first 20 hours of curve is linear, we can use linear interpolation to find the value attained at 1.5 hours on the lines to 48.7g at 20 hours from the starting amounts of water dictated

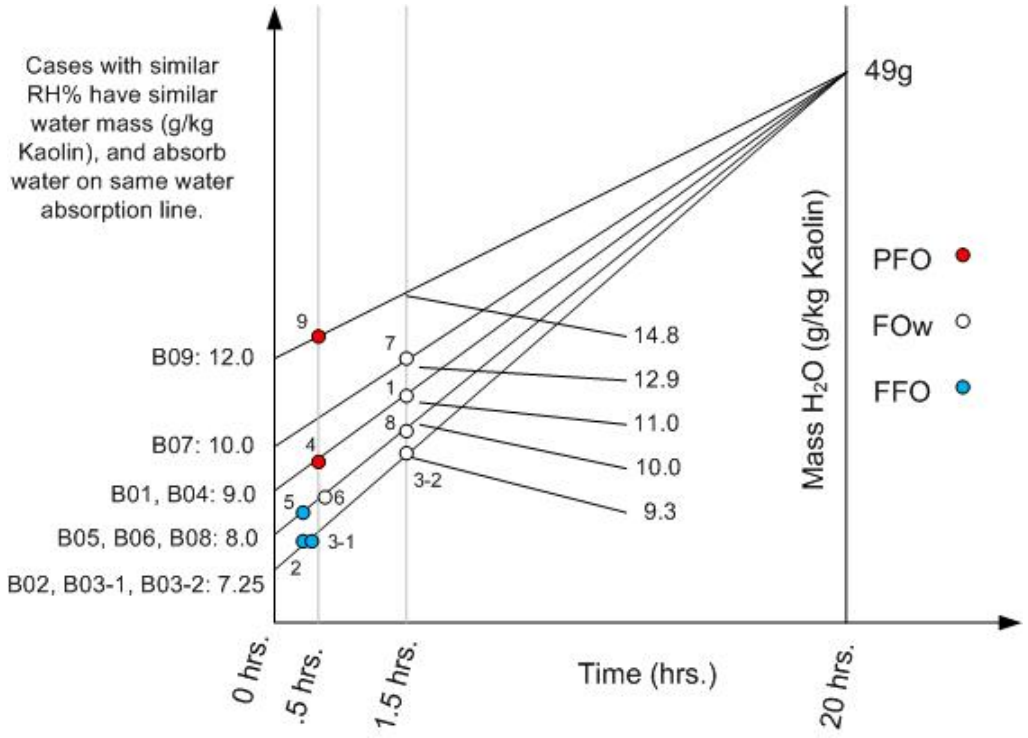

Figure 5.9: Water Absorption Lines for Cases B01-B09 Grouped According to Starting Relative Humidities.

for each of the B01-B09 cases as a function of their starting relative humidity values. This approach is illustrated in Figure 5.9.

From these lines we have the level of water absorbed in the nine cases from start to 1.5 hours with no current heating of the surface (i.e. the current is turned off in the simulation and the surface temperature equals the ambient temperature). Although the amount of moisture absorbed was measured for an ambient temperature of 24°C, it is assumed that the difference between this value and the typical ambient temperature of 22°C is negligible. However, this should be verified in future experimental work.

With the water absorption curves, five base cases are set up for the ten flashover cases exhibiting five starting levels of water already absorbed (due to the hot stick sitting in the environment of the laboratory at five different levels of relative humidity prior to the

experiment). As there is 2.1 μg/cm^2 of salt is on the surface (measured ESDD) and the original spray had 480 g Kaolin to 4.16 g salt, we can calculate out the total Kaolin deposit on the surface to be 115.4 g Kaolin per gram salt. Multiplying by 2.1 μg/cm^2, this gives us 2.42 $\times 10^{-4}$ g Kaolin per cm^2. Multiplying this by the test area of 2.714 $\times 10^3$ cm^2 gives 0.6526 g of Kaolin on the surface. For the B09 case with a different ESDD of 1.9 μg/cm^2 of salt density, we arrive at a value of 0.59 g Kaolin on the test surface area. Multiplying these figures by the grams of water absorbed per 1000 g Kaolin from Figure 5.9 gives us an estimate for the amount of water absorbed on the surface at the beginning and end points of the five curves in Figure 5.9. The amounts are listed in Table 5.3. Note that these levels are only for the hot stick sitting in an environment with the relative humidity rising to approximately 95 percent, without any leakage current heating up the surface and evaporating surface water.

Table 5.3: Start and End Water Absorption, and κ_c values for the Five Absorption Profiles in Figure 5.9

Cases	Start Water Level $10^{-3}g$	End Water Level $10^{-3}g$	κ_c
B09	7.085	8.723	2.60
B07	6.526	8.434	2.87
B01, B04	5.873	7.178	2.27
B05, B06, B08	5.220	6.558	2.31
B02, B03-01, B03-02	4.731	6.093	2.34

With these targets, the condensation coefficient κ_c is set relative to $\kappa_e = 1$, and $\left(\frac{dM}{dt}\right)^{(1)}_{Kaolin\ scale}$ is also scaled so the upward water absorption curve lags behind the relative humidity, but reaches the calculated value of surface water attained on the absorption line in Figure 5.9 for the respective case being adjusted for, after running the simulation for 90 minutes with the current turned off in the simulation. From this set up, these three constants are locked for the five case types based on water absorption. Thus, constants

and scaling factors are arrived at for each absorption line to be applied to the cases associated with that line. The common scaling factor $\left(\frac{dM}{dt}\right)^{(1)}_{Kaolin\ scale}$ is 7.9 $\times 10^{-12}$, and the values for the condensation coefficient κ_c for each case is listed in Table 5.3. As NaCl has a solubility of 35.7 g per 100 g or 100 cm^2 H_2O, multiplying this by the test area of 2714 cm^2 gives 1.59 $\times$ 10^{-2} g or cm^2, the water limit that must be reached before solution rises out of maximum salt saturation. Therefore, the water on the surface in the cases is always at maximum salt saturation, i.e. 357,000 mg per kg or Liter of water.

The next parameter to be set is the scaling constant $R1'$ numerator in the expression for the reference resistivity in the Hilchie equation, as was presented in Chapter 5:

$$\rho_p(t) = R1(t)\left\{\frac{T1_{\circ F} + x(t)}{T_{s^{\circ}F}(t) + x(t)}\right\}, \tag{2.15}$$

with $R1$ given by

$$R1(t) = \frac{R1'}{[NaCl(t)]}. \tag{5.19}$$

It was stated that the reference resistivity $R1'$ was determined by curve fitting the resistance points through the reference temperature line in Figure 2.7 at 50°C (122°F). However, this would just be for a saline solution, not taking into account the unknown effects of Kaolin and the geometry itself on the resistivity. As no resistance measurements were taken in the IREQ experiments, we are forced to estimate the resistivity. One source for a transformation from an ESDD value to an estimation of surface resistivity for an artificially polluted suspension insulator is in CIGRE 158 Polluted Insulators: A Review of Current Knowledge [45]. Figure 5.10 from CIGRE 158 gives a scaled translation to allow for calculation of surface conductivity in μS from ESDD in mg/cm^2 for solid layer experiments conducted under the clean fog test according to the standard IEC 61245 for

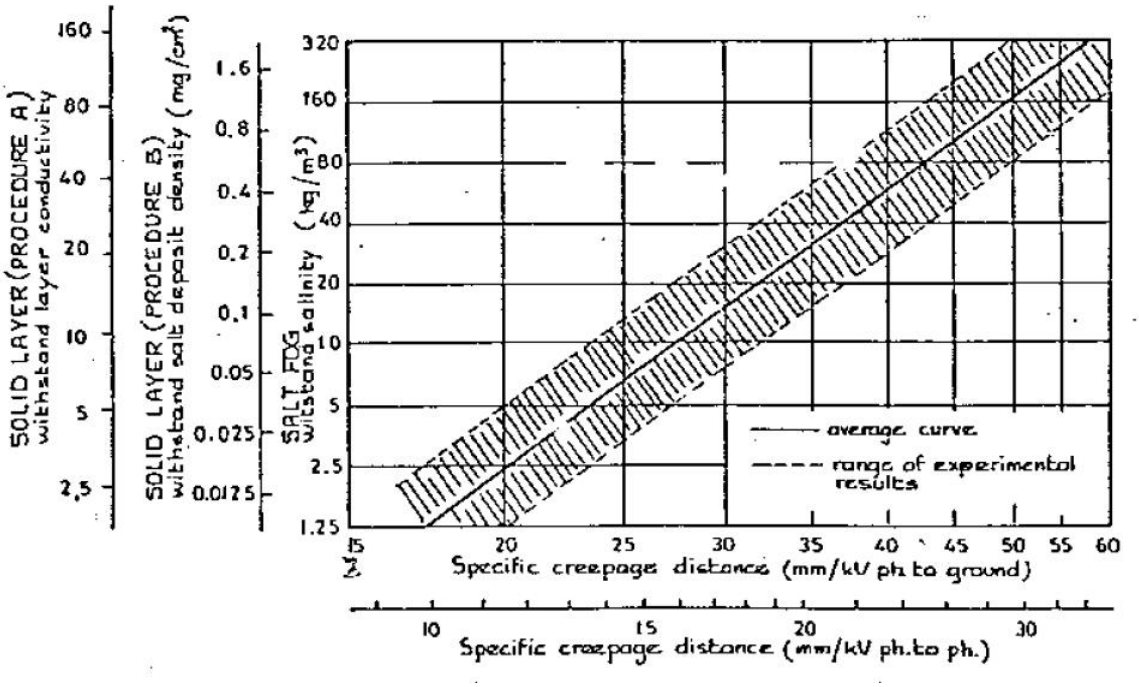

Figure 5.10: Relationship Between ESDD in mg/cm^2 and Surface Conductivity in μS. Adopted from [12], ©2000 CIGRE. Used by Permission.

which the IREQ experiments adhered to.

In using Figure 5.10, although we extrapolate outside the boundary of the figure to get to a ESDD of 2.1μg/cm^2, we stay within the boundary of the linear extrapolation of the range of experimental results. Calculating a creepage distance for our pollution flashover cases of 2700mm/315kV = 9mm/kV, we find that an ESDD of 2.1μg/cm^2 intersects with a specific creepage distance of 9mm/kV within the linear extended range of experimental results.

To extrapolate along the y-axis to get a value of conductivity from our ESDD value, we have two geometric series on two different scales. Points were tabulated between the two scales and a polynomial curve was fit to the data. Surface conductivity σ_s values of 0.879 and 0.855 μS are found for 2.1 and 1.9 μg/cm^2 respectively. These two values are used to find the resistance of the pollution layer from the formula given by Sundararajan

and Gorur [46] and by Kuffel et al. [4], given as

$$R = \frac{1}{\sigma_s} f, \tag{5.22}$$

where f is a form factor that takes into account the geometry of the insulator, expressed by

$$f = \int_0^L \frac{dl}{\pi D\left(l\right)}. \tag{5.23}$$

where $D(l)$ is the diameter of the insulator at the distance l along the leakage path. As the diameter of the hot stick is constant, the form factor is just the length of the test area 270 cm divided by π3.2 cm, with 3.2cm the diameter of the hot stick. This gives a form factor of 26.86. We can then calculate the resistance from the surface conductivities at 2.1μg/cm^2 and 1.9μg/cm^2 for B01-B08 and B09, and arrive at resistance values of 30.55 and 31.42 MΩ respectively. Working backwards from the resistance to the resistivity using equation 5.3, we calculate the resistivity

$$\rho_p\left(t\right) = \frac{R_p\left(t\right) A_{H_2O}^{r\varphi}\left(t\right)}{\left(L - x\left(t\right)\right)}, \tag{5.24}$$

which comes out to 0.0246 $\Omega\cdot$ m for the test area length and the calculated cross section for 5.873 $\times 10^{-3}$ cm^2 of water. Various values of $R1$ were iteratively entered into an Excel spreadsheet with Hilchie's equation to find an $R1$ that would produce the resistivity of 0.0246 $\Omega\cdot$ m, which was 0.015636. With this $R1$ value and knowing $[NaCl]$ = 357,000 mg/kg H_2O, we can calculate out $R1'$ by rearranging equation 5.19

$$R1' = R1\left(t\right) \cdot \left[NaCl\left(t\right)\right], \tag{5.25}$$

multiplying 0.015636 by 357,000 to get an R1' of 5582.

Estimates for surface resistivity vary widely in the literature. Another estimate taken from Farzaneh and Chisholm [47] gives a calculation for a 2.1 μg/cm^2 ESDD surface at 10,275 Ω/cm^2, or only 2.774 MΩ over the test length of the hot stick. Using Equation 5.16, we calculate an A value for these resistances with a $V_{c,\,50\%}$ of 315kV, we obtain values of A of 38 and 3.5 respectively. Various values for A are employed by different researchers for polluted surfaces, with A as wide as from 31 to 138 according to Farzaneh and Chisholm, and up to 530 according to Patni [48].

For the calculation of the heat transfer coefficient h, seven values for h were calculated at six temperature differences between the surface and ambient temperatures. The program interpolates between these when calculating h during the program run during each iteration for the difference between the surface temperature T_s and ambient temperature T_a. Values of $T_s - T_a$ = 1, 4, 10, 20, 60, and 80 were selected for a base $T_a = 20°C$, and values were calculated for the film temperature T_f and thermal expansion coefficient β. For each film temperature, values were read from tables at the back of Welty et al. for the thermal conductivity k, heat coefficient c_p, dynamic viscosity μ, and the kinematic viscosity ν [36]. From these elementals, the dimensionless numbers Prendtl Pr, Grashof Gr_L, Raleigh Ra_L, and the Nusselt Nu_L and the resulting value of h were calculated according to the formulas in Chapter 5. The calculated values are shown in Tables 5.4 - 5.5.

After calculating h for each of the seven breakpoints of $T_sK - T_aK$, the $D/L \geq 35/Gr_L^{0.25}$ condition was checked to see that this value of h could indeed be used. The condition (equation 2.30) is not met, as it is seen that $D/L = 0.0119$ never exceeds or even equals any of the seven calculated $35/Gr_L^{0.25}$ values in Table 5.6. Therefore, we use the Cebeci correction factor as discussed at the end of Chapter 2. We calculate ξ according to

Table 5.4: Table Values and Calculated Values for the Heat Transfer Coefficient h Calculations. $T_aK = 293.15$.

T_sK	T_fK	β	c_p	k	$\mu(\times 10^{-5})$	$\nu(\times 10^{-5})$	$\nu^2(\times 10^{-10})$
294.15	293.65	0.00340	1006	0.0257	1.813	1.51	2.27
297.15	295.15	0.00348	1006	0.0259	1.827	1.53	2.35
303.15	298.15	0.00335	1006	0.0260	1.837	1.55	2.41
313.15	303.15	0.00329	1006	0.0264	1.860	1.61	2.55
333.15	313.15	0.00319	1007	0.0273	1.910	1.69	2.86
353.15	323.15	0.00309	1008	0.0280	1.950	1.79	3.19
373.15	337.15	0.00300	1008	0.0287	2.010	1.90	3.56

Table 5.5: Table Values and Calculated Values for the Heat Transfer Coefficient h Calculations, cont. $T_aK = 293.15$.

T_fK	$Gr_L(\times 10^{10})$	Pr	$Rr_L(\times 10^{10})$	Nu_L	h
293.65	0.290	0.7162	0.21	154.3	1.47
295.15	1.112	0.7170	0.80	267.0	2.56
298.15	2.690	0.7175	1.93	347.5	3.36
303.15	4.990	0.7072	3.53	376.3	3.68
313.15	8.610	0.7047	6.07	447.4	4.51
323.15	11.200.	0.7024	7.87	486.1	5.04
337.15	13.010.	0.7004	9.12	509.3	5.43

its formula

$$\xi = \frac{\sqrt{32}}{Gr_L^{0.25}} \frac{L}{2r}, \tag{2.36}$$

and use this number with the Prendtl number Pr to find the Cebeci correction factor from the tables in [37]. They are incorporated into our calculations to find the final values of h for our hot stick geometry, calculated in Table 5.6.

5.3 Simulation Results and Discussion

The flashover algorithm was coded into MATLAB and was run on the case data. It was found that the simulations failed. After investigation, it was discovered that the algorithm was effectively boiling or evaporating all the water off of the surface of the hot stick for all

Table 5.6: $D/L \geq 35/Gr_L^{0.25}$ (with $D/L = 0.0119$) Conditional Validation Check, and Corresponding Cebeci Correction Factors ${}^*Nu_L/Nu_L$.

$T_f K$	$35/Gr_L^{0.25}$	Test Result	ξ Calculated	Pr	${}^*Nu_L/Nu_L$	h final
293.65	0.1508	Fail	2.0571	154.3	1.58	2.32
295.15	0.1077	Fail	1.4695	267.0	1.42	3.65
298.15	0.0864	Fail	1.1785	347.5	1.34	4.51
303.15	0.0741	Fail	1.0099	376.3	1.29	4.78
313.15	0.0646	Fail	0.8811	447.4	1.26	5.68
323.15	0.0605	Fail	0.8248	486.1	1.24	6.28
337.15	0.0582	Fail	0.7946	509.3	1.23	6.71

cases exhibiting leakage current (B01, B03-02, B04, B06 to B09). This was attributable to the Joule heating term evaporating all the surface water causing a breakdown of the model with the creation of negative water volume levels. Reasons for this issue arising were examined according to the following possibilities.

Current discharges or peaks in the current trace last a minimum of 0.5 seconds in the data (the interval of 1 iteration) but in most circumstances lasting much longer as observed on the original data plots (Appendix A). The sourcing of the data from paper printouts is the largest source of error introduced in the research, due to the lack of resolution in the current trace data, being on a fractional minute time scale, and only recoverable to a specific level of resolution (2-4 seconds between data points). Since discharges last in the order of $10^{-3} - 10^{-2}$ seconds, this has caused an overestimation of heating. This was the major source of error.

Absence of other heat removal terms that also should have been implemented in such a model, such as the conduction effects transferring heat away from the water to the Kaolin and the solid hot stick body in parallel, and through the Kaolin mineral to the hot stick. Radiation effects are also not taken into account [31]

Another two sources of error on the part of this model building can be attributed to

the estimation of the water on the surface for which there was no data from the original experiments, and the estimation for resistance. Although an estimate for the salt on the surface was provided, it is not possible to calculate the resistance which changes with time without knowledge of the water density on the surface, which also changes with time. The estimation of the amount of Kaolin on the surface uses the ratio of salt to Kaolin in the original slurry to estimate the Kaolin density from the salt density. This estimation assumes a completely uniform application of the Kaolin salt water slurry. There was no real time information collected during the experiment with regard to non-uniformity of the pollution layer during the experiment, which could be done by thermography, imaging the variation in surface heating to get an assessment of the non-uniformity.

The estimate of the water on the surface by Kaolin absorption of the vapor in the air is done because the ambient temperature trace reveals very little heat detection, indicative of the steam cooling to room temperature by the time it reached the temperature detector. No data exists on whether or not the steam vapor cools to room temperature prior to reaching the hot stick. The estimate of the amount of humidity absorption comes from Kaolin water absorption data found in the literature. The level of absorption of moisture from the surrounding air using the relative humidity data leads to absorption of water onto the surface on the order of 10^{-3}cm^3 for which there is no reference to compare to without experimentation. The critical voltage did not move at all with a value for the empirical coefficient A of 3.5 to correspond to our resistance [47].

For debugging purposes, it was determined to add three scaling factors to the model to account for a possible error due to the assumptions. A two scaling factor solution had to be implemented in front of the Joule heating term in equation 5.15 to prevent negative water volumes from evolving in any of the cases during the simulations. A straight scaling factor

was implemented and adjusted iteratively until the worst case for boiling all the water off the surface, B03-02, kept a positive water volume on the surface. However, this attenuation nullified any effect of the current in the pollution flashover case B04, and especially B09 with its much smaller current trace. Hence another scaling term was also placed to weigh the larger leakage currents in the heating process and attenuate the effect of smaller current levels. A third scaling factor had to be placed in front of the convection term of equation 5.15. After placement and tuning of the scaling factors to prevent negative water volumes, The constant A was adjusted to allow $V_{c,50\%}$ to rise over the applied voltage trace to assess the discrepancy. This did not occur until A=13,800.

Simulations were run on all cases and the results for a pollution flashover (B04), a fast flashover (B03-01), and a flashover withstand (B01). Figures just for the pollution flashover B04 are shown in Figures 5.11 and 5.12. The resistance is dropping as the experiment proceeds (Figure 5.12), which is as expected from high voltage lab experience. This drop exhibits a lag relative to the onset of humidity as observed in Figure 5.11. The resistivity observed in Figure 5.12 is not moving as expected before the current onset. The same is observed with B01.

When we view the fast flashover B03-01 case, we observe no movement in the critical voltage, easily attributable to the absence of current as with all other cases during periods of no current, observed in Figure 5.15. There is movement in the surface resistance per unit length for the fast flashover due to the increase in surface volume of water, as seen in Figure 5.16. However, the critical voltage is insensitive to the magnitude of change in the surface resistance per unit length.

The absence of change in resistivity was expected from the Kaolin absorption values, and the necessity for scaling down the Joule heating term both point towards an inadequate

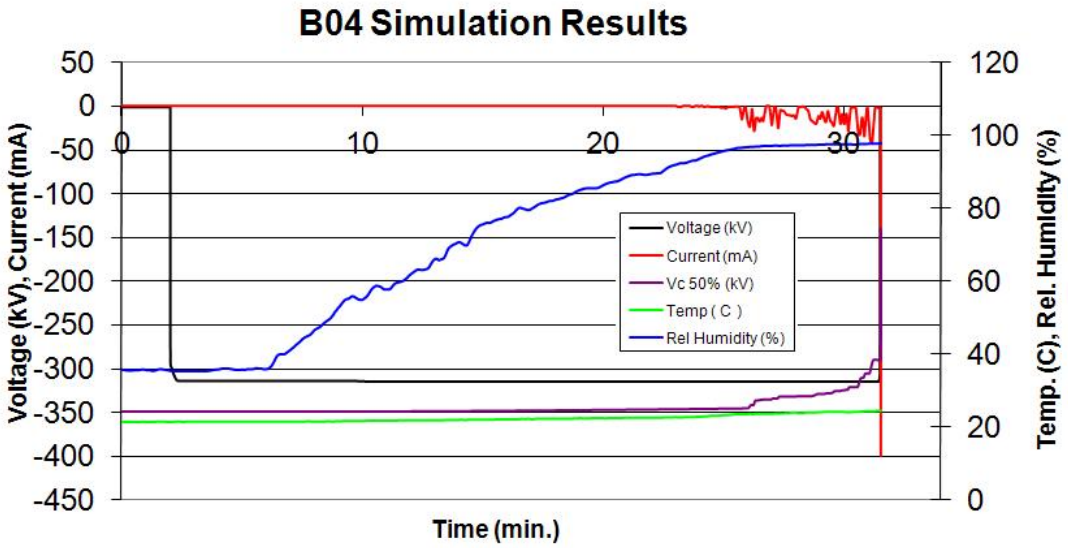

Figure 5.11: B04 Critical Voltage for Pollution Flashover.

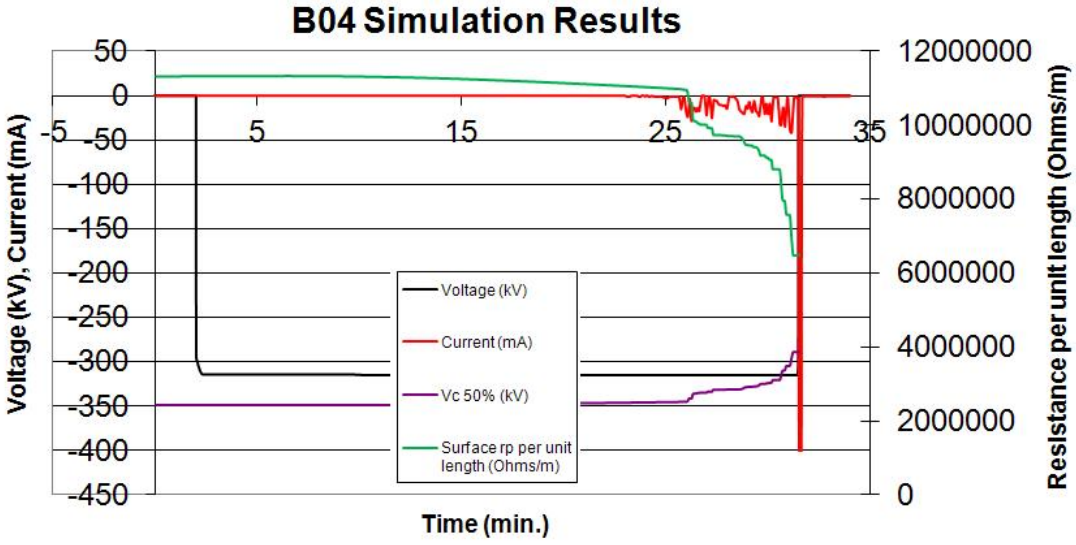

Figure 5.12: B04 Resistance for Pollution Flashover.

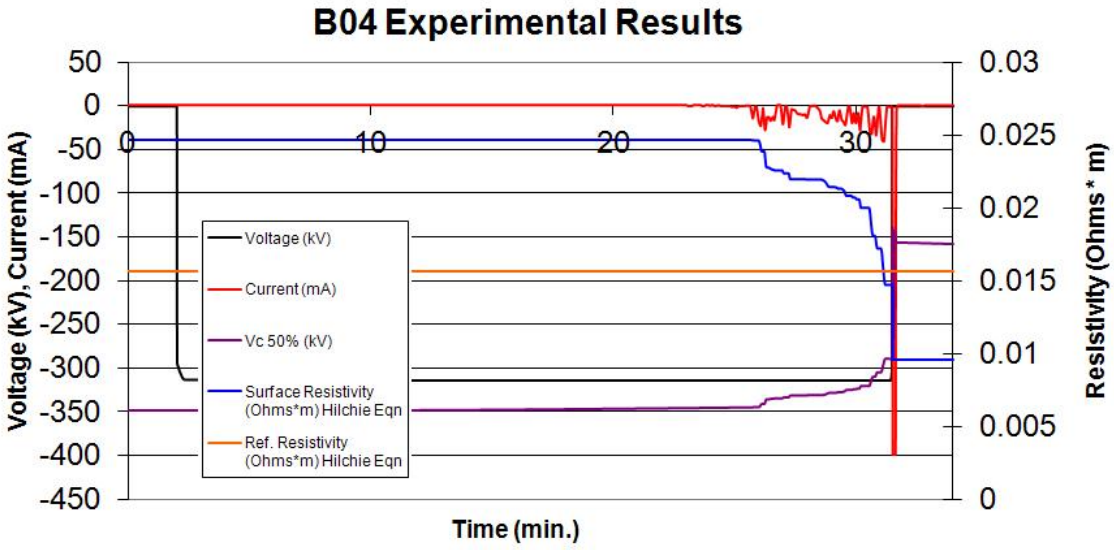

Figure 5.13: B04 Resistivity for Pollution Flashover..

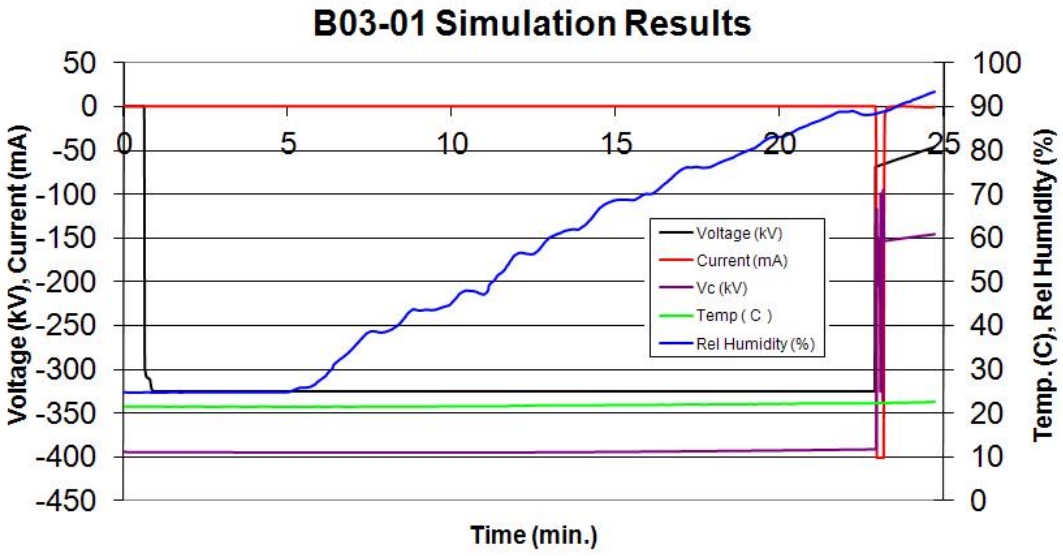

Figure 5.14: B03-01 Critical Voltage for Fast Flashover.

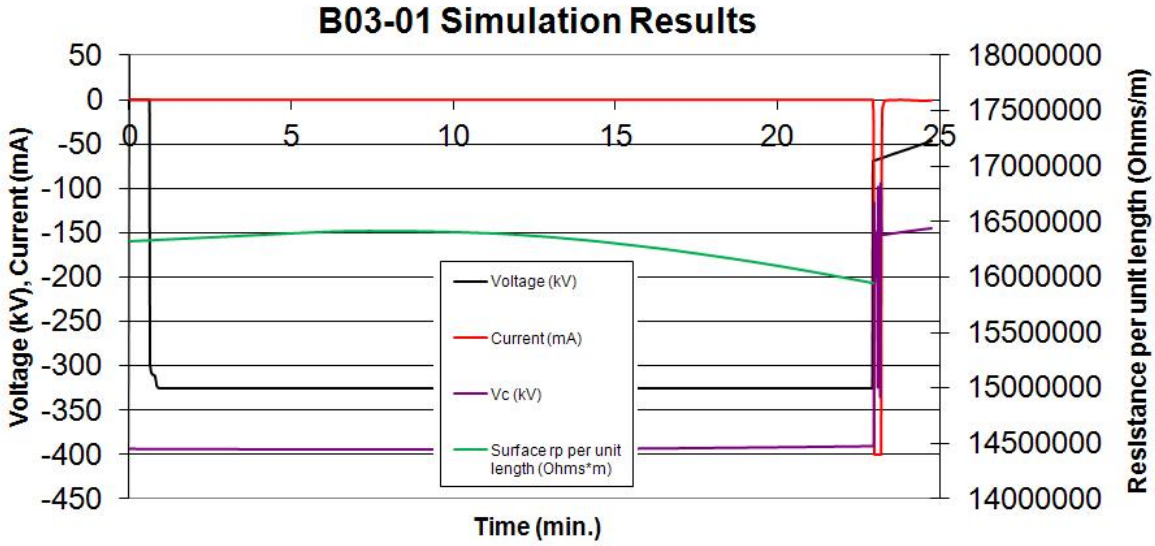

Figure 5.15: B03-01 Resistance for Fast Flashover.

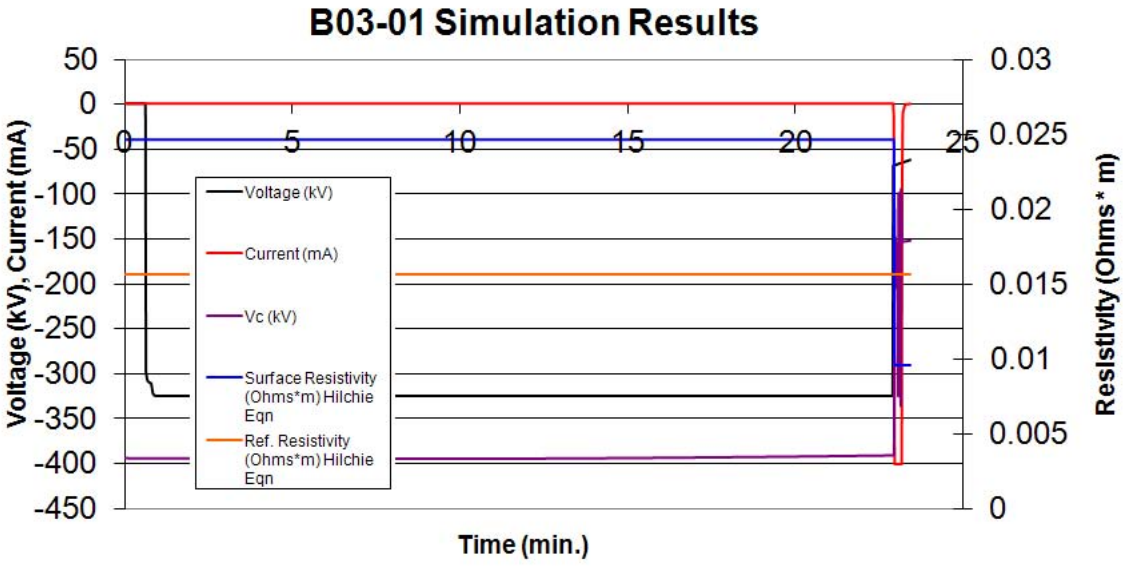

Figure 5.16: B03-01 Resistivity for Fast Flashover..

amount of water on the surface and too low a rate of moisture transfer to the surface that results in water being too aggressively boiled away. This is not what is expected in the physical reality of flashover. As described by Wilkins [28], the water should accumulate until the maximum volume is reached whereby the salt concentration is at the solubility limit, followed by dilution with the drop in conductivity due to incremental dilution. This is counterbalanced by an increasing volume of water in the denominator of the resistance term that keeps the resistance dropping until leakage currents form. Resistivity increase never occurs in all the above cases. However, with larger amounts of water and larger changes in the volume of water, the denominator of the reference resistivity R1 term in the Hilchie equation consisting of the amount of salt divided by the volume of water would have much more impact on the value of the resistivity, most likely allowing for more significant decreases in the pollution flashover cases.

Another point is that a lower pollution resistance as per the estimates of Farzaneh and Chisholm (2.7MΩ) may be more realistic than the CIGRE estimate (30.0MΩ), as the R1' numerator of the reference resistivity term in the Hilchie equation would be lower, making it more sensitive to changes in the denominator to meet the physical reality of a rising resistivity prior to leakage current onset.

The ambient temperature that the temperature sensor is measuring would not be the same temperature at the center of the lab where the hot stick is placed. As it is evident that the steam has lost its energy by the time it diffuses across the lab to the sensor, it may be or may not be cooled to room temperature by the time it reaches the hot stick.

In conclusion, the simulations were performed to examine for differences between the flashover modes with respect to the relative humidity. From the cursory examination of three types of cases, keeping in mind simulation levels were arbitrary due to scaling factors

and only relative changes should be examined, there was no new evidence that gave any insight into the fast flashover mechanism via the effect of relative humidity. Thus, the results were inconclusive. However, this may only apply to the analysis that was done at these low water levels. This analysis has not taken into account the possibility of steam condensation on the hot sticks and much higher rates of water accumulation leading to different outcomes with respect to elevation of the critical voltage curve due to movement in resistivity due to moisture transfer, which can not be ruled out.

Chapter 6

Summary, Conclusion, and Recommendations for Future Research

In concern for protecting against dangerous physical phenomena, the proposition of a new physical mechanism can be a very daunting challenge to gain evidence for. Statistical analysis has offered some support to the proposition of the fast flashover observation being a type of flashover unique from the pollution flashover. However, no further evidence was found to support this assertion. The statistical analysis also gave some evidence for relative humidity having a greater correlation than applied voltage to the type of flashover mechanism that takes place in a discharge over an insulating dielectric surface.

Although the levels of confidence attained in this study would not be sufficient for proving the existence of this mechanism, there are still reasons to go further with investigation. With the idea that there may be some connection between relative humidity and

the type of discharge, the approach was taken to build a pollution flashover model based around a mechanism connecting relative humidity to the outcome of the discharge. It is proposed that the influence of relative humidity can be seen in operation with the pollution flashover mathematically by the observation of the behavior of the intermediate calculated variables. When the fast flashover fails to meet pollution flashover criteria, some insight could be gained in the fast flashover mechanism from the intermediate variables.

The findings of the simulations were inconclusive. Lack of movement in the critical voltage curve in the fast flashover cases could be easily explained by the lack of surface current activity, unlike the pollution flashover and flashover withstand cases that exhibited large levels of activity. However, these movements were expected to come before the leakage current, which would be due to water condensation and temperature changes affecting the resistance of the pollution layer. Higher surface water levels and transfer may still reveal some impact on the resistivity that may impact the critical voltage. The cases exhibited a low level of water buildup due to an assumption that there was no condensation onto the hot stick implied by the temperature trace data.

Although some exposure has been gained into modeling the pollution mechanisms, more work must be done to provide information that will remedy the excessive assumptions that have to be made in the light of unavailable data that may allow for easier investigation to be performed.

6.1 Recommendations for Future Research

In order to allow for future progress in experimental work with artificially polluted insulators or hot sticks, it is essential to see that these deficiencies are remedied that lead to assumptions due to lack of data.

Resistance measurements should be taken off the hot sticks with the specific Kaolin or clay material. Many measurements should be taken of each stick, and a large sample size should be constructed of very carefully prepared artificially polluted hot sticks, similarly coated (essential to be as accurate as possible) to construct a high-confidence estimate of the mean value with a low standard deviation.

It is necessary to assess the true value of moisture buildup on the polluted hot stick or insulator to gain a complete understanding of these flashover mechanisms. During relative humidity changes, a laser refraction method could be employed to measure the level of refraction from the surface fluid level as the accumulation of moisture proceeds during experiments with and without voltage and resulting current applied.

It is absolutely essential to have the highest level of statistical confidence in the rejection of the null hypothesis for any analysis that is attempting to propose a new mechanism [41]. Thus, under the challenge of the economic bounds to experimental repetition, more economical methods must be employed in the laboratory to increase the number of trials in order to increase the sample size to allow for higher confidence.

With regards to the above statement, two additional points must be made. The increase of sample size will by nature decrease the spread of the sample distribution as the frequency of observations increases. However, variation must also be reduced by means of more strict experimental procedures whereby only the variable being studied for the affect of its variation on the dependent variable can be allowed to vary. The other variables must be held constant in the strictest possible sense.

Cameras must be set up to view the entire side of the hot stick or insulator with a wide angle lens if necessary, and two cameras should be used with each placed 180 degrees from the other in order to cover the entire surface. Discharge activity is too fast to capture by

conventional video. High speed video is required with a faster frame rate.

Temperature and relative humidity measurements must be taken near the hot stick being experimented on to assess local ambient temperature and due point in order to contribute to a measurement of condensation. The parameter of ESDD can be used as an index for further estimation. However, moisture level is required in order to move towards a more rigorous appraisal of dynamic surface resistance measurement, and its affect on the flashover phenomenon.

References

[1] T. C. Ltd., *Connectors and Terminals Catalogue 2012*. TE Connectivity Ltd., 2012. [Online]. Available: http://www.te.com/us/en/industries/energy/productsubcontents.aspx?name=1012

[2] U. of Michigan Demonstration Laboratory, "Electric Breakdown Between Electrode and Sphere." [Online]. Available: https://sharepoint.umich.edu/lsa/physics/demolab/DemoLab%20Asset%20Library/Arc%20between%20Electrodes_5C30.50.bmp

[3] K. Schraner, "Electric Breakdown Between 2 Spheres." [Online]. Available: http://twfpowerelectronics.com/~kurt/Marx/6_Marx22cm_Ball1830kl.jpg

[4] E. Kuffel, W. S. Zaengl, and J. Kuffel, *High Voltage Engineering Fundamentals*, 2nd ed. Oxford, U.K.: Newnes, July 2000.

[5] E. Nasser, *Fundamentals of Gaseous Ionization and Plasma Electronics*. New York, NY, USA: Wiley Interscience, April 1971.

[6] U. of Stellenbosch High Voltage Laboratory, "Pollution Flashover," 2001. [Online]. Available: http://research.ee.sun.ac.za/hvlab/download/pictures/ifohd007.jpg

[7] Y. Sabri, M. Farzaneh, and J. Zhang, "Application of Identification Methods for Predicting the Flashover Voltage of Contaminated Insulators Covered with Ice," *IEEE Transactions on Dielectrics and Electrical Insulation*, vol. 17, pp. 451–457, April 2010.

[8] L. Alston and S. Zoledziowski, "Growth of Discharges on Polluted Insulation," *Proceedings of the Institution of Electrical Engineers*, vol. 110, no. 7, pp. 1260 –1266, July 1963.

[9] "Weatherford Log Interpretation Charts, Compact Tool Series. Weatherford, 2007." [Online]. Available: http://www.weatherford.com/ECMWEB/groups/web/documents/weatherfordcorp/WFT051974.pdf

[10] R. Dub and Y. Beausjour, "High Voltage Laboratory Tests on FRP Hot Sticks and FRP Booms," L'Institut de Recherche d'Hydro Quebec (IREQ), Varennes, Canada, Tech. Rep., November 2005.

[11] W. J. Likos and N. Lu, "Water Vapor Sorption Behaviour of Smectite-Kaolinite Mixtures," *Clays and Clay Minerals*, vol. 50, no. 5, pp. 553–561, October 2002.

[12] I. C. on Large Electric Systems (CIGRE), "CIGRE Monograph 158. Polluted Insulators: A Review of Current Knowledge," CIGRE, Tech. Rep., June 2000.

[13] W. McDermid, J. C. Bromley, D. J. Dodds, and D. R. Swatek, "Investigation of the Flashover of a FRP Hot Stick While in Use for Live Line Work at 500 kV," *IEEE Transactions on Power Delivery*, vol. 14, no. 3, pp. 1158 –1166, July 1999.

[14] B. F. Hampton, "Flashover Mechanism of Polluted Insulation," *Proceedings of the Institution of Electrical Engineers*, vol. 111, no. 5, pp. 985 –990, May 1964.

[15] W. McDermid, D. R. Swatek, and J. C. Bromley, "FRP Hot Stick Flashovers During EHV Live Line Work," in *Electrical Insulation Conference and Electrical Manufacturing and Coil Winding Technology Conference, Sept. 23-25, 2003. Proceedings*, September 2003, pp. 7–11.

[16] W. McDermid, "Investigation of FRP Hot Stick Performance for 500 kVdc Applications Under Conditions of Pollution or Non-Uniform Wetting," in *International Conference on High Voltage Engineering and Application (ICHVE) 2008*, November 9-12 2008, pp. 36–39.

[17] ——, "Characterization of Fast Flashover of External Insulation," in *Conference Record of the 2008 IEEE International Symposium on Electrical Insulation (ISEI)*, June 2008, pp. 510–513.

[18] W. Hauschild and W. Mosch, *Statistical Techniques for High Voltage Engineering*. London, U.K.: IET, 1992.

[19] D. C. Jolly, "Contamination Flashover, Part I: Theoretical Aspects," *IEEE Transactions on Power Apparatus and Systems*, vol. PAS-91, no. 6, pp. 2437–2442, November 1972.

[20] L. B. Loeb and J. M. Meek, *The Mechanism of the Electric Spark*. Stanford, CA, USA: Stanford University Press, 1941.

[21] Y. P. Raizer, *Gas Discharge Physics*, J. E. Allen, Ed. Berlin, Germany: Springer-Verlag, 1991.

[22] M. F. Hoyaux, *Arc Physics*. New York, NY, USA: Springer-Verlag, 1968.

[23] M. T. Gencoglu and M. Cebeci, "Computation of AC Flashover Voltage of Polluted HV Insulators Using a Dynamic Arc Model," *European Transactions on Electrical Power*, 2008.

[24] D. C. Jolly, "Contamination Flashover Theory and Insulator Design," *Journal of the Franklin Institute*, vol. 294, no. 6, pp. 483–490, IN27–IN28, 491–500, December 1972.

[25] F. A. M. Rizk, "Mathematical Models for Pollution Flashover," *Electra*, vol. 78, pp. 71–103, 1981.

[26] G. Neumarker, "Verschmutzungszustand und kriechweg," *Monatsberichte der Deutschen Akademie der Wissenschaften zu Berlin*, vol. 1, pp. 352–359, 1959, in German.

[27] D. Halliday, R. Resnick, and J. Walker, *Fundamentals of Physics*, 5th ed. New York, NY, USA: John Wiley & Sons, 1997.

[28] R. Wilkins, "Flashover Voltage of High-Voltage Insulators with Uniform Surface-Pollution Films," *Proceedings of the Institution of Electrical Engineers*, vol. 116, no. 3, pp. 457 –465, March 1969.

[29] P. Glover, "Petrophysics MSc Course Notes. Laval University, Laval, QB, Canada," 2000. [Online]. Available: http://www2.ggl.ulaval.ca/personnel/paglover/CD%20Contents/GGL-66565%20Petrophysics%20English/Chapter%2017.PDF

[30] R. Marek and J. Straub, "Analysis of the Evaporation Coefficient and the Condensation Coefficient of Water," *International Journal of Heat and Mass*

Transfer, vol. 44, no. 1, pp. 39 – 53, January 2001. [Online]. Available: http://www.sciencedirect.com/science/article/pii/S0017931000000867

[31] Y. A. Cengel and M. A. Boles, *Thermodynamics: An Engineering Approach*, 3rd ed. Boston, MA, USA: WCB McGraw-Hill, 1998.

[32] J. G. Speight, *Lange's Handbook of Chemistry*, 15th ed. New York, NY USA: McGraw-Hill, 1999.

[33] R. G. Mortimer, *Physical Chemistry*, 3rd ed. Boston, MA, USA: Elsevier, 2008.

[34] E. C. Salthouse, "Initiation of Dry Bands on Polluted Insulation," *Proceedings of the Institution of Electrical Engineers*, vol. 115, no. 11, pp. 1707–1712, November 1968.

[35] C. Texier, D. Etat, and B. Kouadri, "Model of the Formation of a Dry Band on an NaCl-Polluted Insulation," *IEE Proceedings A: Science, Measurement, and Technology*, vol. 133, no. 5, pp. 285–290, July 1986.

[36] J. Welty, C. E. Wicks, G. Rorrer, and R. E. Wilson, *Fundamentals of Momentum, Heat, and Mass Transfer*, 5th ed. New York, NY, USA: John Wiley & Sons, 2007.

[37] T. Cebeci, "Laminar-Free-Convective-Heat Transfer From the Outer Surface of a Vertical Slender Circular Cylinder," *Proceedings of the Fifth International Conference on Heat transfer, Tokyo, Japan*, vol. 3, pp. 15–19, September 3-7 1974.

[38] C. O. Popiel, J. Wojtkowiak, and K. Bober, "Laminar Free Convective Heat Transfer from Isothermal Vertical Slender Cylinder," *Experimental Thermal and Fluid Science*, vol. 32, no. 2, pp. 607–613, November 2007.

[39] *IEC 61245. Artificial Pollution Tests on High-Voltage Insulators to be Used on D.C. Systems 1993-10.*, International Electrotechnical Commission (IEC) Std. 61 245, 1993.

[40] F. B. Hildebrand, *Introduction to Numerical Analysis*. New York, NY, USA: Dover Books, 1987.

[41] D. S. Moore and G. P. McCabe, *Introduction to the Practice of Statistics*. New York, NY, USA: W. H. Freeman and Company, 1989.

[42] W. W. Daniel, *Applied Nonparametric Statistics*. Boston, MA, USA: PWS-Kent Publishing Company, 1990.

[43] J. Rohlf, *Statistical Tables*. New York, NY, USA: W. H. Freeman and Company, 1995.

[44] N. F. Laubscher, F. E. Steffens, and E. M. Lange, "Exact Critical Values for Mood's Distribution-Free Test Statistic for Dispersion and Its Normal Approximation," *Technometrics*, vol. 10, pp. 497–507, August 1968.

[45] G. Zhicheng and Z. Renyu, "Calculation of DC and AC Flashover Voltage of Polluted Insulators," *IEEE Transactions on Electrical Insulation*, vol. 25, no. 4, pp. 723–729, August 1990.

[46] R. Sundararajan and R. S. Gorur, "Dynamic Arc Modeling of Pollution Flashover of Insulators Under DC Voltage," *IEEE Transactions on Electrical Insulation*, vol. 28, no. 2, pp. 209 –218, April 1993.

[47] M. Farzaneh and W. A. Chisholm, *Insulators for Icing and Polluted Environments*. Hoboken, NJ, USA: IEEE Press, 2009.

[48] P. K. Patni, "Review of Models which Predict the Flashover Voltage of Polluted Insulators," Master's thesis, University of Manitoba, Winnipeg, MB, Canada, June 1997.

Appendix A

Original 2004 IREQ Hot Stick Flashover Experiments: B01 - B09 Raw Data Plots.

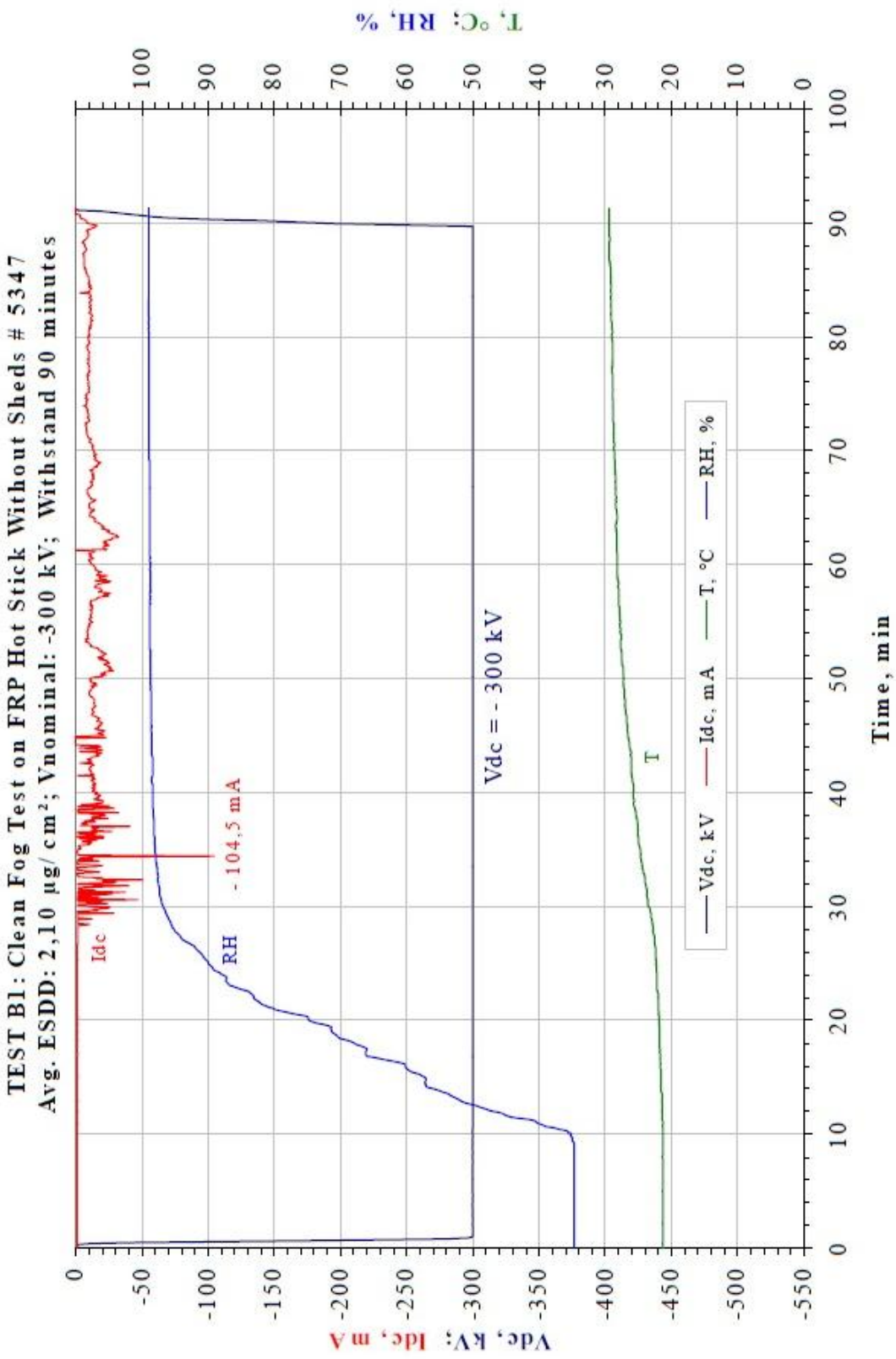

Figure A.1: B01 Pollution Flashover - Original Data.

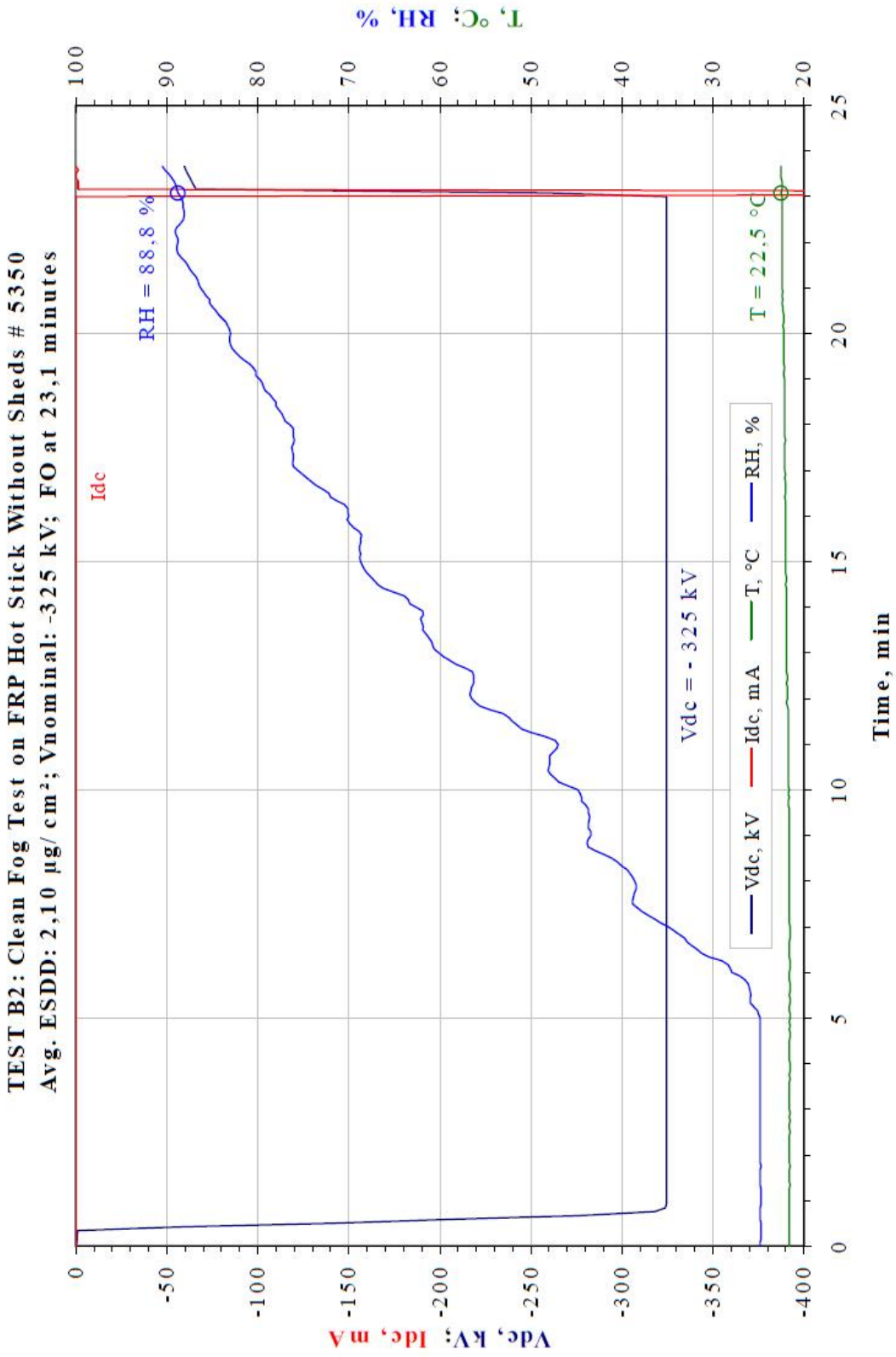

Figure A.2: B02 Fast Flashover - Original Data.

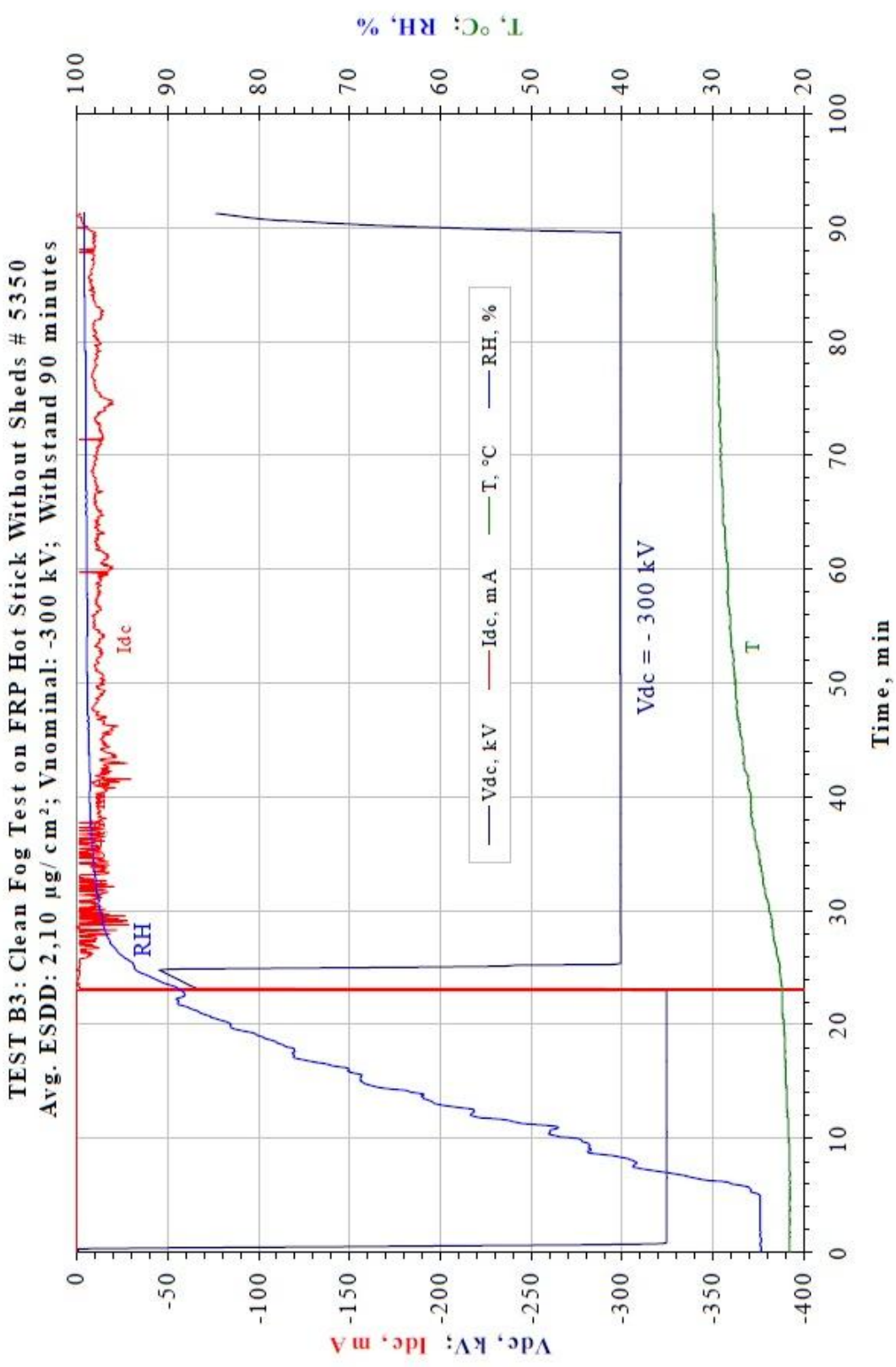

Figure A.3: B03 Fast Flashover (up to 23 min.) and Pollution Flashover Withstand (23 min. to 90 min.) - Original Data.

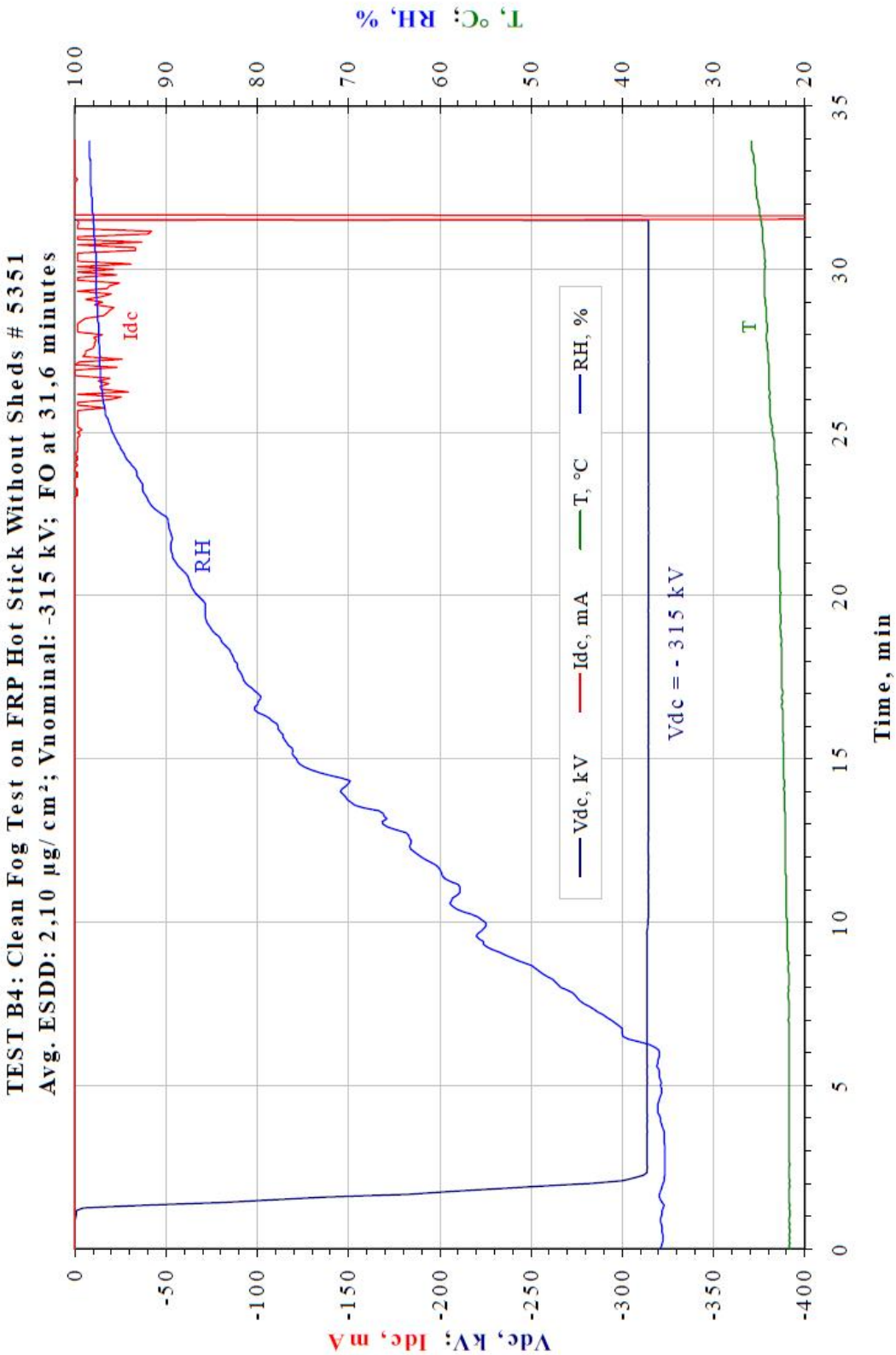

Figure A.4: B04 Pollution Flashover - Original Data.

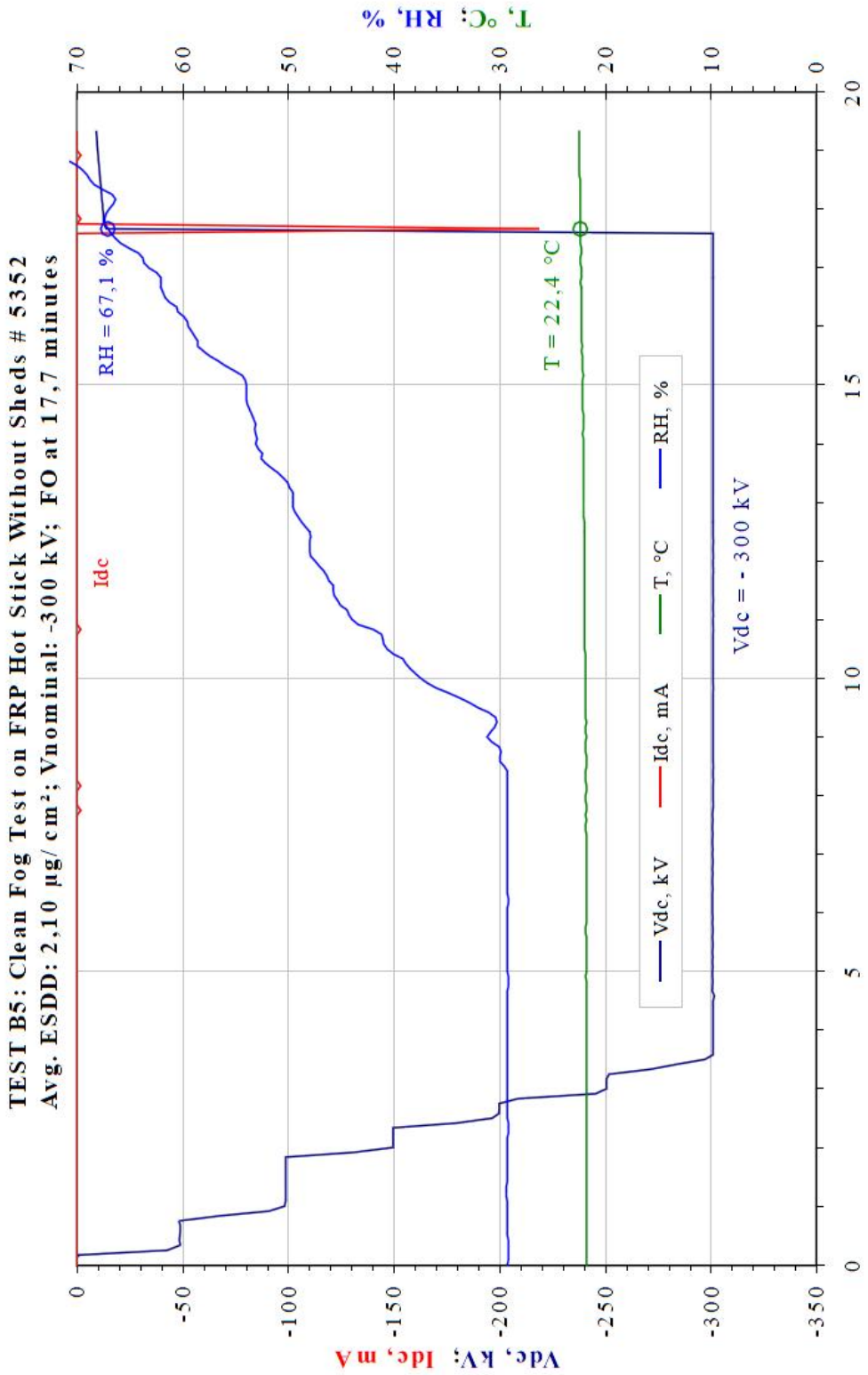

Figure A.5: B05 Fast Flashover - Original Data.

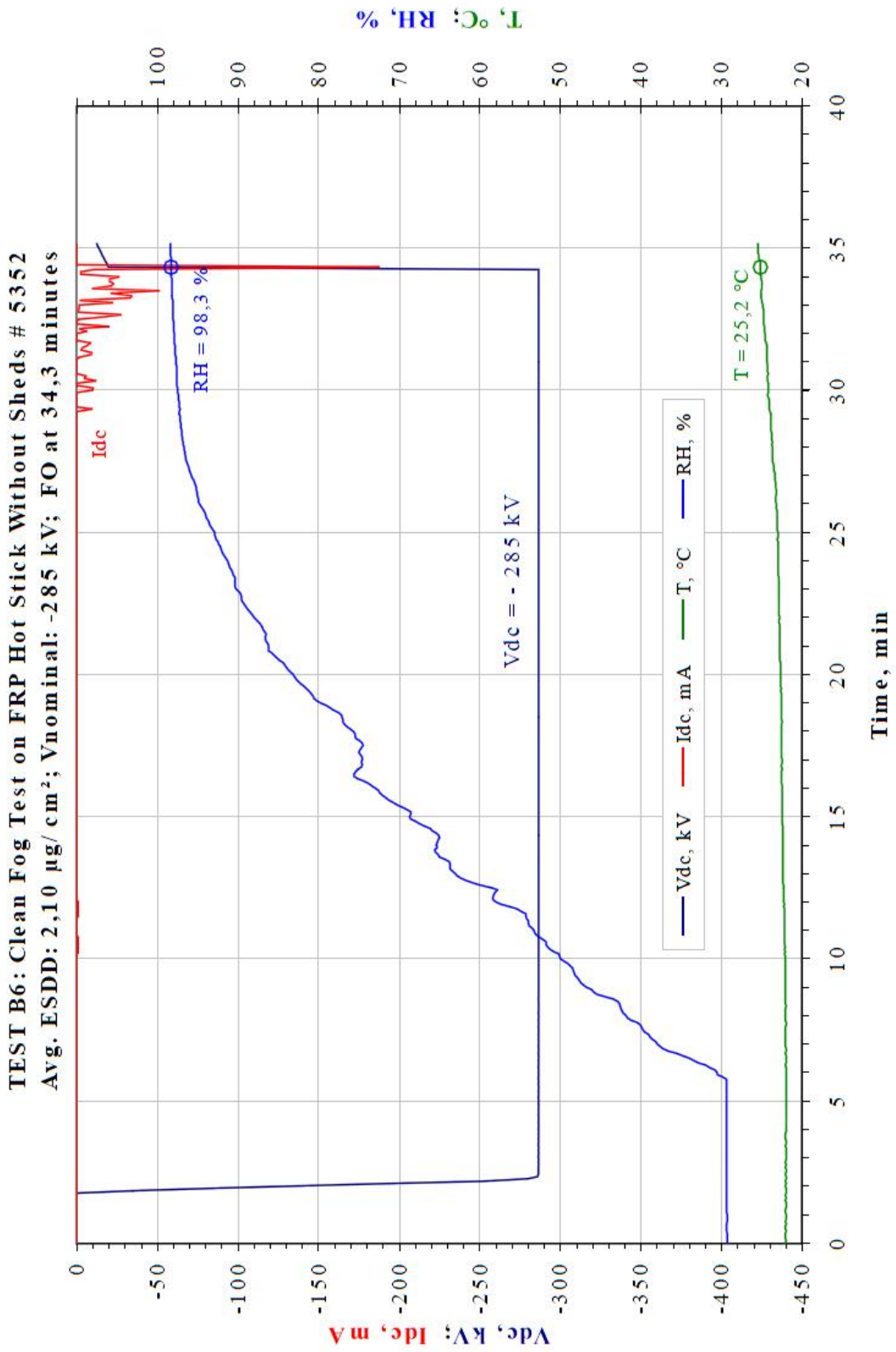

Figure A.6: B06 Pollution Flashover - Original Data.

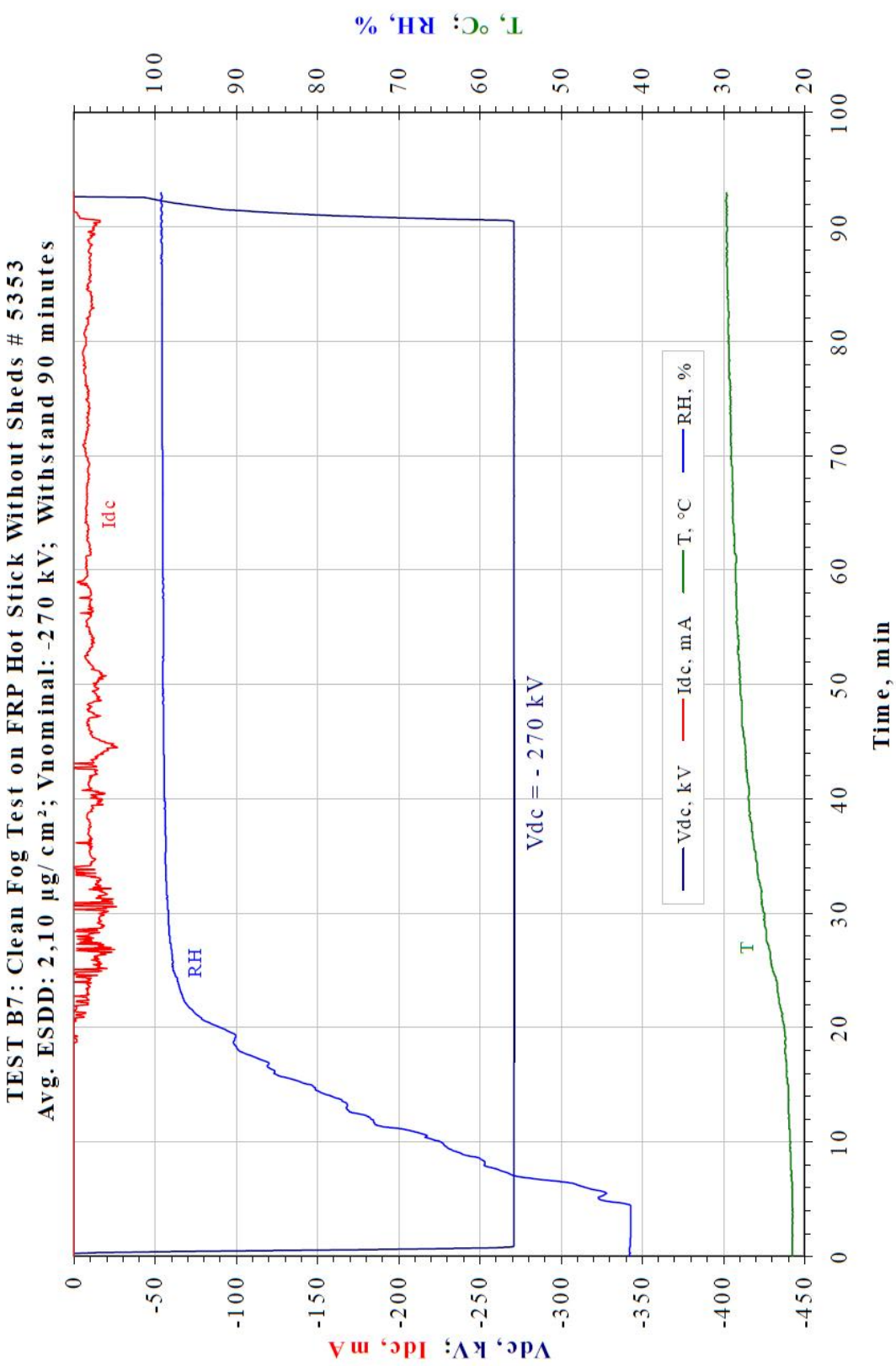

Figure A.7: B07 Flashover Withstand (up to 23 min.) and Pollution Flashover Withstand (23 min. to 90 min.) - Original Data.

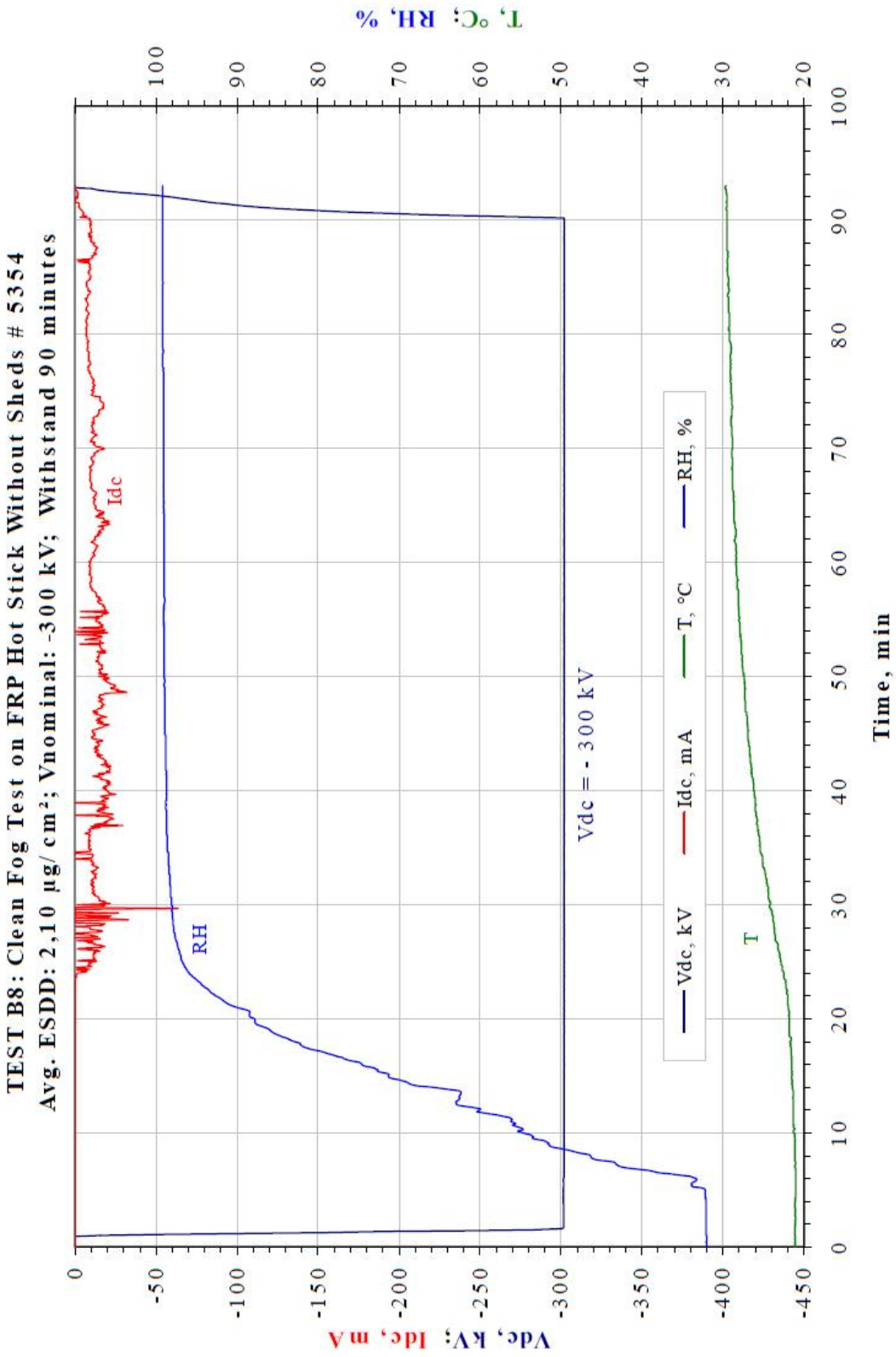

Figure A.8: B08 Flashover Withstand - Original Data.

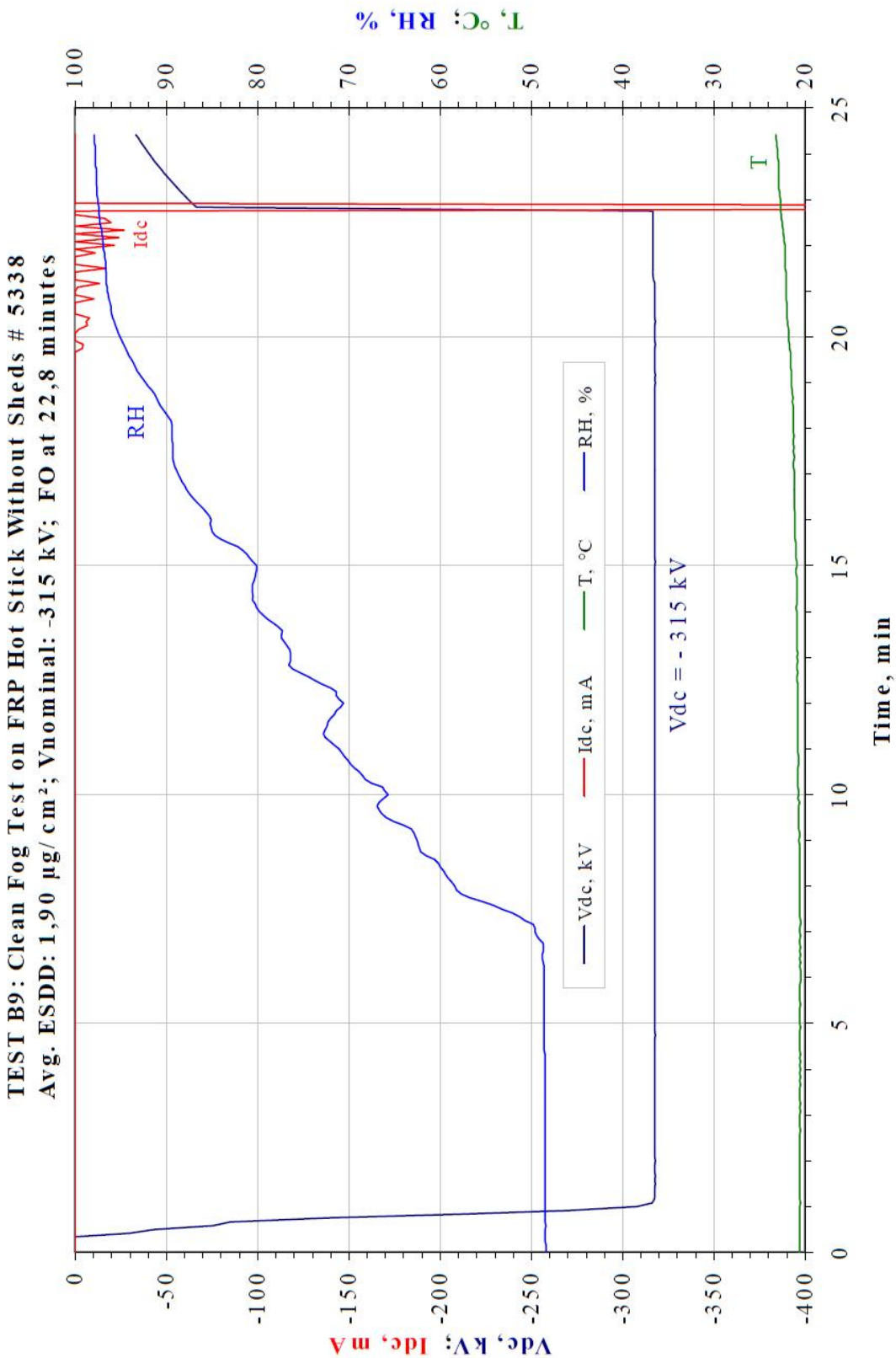

Figure A.9: B09 Flashover Withstand - Original Data.